Università di Roma La Sapienza

Dottorato di Ricerca in Ingegneria

XXII Ciclo

Tecnologia Aeronautica e Spaziale

Finite Element Modeling of Dielectric Elastomer Actuators for Space Applications

Ph.D. : Luca Lampani

Supervisor : Prof. Paolo Gaudenzi

Ai miei genitori

Contents

Table of figures

1

Preface

“ One day the technology of electroactive polymers will drastically change the way we perceive products. Products will gain new dimensions ranging from changing tactile surfaces over active membranes to morphing shapes. Products of the future will be "alive". We´ll have to question future responsibilities of product design, for it will expand from mere shape and function to include topics such as behavior and interaction. ”

Stefan Ulrich, Designer

1.1 Introduction

The technology of adaptive or intelligent structures has encountered a tremendous development in these years and significant potential applications for the space sector were considered first from a theoretical and numerical viewpoint, then on an experimental basis up to on-orbit experiments.

The development of basic studies was increasingly steadily in the last years of the eighties and the first half of the nineties. A classification of smart materials was performed in 1990 and the first assessment study appeared on 1994. A second assessment concerning space applications occurred in 1997. Meanwhile the first on orbit experiment of vibration control were performed first on the Hubble telescope (Fanson and Ealey), then on the Space Technology Research Vehicle (Glaser et al) and then on board the shuttle (Mace experiment, see Miller et al) and the MIR station (Castor, see Bousquet et al). A serie of conferences devoted to the area started in

1990 and have reached now a considerable importance. At the same time the journal of intelligent material systems and structures and the journal of smart structures were founded. In this tremendous effort of research worldwide the leadership was basically under the control of American and Japanese research centres and agencies with Europe recovering the delay starting with the program ARES 1989-1993 (adaptive structural systems) funded by the German state Lower Sachsony with 3 Million €, with the conference ICAST 1993 in Cologne, with an important research national program promoted Germany on “Adaptronics” ("Leitprojekt Adaptronik" involving 26 partners and 25 Million € funding by the federal ministry on education and research) and significant contribution coming from several research centres in France, Belgium and Italy. The focus of this first decade of research in the area was concentrated on piezoelectric materials and especially PZT ceramics, only recently oriented to the development of piezo fibres, and vibration control studies especially in the area of micropositioning and microvibrations control of stiff thin walled aerospace structures. More recently the use of shape memory alloys materials gained interest, especially for the development of thin film technology (see Shin et al) and the possibility of have magnetic films as possible stimula for the development of actuators. Also the techniques for integration of piezoceramics in the frame of composite structures was developed first at basic level and then at the level of space component. In this recent effort towards the recovery of European positions in this area the European Space Agency was keen in funding research projects that allowed companies to develop their internal know how and verify the manufacturing techniques and the control capability of fully integrated smart materials at least at the level of very preliminary space components. Fundamental result of this phase was the incorporation of control techniques in the frame of design and construction of smart structures. This was important both from the viewpoint of control algorithms, developed on purpose for continuous actuators and sensors (not discrete ones as usual for controlled structures) with the opportunity of shaping the geometry of the actuator/sensor for purpose of filtering signals and better adapt to the dynamics of the structure under concern. The result is that everybody considers nowadays the smart structure technology as a multidisciplinary discipline. As a consequence, the engineering for developing such devices needs to embody a fully interdisciplinary and multidisciplinary approach.

The active/adaptive/functional structure systems consist normally of the smart materials (sensor and actuator, from level 1 to 3 and a very futuristic one which we call “level 4”), the structure itself, the control electronics and the power source. Important is that several combinations are possible (Figure 1): a) structure with attached sensors, attached separate actuators, connected with external control electronics and the power; b) smart material which acts both as sensor and actuator attached at a structure and connected with external control electronics and the power; c) smart material which acts as sensor, actuator and structure, connected with external control electronics and the power; d) smart material which acts as sensor, actuator and structure with integrated control electronics and power generator; might be feasible in the far future.

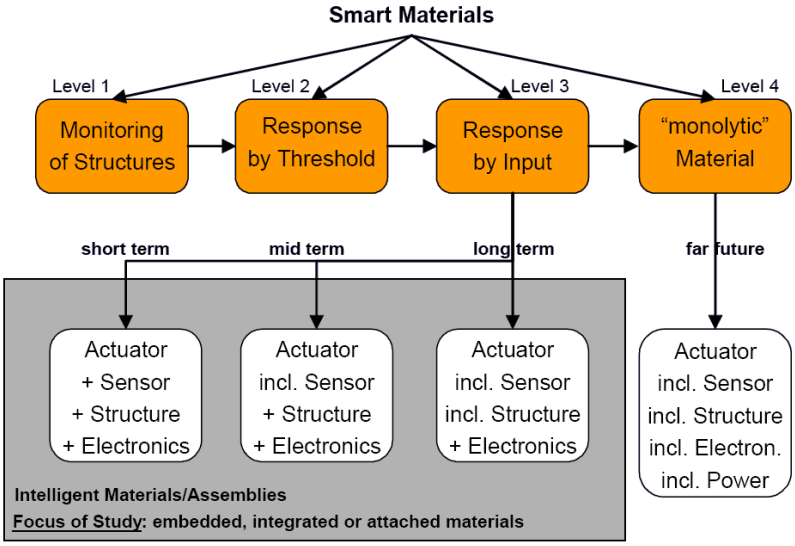

Figure 1. Different Levels of Smart Materials and their complexity.

The development of third-level smart materials aims at addressing the functional and operational requirements of the large flexible space structures that could be conceived for addressing the need of future space missions. In fact one major point to be considered is the development of large membrane structure, deployed along rigid booms (also to be deployed or steered) or inflated by means of some fluid pressure. These structures could also thought as to be rigidized in

a subsequent phase of construction before they could be operated. Inflatable structures were recently considered by the agency in several applications for both manned and unmanned missions and with different objectives, as reported in the roadmap document for technology harmonization. In fact attempts were made to study the possible inclusion of active materials in inflatable membrane structures. The same is true for deployable booms that are the necessary counterpart, in most if not in every case an inflatable structure is considered for space application. Moreover deployable booms are the natural support for membrane structures that are not inflated, such as solar sails. For very different reasons that range from telecom requirements, related to the power of transmission, to the realization of new transportation systems both manned and unmanned for new and long time missions (e.g. Mars missions), large structures cannot be constructed on Earth and need in orbit construction. Inflatable structure offer a very promising opportunity for realizing large structures by keeping mass and volume very low, offering a very good storage capability in the room available on board the space transportation systems. Unfortunately membrane structures encounter instability phenomena that could seriously endanger the mission, as demonstrated by a NASA flight experiment, where the dynamics of the structure was completely out of control. The use of fully integrated intelligent materials could also give a contribution towards an increased level of safety on board being the intelligent material a fundamental basic element of the health management system of the space vehicle of tomorrow. In fact the monitoring and, if needed actuation capability of the material (including in some cases the self repair capability) could be used for detecting incipient or present damage letting the mission control decide the proper decision to be taken. In this view, the “third level” smart material, being a system itself capable of interact with the rest of the vehicle with a continuous flux of information and energy, is fully integrable in the system view of the spacecraft and, due to the interdisciplinary and multidisciplinary characteristics of its behaviour is perfectly addressable to the overall need of the spacecraft mission.

The electro active polymers are one of the most promising technologies for the future.

EAP offers a possible answer to the stringent requirements posed by the new generation of large, flexible, inflatable structures for space. In fact, as already mentioned, the low weight and the possibility of being produced in thin films make these materials particularly suitable for the introduction of the membrane space structure of the future missions.

This thesis is addressed to the analysis and modelling of a category of this wide class of intelligent materials enabling design and manufacturing of large structures, dynamically controlled, to be used in space.

1.2 Structure of the thesis

The work developed and documented with this thesis is subdivided following two different approaches. The first one is a modellistic approach, where a new numerical procedure is developed in order to simulate the behaviour of a class of electroactive polymers. The second is an approach from a designing point of view, where new engineering solution are introduced with the aim of apply these new material in a space framework.

An introduction on the different classes of electroactive polymers and a more detailed one on the specific class of the dielectric elastomers, are edited in the firsts chapters. Such materials are the result of an innovative technology, whose readiness level is the research, and it found proper to describe it at the beginning of this thesis.

In the third chapter the working principle of the dielectric elastomer actuators, their sensing capabilities and typical configuration devices are explained. The mathematical models used in the following chapters to build a numerical procedure to simulate the behaviour of these materials are put in evidence.

In the forth chapter the work sustained for the implementation of a new numerical procedure, thorough the finite element method, to model the electromechanical behaviour of the materials with dielectric elastomer is described. Both the constitutive relations of the mechanical and electrical part of the material show the behaviour with strongly non-linear nature. The first one follows the typical behaviour of the hyperelastic materials and for this reason it is studied and modelled through the introduction of an energetic functional for the elastic deformation based on

the theoretical model of Mooney-Rivlin. The electrical part, to be more precise the relation that states the electromechanical coupling, is based on the Maxwell law. It links the mechanical stress to a component that depends quadratically from the electric field.

The goodness of the numerical procedure is validated in the fifth chapter, where a dielectric elastomer actuator, multilayer type, developed from Risø Danish National Laboratory, a research centre with strong competences in the field of the electroactive polymers, is modelled. In particular at this scope a model, totally new, to reproduce the behaviour of its electrodes (smart metallic compliant electrodes) with a non-linear orthotropic scheme is developed.

A phase of designing approach, through the engineering of such kind of actuator follows. A series of numerical parametric analyses focused to the coupling the actuator with a generic hosting structure, monitoring i.e. the performances of the actuator counteract the stiffness of the hosting structure itself is performed. These analyses are used as backgroung for designing and development of a technological demonstrator for space, optimized in relation with the performances of the actuator.

In the sixth chapter a different kind of polymeric electroactive sensor/actuator, based on a buckling functioning scheme, produced and developed from Centro Piaggio of the University of Pisa, other centre of excellence on research and development of electroactive polymers, is modelled. The choice to model such kind of actuator is motivated for its strong three-dimensionality, in order to validate the numerical procedure also for non-planar deformations.

In the last chapter the development of the demonstrator, such as an active boom, is reported. During this phase a new engineering solution to control the vibration of such kind of structure, based on the morphing of his cross-section and then acting on the inertia moment terms is proposed. This kind of control allows to vary at local level the stiffness of this pipe structure through four sensor/actuators positioned internally. With the aim of develop an adequate control law, a multibody numerical model with flexible elements is built. The finite element model of the boom is associated with the multibody model equipped with sensors and actuators and controlled with a loop implemented in Matlab-Simulink environment. The designing development of this technological demonstrator is then completed with the study of a control algorithm. Moreover the fine-tuning and testing phases I assisted to perform is described.

2

The electro active polymers (EAP)

2.1 EAP Actuators

Despite the advanced state of thermochemical, electromagnetic and pneumatic conventional motor technologies, there is a growing demand in fields such as mechatronics, robotics and bioengineering for polymer actuators with high power-to-weight ratio, high efficiency and large degree of compliance. These devices would provide a major advance in several applications, involving critical and delicate tasks; in particular, such kind of actuators could be advantageously used as "*artificial muscles"*. Aimed at the satisfaction of these and similar needs, in recent years new types of actuators have been proposed. They are based on polymer materials able to change dimensions and/or shapes in response to a specific external stimulus (thermal, chemical, electrical, magnetic, electro-chemical, electro-magnetic, optical). The so-called Electro Active Polymers (EAP) [2] represents a relevant class of such materials. These polymers exhibit interesting properties, such as sizable active strains and/or stresses in response to an electrical stimulus, low specific gravity, high grade of processability and down-scalability and, in most cases, low costs. EAP actuators can be classified in two major categories: ionic (also called "wet" because they often use aqueous component materials) and electric (also called "dry"). The first class comprises polyelectrolyte gels, ionic polymers, conducting polymers, and carbon nanotube actuators. They owe their movement to mass transport processes where ions and solvent molecules are being redistributed. Only low voltages (1-5 V) are needed to activate these materials. In contrast, dielectric elastomer actuators and electrostrictive polymers are driven applying a strong electric field. High voltages (1-5 kV) are needed to activate this class. A new

class of actuators based on liquid crystalline elastomers are driven by thermally induced phase changes. The energy can be supplied through Joule heating in the same way as shape memory alloys work. Table 1 summarises EAP classes and materials and their common abbreviation.

Class	Material	Abbriviation
Ionic	Polyelectrolyte gels	
Ionic	Ionic polymer-metal composite	IPMC
Ionic	Conjugated polymer	CP
Ionic	Carbon Nanotubes	CNT
Electric	Electrostrictive polymers	
Electric	Dielectric elastomer actuator	DE
Other	Liquid crystalline elastomer	LCE

Table 1. Common EAP materials

Electroactive polymers are well suited to provide intermittent displacement and adaptable stiffness on length scales from micrometer to meters. Of prime considerations for space application are flexibility and structural integration; combination of sensing and actuation; stability, reliability and durability; and environmental compliance. In the following sections, we summarize performance characteristics for EAP actuators, modes of sensing and a detailed description for each for EAP material.

2.1.1 Performance characteristics

Performance parameters for EAP actuators include stress, strain, strain rate, work density (and power density), efficiency (including electromechanical coupling efficiency), and cycle life. Each type of EAP has different characteristics and often peak performance for each parameter in optimal test set-up is reported but true working performance of actuators is substantially lower. The behaviour of the materials comprising the actuators is strongly conditioned by the environmental stability. Thermal and vacuum behaviour of physical properties as well as radiation stability are key parameters. For most EAP technologies, environment is likely to affect

performance in a strong manner: performance parameters (under ambient conditions) are quite unaffected by temperatures and pressures in a specific range. Outside of this range, the EAP will not function at all. The Figure 2 illustrates our present understanding of thermal and vacuum stability of EAP. A valuable source has been [3]. We have also indicated a level of maturity (1-10). Ten corresponds to actuators demonstrated to work in an application. One corresponds to a principle just realised. Colour code indicates working pressure range. Black: vacuum compliant. Light: ambient pressure only. Fading colour indicates that performance degrade at the ends of the temperature range. One must keep in mind that no EAP technology is mature, but the best-developed actuators have been demonstrated to work in some kind of lab-scale application.

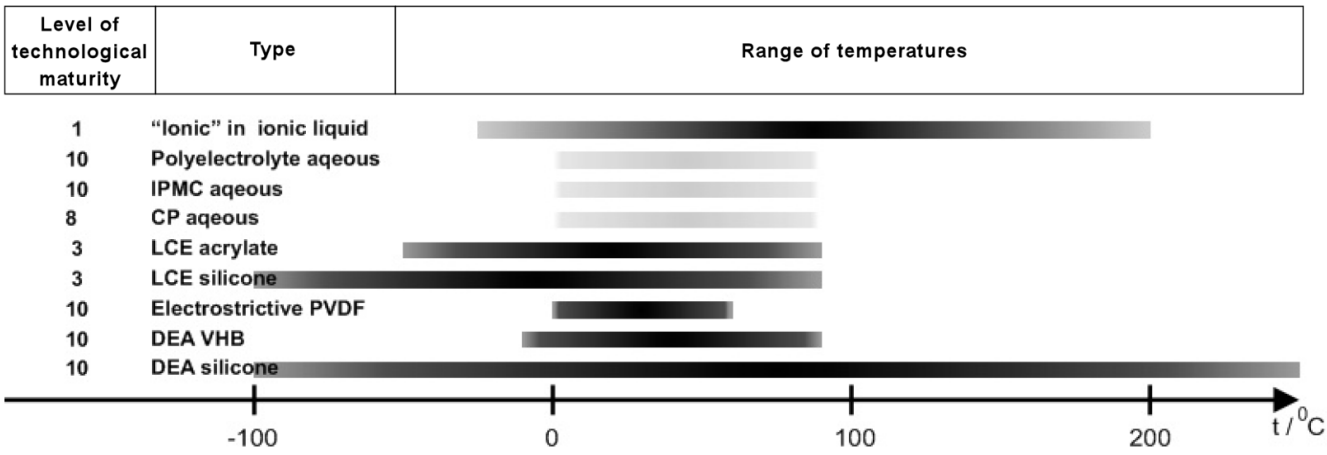

Figure 2. Environmental compliance of EAP actuators and level of maturity.

In general, from Figure 2 it is possible to observe that dielectric elastomer actuators (DEA) show best environmental compliance with a range of temperature of more than 300°C and a high level of technological maturity. Anyway recently, a number of so-called ionic liquids with low vapour pressure have been used for developing both conjugated polymer actuators and ionic polymer-metal composites. Such new solvents may extend the temperature range of ionic actuators considerably below zero degrees Celsius and into vacuum conditions. However it is believed that ionic liquids with lower melting points also lower the EAP performances due to their more bulky chemical structure, but no studies address this issue. Ionic liquid are addressed in the detailed

description of EAP materials. Electronic EAPs show, with respect to ionic EAPs, lower response times and higher efficiency, stability, reliability and durability. Peak performances for stress and strain are however more equally distributed. The data in Table 2 [4] attempts to identify the fundamental material performances of each technology. Note that the tests for each technology were conducted under different conditions, so precise quantitative comparisons are difficult. Practical devices, based on these materials, often achieve a small fraction of their maximum material performance. The materials can be used in very different ways that trade off between stress and strain (e.g., a material that is integrated into a bending beam configuration has a high displacement at the expense of force). Wax and Sands [5] and Bar-Cohen [1], also discuss the comparisons between EAPs and other technologies.

Actuator Type (specific example)	**Maximum Strain (%)**	**Maximum Pressure (MPa)**	**Specific Elastic Energy Density (J/g)**	**Maximum Efficiency (%)**	**Relative Speed (full cycle)**
Dielectric Elastomer					
(Acrylic)	380	7.2	3.4	60–80	Medium
(Silicone)	63	3.0	0.75	90	Fast
Electrostrictive Polymer (P(VDF-TrFE)	4.3	43	0.49	~80 est.	Fast
Carbon Nanotube	> 2.5	> 1.0	> 0.013	< 10?	Medium
Liquid Crystal Elastomer	> 35	> 0.3	> 0.10	< 10?	Slow
Responsive Gels (Polyelectrolyte)	> 40	0.3	0.06	30	Slow
IPMC (Nafion)	10	1.0	0.025	< 10?	Medium
Conducting Polymer (Polypyrrole)	15	20	3	< 10?	Slow
Natural Muscle					
Peaks in nature	100	0.80	0.04	-	Slow-Fast
Human Skeletal	> 40	0.35	0.07	-	Medium

Table 2. Comparison between EAPs and natural muscle.

2.1.2 Previous space studies

Few studies on space-related applications of EAPs have been performed so far. At JPL (Jet Propulsion Laboratory, U.S.A.) Bar-Cohen reported on the so-called “planetary dust wiper” (Figure 3) [1][2]. The figure describes a rover and the front lens of a camera placed on it. The

lens is provided of a wipe, made with ionic polymer-metal composite, that bends periodically under a sine driving voltage to the electrodes. The advantage of this solution is to not be damaged by the dust like for kinematic mechanisms.

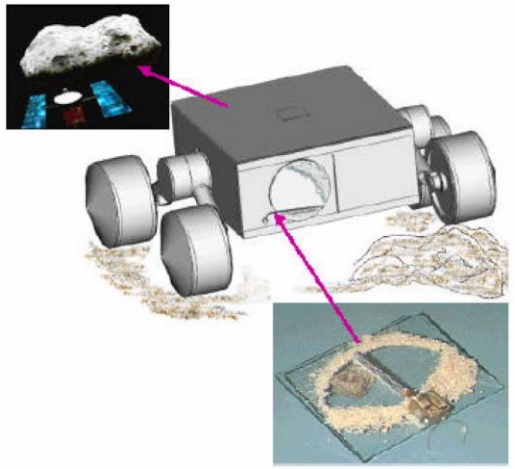

Figure 3. Schematic view of the EAP dustwiper on the MUSES-CN's Nanorover and a photograph of a prototype EAP dust-wiper.

Interestingly, he reported that Joule heating of the actuator allowed it to function down to –100 deg. C. This is an encouraging result for all the "wet" technologies. He also reported that a protective coating is feasible and a sample maintained functionality after storage at ambient conditions for four month. Steven Dubowsky and co-workers at MIT performed a study [6] under a grant from NASA Institute of Advanced Concepts. A lightweight hyper-redundant manipulator based on dielectric elastomer actuators was developed during the project, and a prototype, Binary Robotic Articulated Intelligent Device (BRAID), was successfully tested. Dielectric elastomer actuators have been studied by SRI (Stanford Research Institute) for shape control of lightweight space mirrors [7]. Considered solutions employ laminated or inflatable reflective structures with integrated actuation elements or segmented rigid mirrors driven by external linear actuators [7]. Moreover, this study has proven that a certain silicone rubber (NuSil CV 2287) can withstand an exceptionally broad temperature range with minor degradation of electromechanical actuation performances. In particular, silicone based dielectric elastomer actuators have been successfully tested between -100 and 200 °C [7]. Such an interval would guarantee a quite large operative range for space applications. The use of EAP is of direct relevance for applications like the

Dynamically Responsive Intervention for Tremor Suppression (DRIFTS). In the DRIFTS project, the use of EAP (conjugated polymers) as materials with adaptive stiffness is suggested [8].

2.2 EAP Sensors

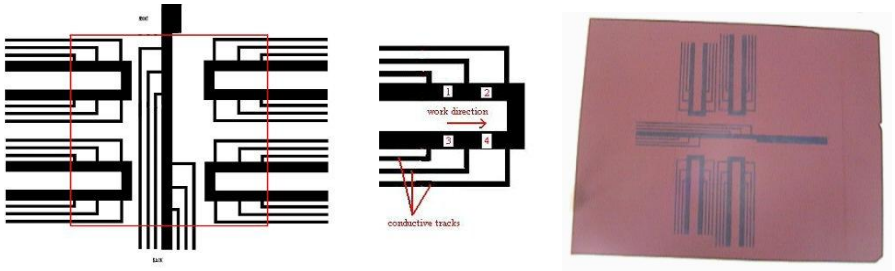

Figure 4. Distributed sensor network.

In order to use electroactive polymers for strain/stress sensing tasks, two different strategies can be adopted:

Lumped sensing:

We define “lumped sensing” the detection of strains and stresses performed by single devices located in specific positions on or into a structure under monitoring. Materials able to show an active response or a passive response can perform such kind of sensing. For instance, using EAP materials capable to generate an electrical signal under a mechanical stimulus can develop active lumped sensing. Differently, *passive lumped sensing* can be performed by EAP based devices presenting a stress- or strain-induced variation of a definite electrical parameter, such as resistance (piezoresistive sensors) or capacitance (piezocapacitive sensors). EAP materials showing active sensing includes IPMCs and piezoelectric polymers. The latter group consists of PolyVinyliDene Fluoride (PVDF) and copolymers and show relatively small strains as actuators. They belong naturally to the group of piezoelectric materials rather than to EAP. IPMC develop a potential difference, in the order of millivolt, when bended. EAP materials showing passive sensing includes conjugated polymers (CP), dielectric elastomer actuators (DEA) and

electrostrictive polymers. CPs are piezoresistive. Both DEA and electrostrictive polymers work as piezocapacitive sensors. In general, for localized sensing of small strains, most suitable sensors are based on piezoelectric materials, whereas for large strains monitoring piezoresistive and piezocapacitive transducers are very performing.

Distributed sensing:

In order to sensorise a large flexible surface for strain/stress distributed monitoring, it is necessary to use a distributed sensor network, which behaves as a "smart skin". In general, a distributed sensor network is defined as a collection of many independent sensing nodes, each one providing modest processing and neighbour-to-neighbour communication capabilities. In literature, several works have mainly focused on silicon based sensors that use piezoresistive effect (i.e. variation of an electrical resistance in response to an external mechanical strain) [9][10] or piezocapacitive effect (i.e. variation of an electrical capacitance in response to an external mechanical strain) [11][12] and polymer-based approaches that use piezoelectric effect (i.e. variation of a polarisation in response to an external mechanical strain) [13][14]. Other works have combined some properties of silicon with polymer-based devices, such as embedding silicon-sensing elements in polymer skins [15][16] or covering silicon-based devices in a protective polymer layer [11][12]. Other sensor arrays are based on polymer micromachining and thin-film metal piezoresistors. More recently, work has been directed towards combining multiple sensing modes, such as contact force and hardness, or normal and shear forces [11][17].

Recently, distributed sensing is investigated with several architectures and new materials used as support for sensors. In particular, fabric substrates are appealing: they are elastic and extendable [18] and supported by a well-known technology. A novel technology consisting in functionalizing fabrics for sensing is emerging. This new approach allows the transduction of pressure and/or strain exerted over a broad piece of fabric by means of piezoresitive or capacitive or piezoelectric sensing.

Here we will focus on flexible sensory "smart skins" based on stand-alone thin polymeric films (active polymeric films) or on sensorised fabrics (functionalisation of substrates).

1. Active polymeric films

Flexible sensors typically consist of thin polymer film realized by microfabrication processes, containing two-dimensional arrays of sensors. The working principle is usually piezoelectric. The variation of polarisation charge is used to transduce strain distribution. Nevertheless, piezoelectric technology is affected by several disadvantages. Mainly, piezoelectric materials are suitable to measure dynamic events only, since they are not able to measure a continuous static event. Furthermore, electronics used to read outputs from piezoelectric sensors is rather more complicated than the one for different types of sensors, such as piezoresistive transducers (described below).

2. Sensorised fabrics

Piezoresistive sensors are the base of the functionalisation of substrates (flexible surfaces). A substrate can be functionalised for sensing by means of several methodologies. Inkjet printing is one of them. In the last few years it has been used as a free-form fabrication method for building three-dimensional components and is being explored as a tool for printing electrical and optical devices, especially where they are made of organic components. This technique can be used for the deposition on substrates of polymeric conducting films, working as piezoresistive sensors. Another way to functionalise a substrate consists in using fabric sensors. In this case the flexible surface can be covered by a sensorized textile structure.

2.3 EAP materials

2.3.1 Polyelectrolyte gels

Polyelectrolyte gels [19][20][21] consist of elastic cross-linked polymer networks having interstitial spaces filled with fluids. The network holds the liquid and gives to the gel its typical compactness. Gels are wet and soft and look like a solid polymer material, but are capable of undergoing large deformations. Polymer gels can be easily deformed by external stimuli, and generate force or execute work externally. If such responses can be translated from the

microscopic level to a macroscopic scale, a conversion of chemical free energy into mechanical work is realized.

Same effects can be obtained causing a pH variation by electrochemical reaction. In other polymer gels the dilatation is obtained using a thermal control or changing the type of solvent in which the polymer is immersed. These transformations are denoted as “mechanochemical reactions”. Those energy conversion systems were considered to have great potential as artificial muscle models. After a pause of more than three decades, research in this field is now becoming active and attempts as a practical utilization such as for actuators [22].

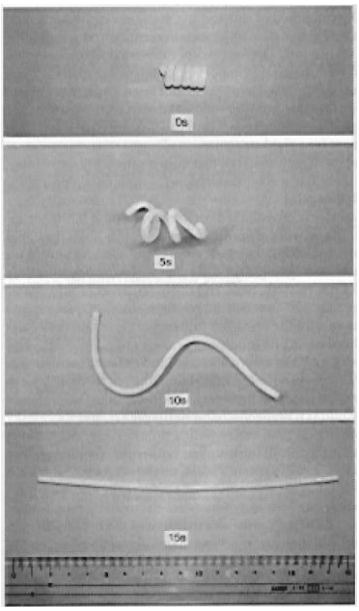

Figure 5. Shape memory gel subjected to winding between 50°C and room temperature

For example gels can be used to construct a thermo-responsive diaphragm capable of automatically opening and closing a valve. The system is based on two specific properties of the polymer gels. One is the hard plastic nature below glass transition temperature and the other is that of the rubber-like soft elastomer with shape memory function. I.e. in Figure 5 it is shown a sequence of morphing of a wire made of shape memory gel, from a coiled shape to a straight one and vice versa, when subjected to winding between 50°C and room temperature [23].

If a water-swollen cross-linked polyelectrolyte gel is inserted between a pair of planar electrodes and a DC voltage is applied, it undergoes anisotropic contraction and concomitant fluid exudation.

The electrically induced contraction of the gel is caused by a transport of hydrated ions and water in the network (electrokinetic phenomena). When an outer electrical field is applied across the gel, both the macro- and the microions are subject to electrical forces in opposite direction. However, the macroions are a stationary phase, since they are chemically fixed to the polymer network, while the counter ions are mobile, capable of migrating along the electric field and dragging water molecules with them.

By using this phenomenon, several active devices can be realized:

- an electrically activated valve membrane, which reversibly expands and contracts its pore size in response to an electrical stimulus and
- a gel-looper: causing a pH variation by electrolysis between the two faces of a gel strip, it is possible to induce a different dilatation along the thickness of the material.

2.3.2 Ion-polymer metal composites

Ion-polymer metal composites (IPMCs) used as actuators show large deformations in presence of low applied voltages and exhibit low electrical and mechanical impedance. They operate best in a humid environment and can be made as encapsulated actuators to operate in dry conditions. These materials have many ionizable groups in their molecular chain. These ionizable groups can be dissociated in various solvents, showing a resulting net charge, which is compensated by the presence of counterions. The net charges of the network of the material macromolecules are called polyions and they develop an electric field of the order of 1010 V/m [24]. The essence of the electromechanochemical deformations shown by IPMCs is represented by their susceptibility to interact with externally applied fields. If the interstitial space of the network is filled with a liquid containing ions, electrophoretic migration (due to an imposed electric field) of these ions inside the structure can cause the macromolecular network to be deformed accordingly [25].

Having an ionic microscopic structure, IPMCs show the ability to shift ions of the same polarity within itself, when they are placed in an electric field, resulting in a ionic attraction or repulsion between the fixed charges of opposite polarity contained in the side groups within the polymer molecular chain. This leads to local collapse or expansion of the polymer membrane. This produces a stress gradient on opposites sided of the membranes, causing it to bend. The Figure 6 shows the IPMC principle of operation. Cations and solvent migrate towards the cathode (fig a), resulting in a bending towards the anode side (fig b). The bending occurs during changes in potential. An AC field, can be used to cause the membrane to bend from site to site with up to 50 Hz.

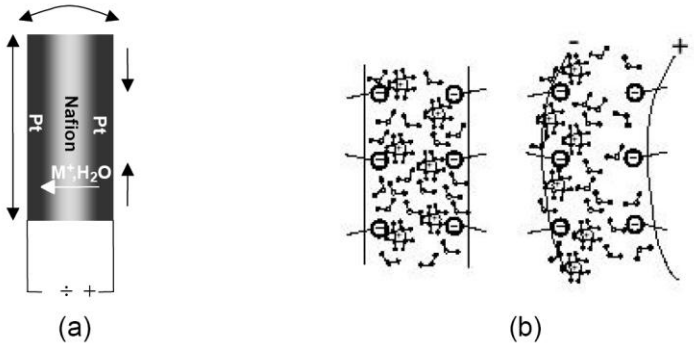

Figure 6. IPMC principle of operation.

The structure and the properties of IPMCs have been subjected to numerous investigations [25][26][27]. The detailed mechanism of is extremely complicated but rather well understood [28]. Several applications have been investigated. Swimming robots structures, cilia assembly-type robotic systems have been constructed for collective vibrational dynamics. Wing flapping flying machines and heart-assist devices have been proposed, as well as multi-finger gripper end effector for a miniature low mass robotic arm (Figure 7).

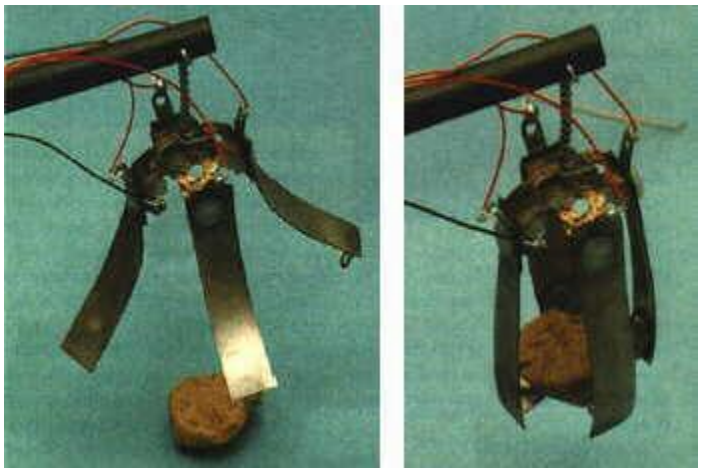

Figure 7. Multi-finger gripper

IPMCs develop mV potential differences when bended [25]. They show a transient response only; hence static bends does not leave static potential differences and static applied potentials do not result in static bending.

2.3.3 Conjugated polymers

Conjugated polymers (CPs) have been studied as materials for polymer actuation for many years [29]-[42]. Conjugated polymers are characterised by a chemical structure, where π-conjugation extends throughout the polymer. They can continuously be oxidised and reduced and show electronic conductance in either the oxidised or reduced form. For that reason, they are also termed “conducting polymers” (CPs). For actuation purposes they are used as one component of an electrochemical cell, whose base structure includes two electrodes immersed in an electrolyte. In particular, the active conducting polymer material constitutes one of the two electrodes of the cell. By applying a potential difference between the electrodes, the one made of conducting polymer shows a dimensional variation and works as an actuator. The observed deformation is due to the diffusion of ions into/from the polymer sample. The applied voltage produces a variation of the polymer oxidation state, which causes an exchange of ions between the conjugated polymer and the surrounding electrolyte medium in order to maintain the global

electroneutrality. The resulting intercalation (or de-intercalation) of doping ions and solvent molecules causes structural and dimensional changes of the material [38]-[43], with a strongly anisotropic volume variation [44]. Figure 8 illustrates the principle. A composite structure results when pyrrole is electropolymerised in the presence of a bulky anion like sodium dodecylbenzenesulphonate (DBS). In the as-prepared (oxidized) form, the polypyrrole is positively charged and electronically conducting. The charges are balanced by DBS counter ions. When the material is reduced, PPy chains are neutralised, and cations and solvent molecules are dragged into the structure in order to compensate the charges of the DBS. In other words: an electrically activated swelling of the material results.

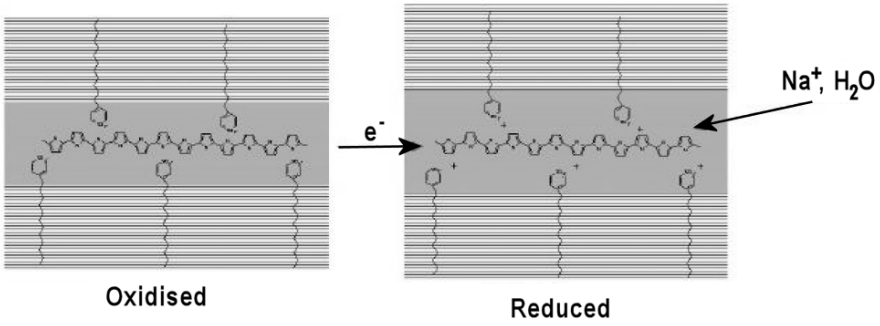

Figure 8. Principle of operation of a polypyrrole (PPy) actuator.

Conducting polymer actuators typically exhibit active strains of the order of 1-10%, high active stresses (up to tens of MPa), and low driving electrical potential differences (order of 1 V). Conducting polymer actuators are frequently implemented in bending mode. However, in direct linear contraction they may produce significant forces. Some research groups are using conducting polymers in this direct mode with reported forces in excess of 1 N and strains approaching 10% [46]. For that reason, a number of groups are investigating the fiber fabrication of conducting polymers, in order to use them as linear actuators. At the end of the nineties, the Research Centre "E. Piaggio" (Italy) has proposed an extruded polyaniline fibre coated with a thin layer of solid polymer electrolyte, whereas a further layer of polypyrrole acts as counter-electrode (Figure 9).

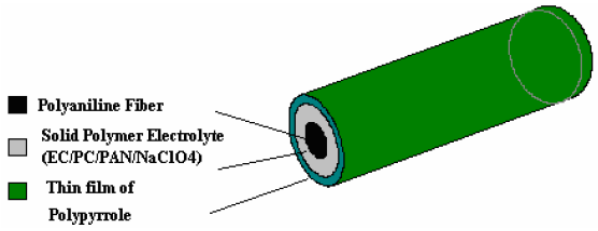

Figure 9. Conducting polymer fiber actuator

Alternatively, the counter-electrode can consist of a metal wire twisted around the fibre (Figure 10). Actuators with such a fibre-like structure have shown strains of about 0.3% and active stresses of about 3 MPa, for driving voltages lower than 1 V.

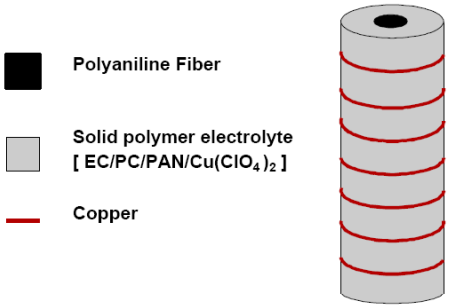

Figure 10. Dry linear actuator based on conducting polymer

2.3.4 Carbon nanotubes

Carbon nanotubes (CNTs) are one of the most recent entry to the class of electroactive materials. Carbon nanotubes have lengths about 1000 times higher than their widths (typical diameters are about 10 Angstrom, while typical lengths about 1 micrometer) and they are usually combined in bundles having diameters of the order of 100 Angstrom. Carbon nanotubes can be divided in two classes: single-wall nanotubes (SWNT) and multi-wall nanotubes (MWNT). A single-wall CNT consists of a single film of graphite rolled to make a tube, whereas a multi-wall CNT is made of several films rolled together.

Unlike conducting polymers, which can act as electrodes in battery-like systems, CNTs can be used as electrodes in electrochemical supercapacitors, owing to the double layer of charge which

originates at a CNT/solution interface. By changing the applied voltage in such a system, an electronic charge is stored in the CNT electrode and is compensated by ions at the CNT/solution interface (Figure 11). As a result of the capacitive effect, the stored charge is proportional to the capacitance of the carbon nanotube/solution interface and the applied potential.

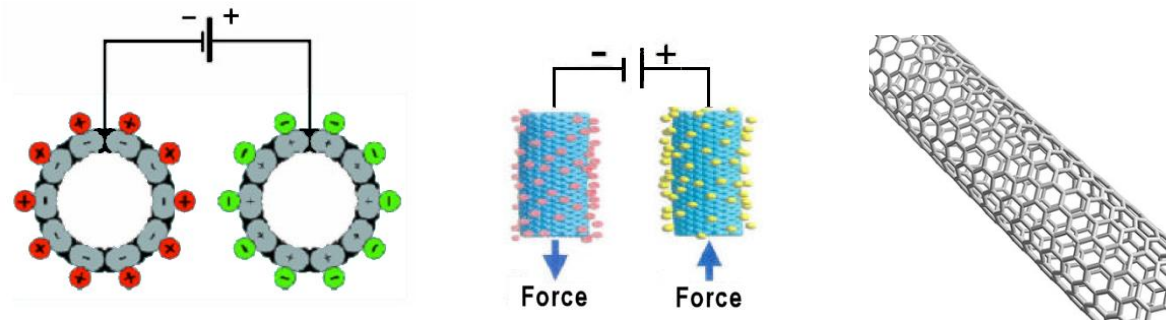

Figure 11. Schematic drawing and principle of operation of a carbon nanotube actuator.

Such a double-layer charge injection, permitted by the very high surface-area of CNT electrodes, is the basis of the principle of operation of a carbon nanotube based actuator (Figure 11). In fact, the electrically induced charge-injection is able to produce dimensional changes of the material, originating from quantum chemical and double-layer electrostatic effects [49].

Typical actuators based on carbon nanotubes consists of single walled nanotubes arranged in felt strips, used as working electrode in an electrochemical cell, so that to implement bending devices (Figure 12). By operating these actuators in 1 M NaCl at low voltages, early investigations showed active strains of fractions of % [49].

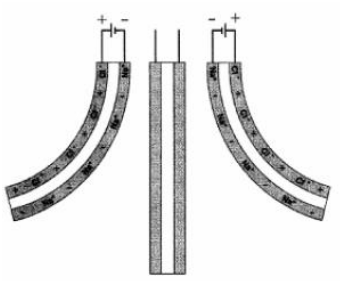

Figure 12. Bending carbon nanotube actuator.

CNTs have been used to realize micro-benders for clamps. By embedding CNTs in a gel matrix (obtained adding CNT in DMA in a mixture of PVA-PAA), a multilayer unimorph micro-bender was realized [50].

2.3.5 Electrostrictive polymers

Electrostriction is one of the main electro-mechanical coupling phenomenon shown by dielectric materials. It consists of a quadratic dependence of the strain and stress on the material polarization, due to an applied electric field. For materials showing a linear relation between polarization and applied electric field (E), the electrostrictive strain (or stress) depends on the square of E: $Strain = QE^2$

Although any dielectric polymer can be electrostrictive in principle, this property is commonly attributed only to those polymers manifesting markedly this effect. In fact, most of polymers present a relatively low degree of electrostriction, mainly due to the low value of their dielectric permittivity.

Polymer electrostriction has been largely studied in ferroelectric polymers, showing spontaneous polarization, which can be inverted by an applied electric field. Mechanism of actuation consists of deformations of polymer networks induced by electrically-driven dipole orientation.

Ferroelectric polymers have an elastic modulus of the order of 1÷10 GPa. By applying an ac high electric field (order of 100 V/μm), strains of the order of 1% can be obtained; hysteresis effects can occur within the operative range.

Actuators realized with electrostrictive ferroelectric EAPs can be operated in air, water or vacuum and in a wide range of temperature. Since these polymers are piezoelectric too, they can be used as both actuators or sensors. In fact, a stress applied to the material induces electrical charges on the material surfaces, generating a useful voltage signal.

2.3.6 Ferroelectric liquid crystalline elastomers

Liquid crystalline elastomers (LCEs) are crosslinked side chain liquid crystalline polymers. The mesogenic units can be ordered nematically and undergo a phase transition to a disordered phase at a temperature considerably higher than the glass transition temperature of the polymer. Ratna and co-workers have demonstrated acrylate-based elastomers that show thermoelastic contraction responses with strain changes, through the nematic-isotropic phase transition, of 30-45% [51]. The Figure 13 shows the thermoelastic response of liquid crystalline elastomer for different stiffness. The strains follow hysteretic cycles around the transition temperature.

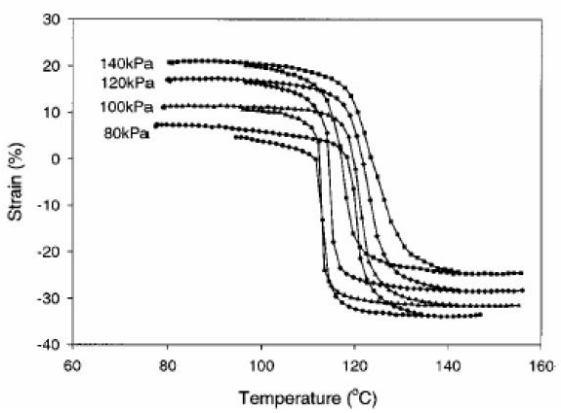

Figure 13. Thermoelastic response of a liquid crystalline elastomer.

Although the phase transition is thermally driven, composites with electric conductivity have been described by Shahinpoor [52]. These materials can be electrically stimulated in the same way as shape memory alloys. Moreover, liquid crystalline elastomers can be electrically stimulated even by the application of an electric field, responsible on an electroclinic effect (Figure 14) [53].

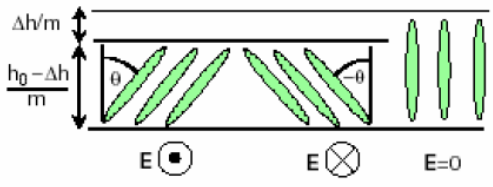

Figure 14. Electroclinic effect in a liquid crystal elastomer film

Despite the interesting electromechanical performances recently reported (4% lateral strain at 1.5 V/μm) [53], currently they do not have any practical use for macroscopic applications.

2.3.7 Dielectric Elastomers

Dielectric Elastomers (DE) are incompressible dielectrics which can experience deviatoric (isochoric) finite deformations in response to applied large electric fields. Thanks to the strong electro-mechanical coupling, DE intrinsically offer great potentialities for conceiving novel solid-state mechatronic devices, in particular linear actuators, which are more integrated, lightweight, economic, silent, resilient and disposable than equivalent devices based on traditional technologies. For actuation usage, DE are typically shaped in thin films coated with compliant electrodes on both sides and piled one on the other to form a multilayered DE. Pelrine, Kornbluh and others at SRI International pioneered the use of dielectric elastomers as actuators beginning in the early 1990s. This kind of material is object of this thesis and will be described with more accuracy in the next chapter.

2.4 References

[1] Bar-Cohen Y., Leary S., Shahinpoor M., Harrison J.O. and J. Smith J. - Electro-Active Polymer (EAP) actuators for planetary applications - In Y. Bar-Cohen (Ed), *Smart Structures and Materials 1999: Electroactive Polymer Actuators and Devices*, Proceedings of SPIE, 3669 (1999) 57-63.

[2] Bar-Cohen Y., Leary S., Yavrouian A., Oguro K., Tadokova S., Harrison J., SmithJ. and Su J. - *Challenges to the transition of IPMC artificial muscle actuators to practical application* - MRS Symposium Proceedings (1999).

[3] Madden J.D.W., Vandesteeg N.A., Anquetil P.A., Madden P.G.A., Takshi A., Pytel R.Z., Lafontaine S.R., Wieringa P.A. and Hunter I.W. *Artificial muscle technology: physical*

principles and naval prospects. IEEE J. Ocean. Eng. (USA), Volume 29, Number 3, p.706-28 (2004)

[4] Pelrine R. and Kornbluh R., SRI International, 1999

[5] Wax S.G., Sands R.R. *Electroactive polymer actuators and devices*. Proc. SPIE Vol. 3669, p. 2-10, Smart Structures and Materials 1999

[6] Wingert A., Lichter M., Dubowsky S. and Hafez M. - *Hyper-redundant robot manipulator actuated by optimized binary dielectric polymers* - In Bar-Cohen, Y. (ed.), Proceedings of SPIE Vol. 4695, p. 415-423 (2002).

[7] Kornbluh R.D. et al. - *Shape control of large lightweight mirrors with dielectric elastomer actuation* - In Y. Bar-Cohen (Ed), Smart Structures and Materials 2003: Electroactive Polymer Actuators and Devices, Proceedings of SPIE, 5051 (2003) 143-158.

[8] Manto M., Topping M., Soede M., Sanchez-Lacuesta J., Harwin W., Pons J., Williams J., Skaarup S. and Normie L. - *Dynamically Responsive Intervention for Tremor Suppression* - IEEE Engineering in Medicine and Biology Magazine 22 (3), 120-132 (2003).

[9] Kane B.J., Cutkosky M.R. and Kovacs G.T.A. *A Traction Stress Sensor Array for Use in High-Resolution Robotic Tactile Imaging*. J. of Microelectromechanical Sys., vol. 9, pp. 425-434, 2000

[10] Beebe D.J., Hsieh A.S., Denton D.D. and Radwin R.G. *A silicon force sensor for robotics and medicine*. Sensors and Actuators A 50 (1995) 55-56

[11] Gray B.L. and Fearing R.S. *A surface-micromachined microtactile sensor array*. Proceedings of IEEE International Conference on Robotics and Automation, volume 1, pages 1-6, 1996.

[12] Leineweber M., Pelz G., Schmidt M., Kappert H.and Zimmer G. *New tactile sensor chip with silicone rubber cover*. Sensors and Actuators. A, Vol.84 (2000), No.3, pp.236-245

[13] Kolesar E.S. and Dyson C.S. *Object Imaging with a Piezoelectric Robotic Tactile Sensor*. J. of Microelectromechanical Sys., vol. 4, pp. 87-96, 1995

[14] Reston R.R. and Kolesar J.E.S. *Robotic Tactile Sensor Array Fabricated from a Piezoelectric Polyvinylidene Fluoride Film*. Proc. IEEE 1990 Nat'l Aerospace and Electronics Conf. (NAECON 1990), pp. 1139-1144, May 1990

[15] Jiang F., Tai Y.C., Gupta B., Goodman R., Tung S., Huang J.B. and Ho C.M.. *Micromachined shear stress sensor array*. Proc. IEEE MEMS-96 Workshop, San Diego, 1996, pp. 110–115.

[16] Beebe D.J. and Denton D.D. *Flexible polyimide-based package for silicon sensors*. Sensors and Actuators A A44 (1994) 57–64.

[17] Cao L., Kim T.S., Mantell S.C. and Polla D.L. *Simulation and fabrication of piezoresistive membrane type MEMS strain sensors*. Sensors and Actuators 80 (2000) 273–279

[18] Lumelsky V., Shur S.M. and Wagner S. *Sensitive skin*. IEEE Sensor Journal, 1(1), June 2001, 41–51.

[19] Kuhn W. – *Experimentia* - v. 5 (1949), 318.

[20] Breitenbach J.W. and Karlinger H. - *Monatsh Chem* - v. 80 (1949), 211.

[21] Katchalsky A., Optlatka A. in Lee E.H., Copley A.L. (eds) - *Proc. 4th Intern. Cong. Rheology, part. 1* - Interscience Publishers (1965), 73.

[22] De Rossi D., Kajivira K., Osada Y., Yamauchi A. (eds) - *Polymer gels – Foundamentals and biomedical applications* - Plenum Press-New York (1990).

[23] Tanaka Y., Kagamo Y., Matsuda A. and Osada Y. – *Macromolecules* - v. 28 (1995), 2574.

[24] Alexanderowica A. and Katchalsky A. - *J. Polymer Sci*. - v. 1A (1963), 3231

[25] Shahinpoor M., Bar-Cohen Y., Simpson J.O. and Smith J. - *Ionic polymer-metal composites (IPMCs) as biomimetic sensors, actuators and artificial muscles - a review* - Smart Materials & Structures, **7**, 6 (1998) R15-R30.

[26] Oguro K., Kawami Y. and Takenaka H. - *J. Micromachine* - Soc 5, 27-30, 1992.

[27] Tadokoro S., Takamori T. and Oguro J. - *Modeling IPMC for design of actuation mechanisms* - in Osada Y, De Rossi D. (editors), Polymer sensors and Actuators, Springer, Berlin, Germany (2000).

[28] Nemat-Nasser S. - *Micromechanics of actuation of ionic polymer-metal composites* - Journal of Applied Physics, 92 (5), 2899-2915 (2002)

[29] Mazzoldi A., Della Santa A. and De Rossi D. - *Conducting polymer actuators* - in: Polymer sensors and actuators, edited by Osada Y. and De Rossi D., Springer Verlag - Heidelberg (2000).

[30] Baughman R.H. and Shacklette L.V. - *Science and Application of Conducting Polymers* - SalaneckW.R., Clark D.T. and Samuelsen E.J., ed. Adam Hilger, New York (1990).

[31] Baughman R.H. - *Makromol. Chem. Macromol Symp*. - 51, 193, 1(991)

[32] Baughman R.H. - *Conducting polymer artificial muscles* - Synth. Met., vol. 78, pp. 339-353, 1996.

[33] Spinks G.M., Liu L., Wallace G.G. and Zhou D. - *Strain response from polypyrrole actuators under load* - Advanced Functional Materials, vol. 12 (6-7), pp. 437-440, 2002.

[34] Lewis T.W, Spinks G.M., Wallace G.G., Mazzoldi A. and De Rossi D. - *Investigation of the applied potential limits for polypyrrole when employed as the active components of a two-electrode device* - Synth. Met., vol. 122, pp. 379-385, 2001.

[35] Jager E.E.H., Smela E. and Inganas O. - *Microfabricating conjugated polymer actuators* - Science, vol. 290, pp.1540-1545, 2000.

[36] De Rossi D., Della Santa A. and Mazzoldi A. - *Performance and work capacity of a polppyrrole conducting polymer linear actuator* - Synthetic Metals, vol. 90, pp. 93-100, 1997.

[37] Della Santa A., De Rossi D. and Mazzoldi A. - *Characterisation and modelling of a conducting polymer musclelike linear actuator* - Smart Material and Structures, vol. 6 (1997), pp. 23-34.

[38] Gandhi M.R., Murray P., Spinks G.M. and Wallace G.G. - *Mechanism of electromechanical actuation in polypyrrole* - Synth. Met., vol. 73, pp. 247-256, 1995.

[39] Kaneto K., Kaneko M., Min Y. and MacDiarmid A.G. - *'Artificial muscle': Electromechanical actuators using polyaniline films* - Synth. Met., vol. 71, pp. 2211-2212, 1995. 1995.

[40] Chiarelli P., De Rossi D., Della Santa A. and Mazzoldi A. - *Doping induced volume change in a π-conjugated conducting polymer* - Polymers Gels and Networks, 2 (1994), pp.289-297.

[41] Otero T.F., Angulo E., Roddguez J. and Santamaria C. - *J. Electroanal. Chem* - 341, 369 (1992)

[42] Pei Q. and Inganäs O. - *Advanced Materials* - 4, 277 (1992).

[43] Bay L., Jacobsen T., Skaarup S. and West K. - *Mechanism of Actuation in Conducting Polymers: Osmotic Expansion* - J.Phys.Chem.B 105(36) 8492-7 (2001).

[44] Smela E. and Gadegaard N. - *Advanced Materials* - vol 11 n. 11 (1999), 953.

[45] Ding J., Zhou D., Spinks G., Wallace G., Forsyth S., Forsyth M. and MacFarlane D. - *Use of Ionic Liquids as Electrolytes in Electromechanical Actuator Systems Based on Inherently Conducting Polymers* - Chemistry of Materials, Vol 15, 2003, pp. 2392 – 2398.

[46] West K., Bay L. and Skaarup S. - *Optimisation of the actuator properties of polypyrrole doped with alkyl benzene sulfonates.* - Int. workshop: "Electroactive Polymers and Biosystems: New Directions in Electroactive Polymer Materials for Biomimetic and Interactive Processes", Lucca, July 2001, p 71-74 (2002).

[47] Randdriamahazada H., Plesse C., Vidal F., Gaunthier C., Chevrot C. and Teyssie, D. - *Actuators based on Poly(3,4ethylenedioxythiophene)/PEO/elastomer IPNs* - In "Smart Structures and Materials 2004: Electroactive polymer actuators and devices (EAPAD), Ed. Y. Bar-Cohen, Proc. Of SPIE 5385, 294-301 (2004)

[48] Wu B., Reddy R.G. and Rogers R.D. - *Novel ionic liquid thermal storage for solar thermal electric power systems* - Proc. of "Solar Forum 2001, Solar Energy: The power to Choose", April 21-25, Washington DC (2001)

[49] Baughman R.H., Cui C., Zakhidov A.A., Iqbal Z., Barisci J.N., Spinks G.M., Wallace G.G., Mazzoldi A., De Rossi D., Rinzler A.G., Jaschinski O., Roth S. and Kertesz M. – *Science* - v. 284 (1999), 1340.

[50] Ahluwalia A., Baughman R., De Rossi D., Mazzoldi A., Tesconi M., Tognetti A. and Vozzi G. - Electroactive Polymer Actuators and Devices (EAPAD)-SPIE (Newport Beach, CA, March, 2001).

[51] Thomsen III D.L., Keller P., Naciri J., Pink R., Jeon H., Shenoy D. and Ratna B.R. – *Macomolecules* - 34 (2001) 5868-5875.

[52] Finkelmann H. and Shahinpoor M. - *Electrically-controllable liquid crystal elastomer-graphite composite artifical muscles* - In Y. Bar-Cohen (Ed), Smart Structures and Materials 2002: Electroactive Polymer Actuators and Devices, Proceedings of SPIE, Vol. 4695 (2002) 459-464.

[53] Lehmann W., Skupin H., Tolksdorf C., Gebhard E., Zentel R., Krüger P., Lösche M. and Kremer F. - *Giant lateral electrostriction in ferroelectric liquid-crystalline elastomers* - Nature, vol. 410, pp. 447-450, 2001.

3

The dielectric elastomer actuators (DEA)

In this chapter the working principle of the dielectric elastomer actuators, their sensing capabilities and typical configuration devices are described. The mathematical models used in the following chapters to build a numerical procedure to simulate the behaviour of these materials are put in evidence.

3.1 Working principle of dielectric elastomer actuators

Simplicity in mechanism and design combined with superiority in performance has made Dielectric Elastomer Actuators (DEAs) [8][10][11][14]-[20] a preferred choice for an increasing number of R&D groups and companies developing EAP applications. This kind of EAP consists of an elastomer dielectric material that is coated on both sides with an expandable film that acts as a conducting electrode, as illustrated in Figure 15. When exposed to high electric fields, the dielectric elastomers, such as silicones and acrylics, contract in the direction of the electric field lines, and expand perpendicularly to them. The stress state induced by the electromechanical coupling is known as the Maxwell stress (see [1] Sec.1.5.1.2 pp.23-24, [2] Chap.1). The device is basically a flexible rubbery capacitor composed of two charged compliant parallel plates sandwiching a dielectric material.

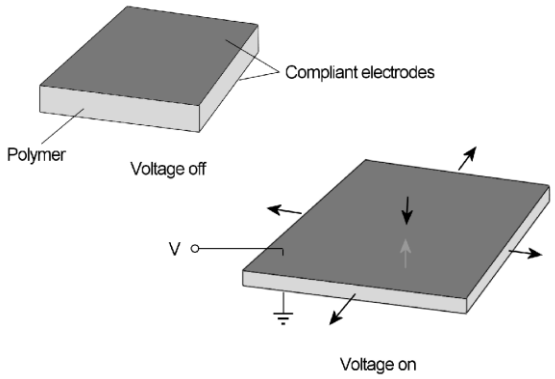

Figure 15. Working principle of dielectric elastomer actuators.

Two types of elastomers are commonly used for DEAs: an acrylate elastomer from 3M™ (VHB™ 4910) and silicone elastomers (PDMS - polydimethylsiloxane). The former shows better electromechanical properties but it comes as an adhesive tape that cannot be processed further, whereas two-component silicone rubbers are easily cast and moulded into any thickness and form. In case of the VHB tape, compliant electrodes are simply made of micron or sub-micron sized conducting particles (i.e. graphite or metal) brushed, painted or sprayed on the film. Such electrodes also work for silicone actuators, but here more elaborate designs like the smart compliant electrodes (SCE) [4], developed in the ARTMUS project by Risoe, have the advantage of reliability and reproducibility. In Figure 16 a schematic of an elastomer actuator/sensor with smart metallic compliant electrodes is illustrated. A "smart" compliant electrode is a thin metal film deposited on the corrugated side of an elastomeric film. The electrode is compliant in the direction of the wave-pattern but it is stiff in the perpendicular direction.

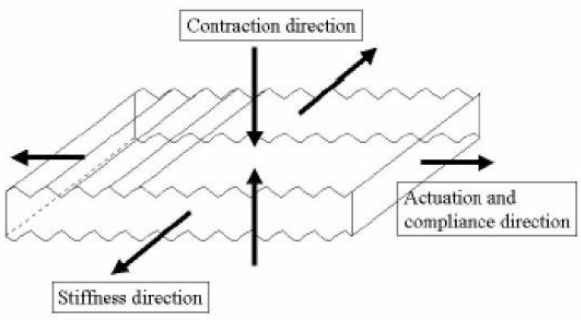

Figure 16. Schematic of an elastomer actuator/sensor with smart metallic compliant electrodes.

The polymers exhibit large strains, therefore the electrodes would have to be expandable as well. To this aim compliant electrodes based on conductive particles in an elastomer matrix have been developed. Because the electrodes expand along with the plastic, they can maintain the electric field across the entire active region. Stretching the polymers prior to electric activation vastly improves the polymer performance [3]. The prestretching orients the molecular chains along the plane, and makes it stiffer in that direction. To achieve this prestretching effect, the actuators contain an external bracing structure. Such prestretching may be anisotropic and thus may cause the effective elastic modulus to be anisotropic [4].

Acrylic polymers (or acrylates) are soft and highly viscoelastic materials, having the molecular structure represented in Figure 17a. Silicone polymers structure and the molecular origin of silicone elasticity are shown respectively in Figure 17b and Figure 17c.

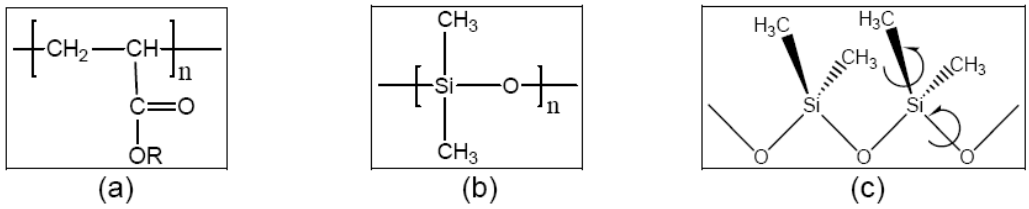

Figure 17. Molecular structure of acrylic polymers (a) and silicone polymers (b). Molecular origin of silicone elasticity (c).

They can exhibit high-level actuating capabilities: thickness strains up to 60-70% at 400 V/μm, area strains (Figure 18a and b) up to 200% at 200 V/μm (with and corresponding stresses of the order of 1 MPa have been demonstrated [10].

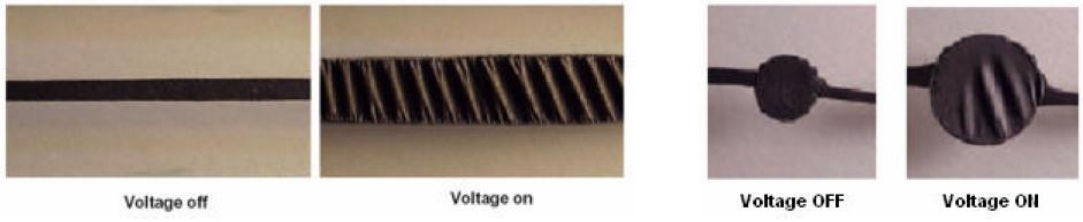

a) b)

Figure 18. Images showing electrically-activated electrode expansions for an acrylic elastomer.

Such performances are enabled by low elastic moduli and high dielectric strengths (dielectric breakdown can occur at electric fields of about 500 V/μm), which permit the application of high electric fields.

Material prestretching, before the application of the electric field, has been demonstrated to increase active performances, due to the improved elasticity and dielectric strength of the polymer [10]. Ever reported peak performances of DE actuators are impressive: strains up to 300%, response faster than 100 Hz and work density higher than 100 kJ/m3 [10][26]. These peak performances are not obtained under the same conditions and in order to evaluate the working performance of an actuator, its mechanical properties must be carefully considered – after all, it is a rubber band that extends and contracts. Sommer-Larsen have addressed the dynamical and static performance of DE actuators in a series of papers [27][9][28][29].

Silicone elastomers are amorphous polymers, having the molecular structure represented in Figure 17b. These materials are easily processable (by spin coating, casting,…) and permit the realization of good elastomers, with low glass transition temperature owing to the low barrier for rotation around the Si-O and Si-C bonds, which confer high mobility to the main chains, as shown by Figure 17c. Dielectric breakdown of silicones occurs at electric fields ranging from 100 to 350 V/μm, enabling thickness strains up to 40-50 % and area strains up to 100 % with related stresses of 0.3-0.4 MPa [10].

The excellent figures of merit possessed by dielectric elastomers in several respects (high actuation strains and stresses, fast response times, high efficiency, stability, reliability and durability) make them the most performing materials currently available for polymer actuation. The price for achieving these high-level capabilities is represented by the high driving electric fields needed (order of 100 V/μm). For a definite polymer thickness, such field levels can be reached by using high voltages, which may be disadvantageous in many applications. In order to reduce the driving electric fields, polymers with high dielectric constant are necessary. In fact, the strain generated by a dielectric elastomer actuator is proportional to both the square of the applied electric field and the material dielectric constant. Therefore, elastomers with higher permittivity can be advantageously driven with lower fields.

3.2 Actuating configurations

So far, many actuating configurations have been proposed and demonstrated, including planar, tube, rolled, extender, diaphragm, bimorph and unimorph bender (Figure 19).

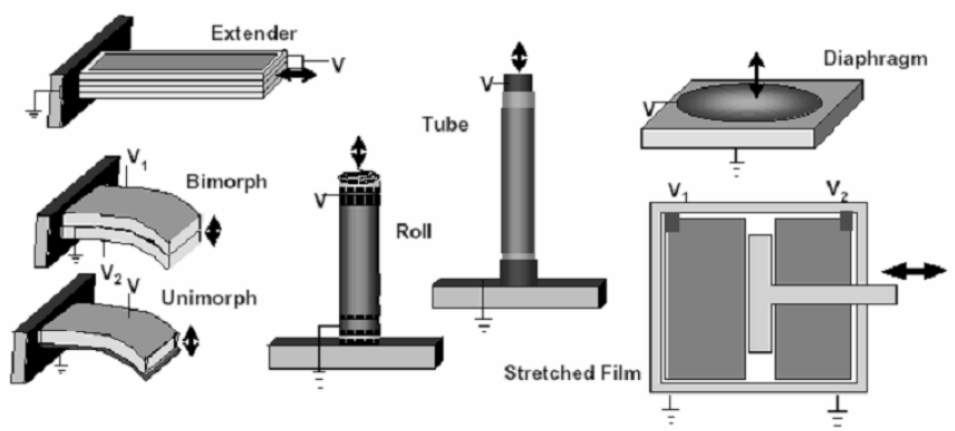

Figure 19. Most used configurations for dielectric elastomer actuators.

Tube and, mainly, roll actuators (Figure 20) are flexible devices suitable for linear (along a line) actuation, consisting of an axial elongation under electrical stimulation.

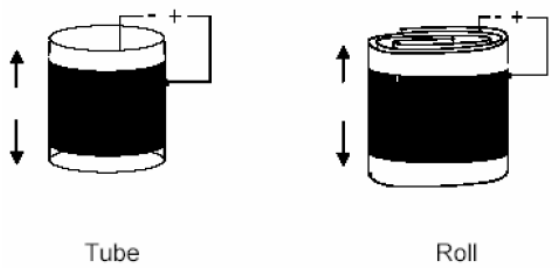

Figure 20. Tube and roll dielectric elastomer actuators.

Dielectric elastomer actuators can be advantageously used for each application requiring high axial elongations or contractions activated and modulated by an electrical signal. They share application areas with electrostrictive polymers but, because of their large strain capabilities, can also be used directly as replacements for many linear actuators, such as pneumatic cylinders and

electromagnetic solenoids (such as for industrial valves). Dielectric elastomers have a stress strain response that can duplicate that of natural muscle and consequently are well suited to applications in robotics, prosthetics, and animatronics. Because rubbers used in dielectric elastomers are already often used in vibration control applications as passive devices, dielectric elastomers can be suited for active vibration control applications, although such a kind of application has never been investigated.

3.3 Sensing capabilities

Performances of elastomeric materials have been reviewed in terms of actuation properties only. However, rubbery materials are also suitable for an use as strain sensing elements. In particular, two basic principles of sensing can be distinguished:

Piezocapacitive strain sensing

According to the basic structure of a dielectric elastomer actuator, such a device represents a variable capacitor, whose electrical capacitance changes in relation to an imposed deformation. This property can employed in order to use the device as a piezocapacitive strain sensor.

Piezoresistive strain sensing

A different principle of sensing can be exploited when the elastomeric material is filled with conducting particles (e.g. carbon black, metal powder, etc.), in order to make it electrically conductive. Since the electrical resistance of the material changes in relation to an imposed deformation, this effect can be used to implement piezoresistive transducers of strain. Such a simple sensing strategy has been successfully adopted in order to integrate distributed elastomeric strain sensors into wearable textile substrates.

3.4 Constitutive models

In order to obtain a numerical model that can simulate correctly the behavior of these actuators it is necessary to determine the following three items:

- the mechanical behavior of the polymer under electrical load;
- the electrical behavior and coupling with the mechanical one because the strongly dependence on a local thickness of the polymeric film;
- the prestretched configuration.

Smart materials are used in manufacturing the smart structures for the purpose of developing actuation and sensing capabilities. In general the constitutive behavior of these materials couples their structural response (stress and strain) with other physical fields. The coupled behavior of smart materials can also be viewed as energy transduction between different physical fields (e.g. elastic and kinetic energy transformed into electrostatic energy or vice versa). For this reason smart structures are a typical example of a mechanical system governed by a multi-physics behavior.

In this way, a mechanical excitation can be transformed into a non-mechanical effect and, conversely, a non-mechanical excitation can be converted into a mechanical effect. This is what happens in piezoelectric materials, where the electric behavior is coupled with the mechanical one due to the direct and converse piezoelectric effect. This effect enables the material to behave as an actuator or a sensor.

For the dielectric elastomers, the capability to sense is “indirect”; it means that a mechanical stimulus is not converted in an electrical signal but reading a variation of the physical characteristics as resistance or capacitance is needed for implementing the sensing.

From an engineering point of view, rubbers are homogeneous, isotropic materials that exhibit very large elastic strains (in a tensile test, a sample could reach ten times its original length). Moreover, one can observe from a tension test that the stress-strain behavior is strongly

nonlinear. Rubber and rubber-like materials are usually modeled as incompressible hyperelastic materials.

The nonlinear theory of elasticity is applied for the description of their mechanical behavior because structural components in the practice undergo large strain conditions. The finite-element method is suitable for the analysis of rubber and rubber-like materials provided that a nonlinear constitutive law and an iterative approach are used. In fact it is necessary to properly model the nonlinear stress-strain relations and take into account incompressible behavior of these materials and the presence of large deformation.

3.4.1 Mechanical constitutive model

Consider a body at a generic time t, a fundamental measure of the deformation of the body ${}_0^tF_{ik}$ is the *material deformation gradient tensor*, defined as:

$$ {}_0^tF_{ik} = \delta_{ik} + \frac{\partial {}^tu_i}{\partial {}_0x_k} \qquad (1) $$

where:

δ_{ik} : Kroneker's delta

${}^tu_i$: displacement components at time t

${}_0x_k$: material coordinate in a Cartesian reference system

$\frac{\partial {}^tu_i}{\partial {}_0x_k}$: displacement gradient tensor components

The *right Cauchy-Green deformation* tensor, in component notation, is defined as:

$$ {}_0^tC_{ij} = {}_0^tF_{ki}\ {}_0^tF_{kj} = \frac{\partial {}^tu_k}{\partial {}_0x_i}\frac{\partial {}^tu_k}{\partial {}_0x_j} = 2{}_0^t\epsilon_{ij} - \delta_{ij} \qquad (2) $$

where ${}_0^t\epsilon_{ij}$ is the *Green-Lagrange strain* tensor; this can be written in terms of Cauchy-Green deformation tensor as:

$$ {}^{t}_{0}\epsilon_{ij} = \frac{1}{2}\left({}^{t}_{0}C_{ij} - \delta_{ij}\right) \qquad (3) $$

The energy conjugate stress measure to use with the Green-Lagrange strain tensor is the *second Piola-Kirchhoff stress* tensor ${}^{t}_{0}S_{ij}$ ([5] Sec.6.2.2 p.515). The Piola-Kirchhoff stress tensor is used to express the stress relative to the reference configuration. This is in contrast to the Cauchy stress tensor which expresses the stress relative to the present configuration. For infinitesimal deformations or rotations, the Cauchy and Piola-Kirchhoff tensors are identical.

Hyperelastic material models assume that materials response is isotropic and isothermal. This assumption allows that the strain energy potentials are expressed in terms of strain invariants or principal stretch ratios. Except as otherwise indicated, the materials are also assumed to be nearly or purely incompressible. Material thermal expansion is also assumed to be isotropic.

The constitutive behavior of hyperelastic materials are usually derived from the strain energy potentials. The isotropic hyperelastic effects are mathematically described by specifying the dependence of the strain energy density (per unit original volume) W on the Green-Lagrange strain tensor.

Depending on the specific material model used, several forms of strain energy potential, such as Neo-Hookean, Mooney-Rivlin, Polynomial Form, Ogden Potential, Arruda-Boyce, Gent, and Yeoh are available ([6] Sec.3.8 p.325).

In this thesis the Mooney-Rivlin model is adopted. The use to describe the mechanical response is justified by the strain range of the DEA materials. As it will be shown in the next section, for a strain of 100% this model will allow a good fit of the constitutive behavior.

The conventional Mooney-Rivlin model [5] is described by the strain energy density per unit original volume:

$$ {}^{t}_{0}\widetilde{W} = c_1({}^{t}_{0}I_1 - 3) + c_2({}^{t}_{0}I_2 - 3) \qquad {}^{t}_{0}I_3 = 1 \qquad (4) $$

where c_1 and c_2 are material constants and the invariants ${}^{t}_{0}I_i$ are given in terms of the components of the Cauchy-Green deformation tensor and the three principal stretches ${}^{t}_{0}\lambda_i$:

$$
\begin{aligned}
{}_0^tI_1 &= {}_0^tC_{kk} = {}_0^t\lambda_1{}^2 + {}_0^t\lambda_2{}^2 + {}_0^t\lambda_3{}^2 \\
{}_0^tI_2 &= \frac{1}{2}\left[({}_0^tI_1)^2 - {}_0^tC_{ij}\,{}_0^tC_{ij}\right] = {}_0^t\lambda_1{}^2\,{}_0^t\lambda_2{}^2 + {}_0^t\lambda_2{}^2\,{}_0^t\lambda_3{}^2 + {}_0^t\lambda_3{}^2\,{}_0^t\lambda_1{}^2 \qquad (5)\\
{}_0^tI_3 &= det\,{}_0^t\boldsymbol{C} = {}_0^t\lambda_1{}^2\,{}_0^t\lambda_2{}^2\,{}_0^t\lambda_3{}^2
\end{aligned}
$$

Eq. (4) assumes that the material is totally incompressible (since ${}_0^tI_3 = 1$). A better assumption is that the bulk modulus is several thousand times large with respect to the shear modulus, which means that the material is almost incompressible. This assumption is incorporated by dropping the restriction that ${}_0^tI_3 = 1$ and including a hydrostatic work term W_H in the strain energy function to obtain

$$
{}_0^t\widetilde{W} = c_1({}_0^tI_1 - 3) + c_2({}_0^tI_2 - 3) + W_H({}_0^tI_3) \qquad (6)
$$

However, this expression cannot be used directly in the displacement/pressure formulations because all the three terms contribute to the pressure. To obtain an appropriate expression, it is possible to define the reduced invariants:

$$
\begin{aligned}
{}_0^tJ_1 &= {}_0^tI_1({}_0^tI_3)^{-\frac{1}{3}} \\
{}_0^tJ_2 &= {}_0^tI_2({}_0^tI_3)^{-\frac{2}{3}} \qquad (7)\\
{}_0^tJ_3 &= ({}_0^tI_3)^{\frac{1}{2}}
\end{aligned}
$$

so that it is possible to write:

$$
{}_0^t\overline{W} = c_1({}_0^tJ_1 - 3) + c_2({}_0^tJ_2 - 3) + \frac{1}{2}\kappa({}_0^tJ_3 - 1)^2 \qquad (8)
$$

where the strain energy density ${}_0^t\overline{W}$ is expressed in terms of the bulk modulus κ that measures the resistance to a uniform pressure ${}^t\bar{p}$ defined as:

$$
{}^t\bar{p} = \kappa({}_0^tJ_3 - 1) \qquad (9)
$$

With the knowledge of how the strain energy density *W* depends on the Green-Lagrange strain tensor (through the invariants or stretches), the 2nd Piola-Kirchhoff stress tensor is evaluated using:

$$S_{ij} = \frac{1}{2}\left(\frac{\partial W}{\partial \epsilon_{ij}} + \frac{\partial W}{\partial \epsilon_{ji}}\right) \qquad (10)$$

and the elasticity tensor is evaluated using the following expression:

$$C_{ijrs} = \frac{1}{2}\left(\frac{\partial S_{ij}}{\partial \epsilon_{rs}} + \frac{\partial S_{ij}}{\partial \epsilon_{sr}}\right) \qquad (11)$$

3.4.2 Electromechanical constitutive model

Stresses and strains induced in dielectrics by an electrostatic field have two sources [7]. The first one is the *Maxwell stress effect* which originates from the coulombic interaction between charges on electrodes needed for establishment of electric field. The second one is related to the change in dielectric properties of the material with strain and is referred to as *electrostriction*. Stresses and strains resulting from the both effects are quadratic with the magnitude of the electric field [8][9].

If a Cartesian reference system of coordinates is chosen in such way that the electric field vector lies in z direction, the principal electrically induced stresses are:

$$\sigma_{xx} = \sigma_{yy} = +\frac{1}{2}\varepsilon_R \varepsilon_0 E^2 \left(1 + \frac{a_2}{\varepsilon_R}\right) \qquad (12)$$

$$\sigma_{zz} = -\frac{1}{2}\varepsilon_R \varepsilon_0 E^2 \left(1 - \frac{a_1 + a_2}{\varepsilon_R}\right) \qquad (13)$$

where

- E is the electric field
- ε_R is the relative permittivity of the material

- ε_0 is the permittivity of vacuum
- a_1 and a_2 are two parameters describing the change of dielectric properties of the material in shear and bulk deformation.

The material is considered isotropic in terms of permittivity, for this reason it is possible to express $\sigma_{xx} = \sigma_{yy}$. Some studies [10][11] shows that the dielectric permittivities of some polymers are slightly affected by strain. This is true for low dielectric constant elastomers. In this case the electrostriction effect is negligible. The electrostrictive coefficients a_1 and a_2 assume a little importance [12], hence we will neglect their contribution, such that:

$$\sigma_{ij} = \varepsilon_R \varepsilon_0 E_i E_j - \frac{1}{2} \varepsilon_R \varepsilon_0 E^2 \delta_{ij} \qquad (14)$$

In case of an incompressible dielectrically isotropic material eq.(14) represents adequately a simplified version of the electrostatic stress [13]

When a capacitor is charged by the application of an electric field, positive charges reside on one electrode, balanced by negative charges on the other electrode. The compliance of the elastomer allows the charges to move closer by squeezing the capacitor. Like charges on a given electrode repel each other and expand the polymer in transverse direction (Figure 21).

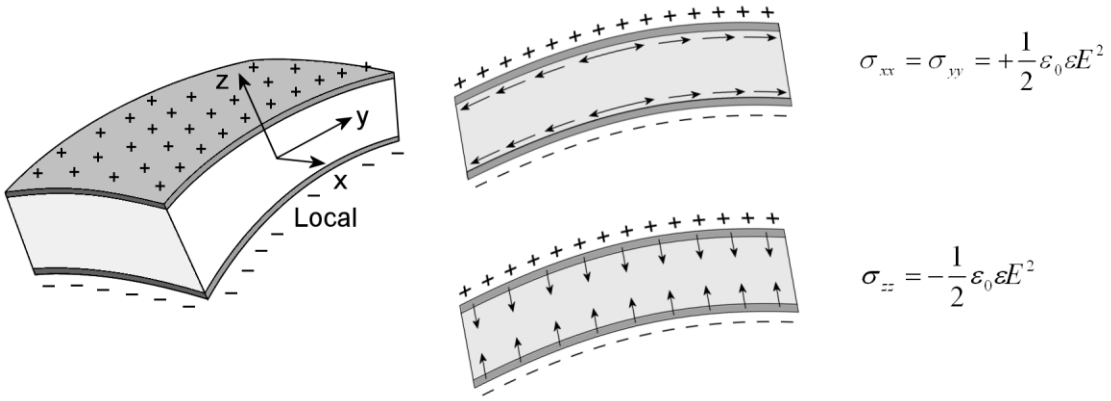

Figure 21. Maxwell stress effect.

The electric flux density in the material can be expressed as:

$$D_i = \varepsilon_{ij} E_j \qquad (15)$$

The above mechanical and electrical constitutive equations are rearranged now to represent the coupled behavior of the material.

$$\begin{cases} \Sigma_{ij} = \sigma_{ij} + \sigma_{ij}^M & (16) \\ D_i = \varepsilon_{ij} E_j & (17) \end{cases}$$

where $\varepsilon = \varepsilon_R \varepsilon_0$ is the permittivity of the material and σ_{ij}^M represents the Maxwell's stress.

The attraction of the electrodes compress the elastomer along thickness and volume conservation forces the elastomer to expand transversely to electric field, increasing the area of electrodes. At the same time the repulsion of like charges on the same electrode expand transversely the elastomer and volume conservation forces the elastomer to compress in thickness. This is the double effect of actuators with compliant electrodes. The value of the compression results to be twice than for conventional stiff electrodes.

The effect that Pelrine et al. [14] include by doubling the value of eq.(14) is taken into account in the present formulation by assuming an incompressible Mooney-Rivlin model for the mechanical (namely the elastic part) of the constitutive model of DEA. In fact the proposed approach assumes an iterative form of solution that solves the electrical and the mechanical part of the DEA behavior. This allows also very general kind of loading to be applied to the material (e.g. pretension) and to evaluate in a proper way the stiffness of the material that experiences, as well known, a highly non-linear behavior. In the mechanical iteration of analysis the electrostatic (Maxwell) stress and the elastic are combined. As results we can obtain the same "double effect". Moreover this method allows to consider the stiffness of the compliant electrodes separated from the expression of the electrostatics and then to take into account their anisotropy and non-linear behavior. For this reason the effect is not exactly twice as for electrodes that are compliant in both directions.

3.5 References

[1] Bar-Cohen, Y. - *Electroactive Polymer (EAP) Actuators as Artificial Muscles - Reality, Potential and Challenges* - SPIE Press, Vol. PM98, 2001.

[2] Carpi F., De Rossi D., Kornbluh, R. Pelrine R. and Sommer-Larsen P. - *Dielectric Elastomers as Electromechanical Transducers Fundamentals, Materials, Devices, Models and Applications of an Emerging Electroactive Polymer Technology* - Elsevier Science, March 10, 2008

[3] Kofold G. - *The static actuation of dielectric elastomer actuators how does pre-stretch improve actuation?* - Journal of physics D: Applied Physics. 41(2008)

[4] Benslimane M., Gravesen, P., Sommer-Larsen P. - *Mechanical properties of dielectric elastomer actuators with smart metallic compliant electrodes* - Smart Structures and Materials 2002: Electroactive Polymer Actuators and Devices (EAPAD) Edited by Bar-Cohen, Yoseph. Proc. SPIE Vol. 4695, p. 150-157

[5] Bathe K.J. - *Finite Element Procedures* - Prentice Hall, 1996

[6] *Theory and Modeling Guide* - Volume I: ADINA, ADINA R&D, Inc., Report ARD 04-7, September 2004

[7] Krakowsky I., Romijn T. and Posthuma de Boer A. - *A few remarks on the electrostriction of elastomers* - Journal of Applied Physics Vol.85 N.1 (1999)

[8] Kofod G., Kornbluh R., Pelrine R. and Sommer-Larsen P. - *Actuation response of polyacrylate dielectric elastomers* - Journal of Intelligent Material Systems and Structures, Vol.14 December 2003.

[9] Sommer-Larsen P. and Larsen A.L. - *Materials for dielectric elastomer actuators* - Smart Structures and Materials: Electroactive Polymer Actuators and Devices (EAPAD). Edited by Bar-Cohen, Yoseph. Proceedings of the SPIE, Volume 5385, pp. 68-77, 2004.

[10] Pelrine R., Kornbluh R., Pei Q. and Joseph J. - *High-Speed Electrically Actuated Elastomers with over 100% Strain* - Science Vol.287 N.5454

[11] Pelrine R., Kornbluh R., Heydt J.J.R., Pei Q. and Chiba S. - *High-field deformation of elastomeric dielectrics for actuators* - Materials Science and Engineering C Vol.11 N.2 (2000)

[12] Yamwong T., Voice A.M. and Davies G.R. - *Electrostrictive response of an ideal polar rubber* - Journal of Applied Physics Vol.91 1472-6 (2002)

[13] McMeeking R.M. and Landis C.M. - *Electrostatic forces and stored energy for deformable dielectric materials* - Journal of Applied Mechanics. 72 581-90 (2005)

[14] Pelrine R.E., Kornbluh R.D. and Joseph J.P. - *Electrostriction of polymer dielectrics with compliant electrodes as a means of actuation* - Sensors and Actuators A 64 (1998) 77-85.

[15] Heydt R., Kornbluh R., Pelrine R. and Mason V. - *Design and performance of an electrostrictive polymer film acoustic actuator* - Journal of Sound and Vibration 215 (2) (1998) 297-311.

[16] Pelrine R., Kornbluh R. and Kofod G. - *High-strain actuator materials based on dielectric elastomers* - Adv. Mater, vol. 12 (16), pp. 1223-1225, 2000.

[17] Pei Q., Pelrine R., Stanford S., Kornbluh R. and Rosenthal M. - *Electroelastomer rolls and their application for biomimetic walking robots* - Synthetic Metals 135-136 (2003) 129-131.

[18] Ashley S - *Artificial muscles* - Scientific American, October Issue, pp. 52-59, 2003.

[19] Carpi F., Chiarelli P., Mazzoldi A. and De Rossi D. - *Electromechanical characterisation of dielectric elastomer planar actuators: comparative evaluation of different electrode materials and different counterloads* - Sensors and Actuators A 107 (2003) 85-95.

[20] Carpi F. and De Rossi D. - *Dielectric elastomer cylindrical actuators: electromechanical modelling and experimental evaluation* - Mater. Sci. Eng. C, vol. 24 (4), pp. 555-562, 2004.

[21] Kornbluh R., Pelrine R. and Joseph J., in Proc. Third IASTED International Conference on Robotics and Manufacturing, Cancun, Mexico, 1–6 (1995).

[22] Artificial Muscles Inc, web site: http://www.artificialmuscle.com.

[23] ARTMUS - Artificial Muscles. A feasibility Study of polymer based materials for actuator purposes. Report for project period I. (pp. 1-66), II. (pp. 1-46), Final Report. (pp. 1-41), Ed. Peter Sommer-Larsen, Per Elgård Pedersen. Risø National Laboratory (1996).

[24] Wingert A., Lichter M., Dubowsky S. And Hafez M. - *Hyper-redundant robot manipulator actuated by optimized binary dielectric polymers* - In Bar-Cohen, Y. (ed.), Proceedings of SPIE Vol. 4695, p. 415-423 (2002).

[25] Jeon J., Park K., An S., Nam J., Choi H., Kim H., Bae S. and Tak Y., in Y. Bar-Cohen (Ed.), Proceedings of SPIE Vol. 4329, 380–388, (2001).

[26] Kornbluh R., Pelrine R., Pei Q., Heydt R., Stanford S., Oh S. and Eckerle J., in Proc. SPIE, Smart Structures and Materials 2002: Industrial and Commercial Applications of Smart Structures Technologies 4698 (2002).

[27] Sommer-Larsen P. - *Polymer actuators- How do they work?* - In: Conference proceedings. Actuator 2004, 2Borgmann, H. (ed.), (Messe Bremen GmbH, Bremen, (2004).

[28] Sommer-Larsen P., Kofod G., Shridhar M.H., Benslimane M. and Gravesen P. - *Performance of dielectric elastomer actuators and materials* - In Bar-Cohen, Y. (ed.), Proceedings of SPIE Vol. 4695, p.158-166 (2002).

[29] Sommer-Larsen P., Hooker J.C., Kofod G., West K., Benslimane M. and Gravesen, P. - *Response of dielectric elastomer actuators* - In Bar-Cohen, Y. (ed.), Proceedings of SPIE Vol. 4329, p. 157-163 (2001).

4

Finite element modelling

The work sustained for the implementation of a new numerical procedure, thorough the finite element method, to model the electromechanical behaviour of the materials with dielectric elastomer is described in this chapter. Both the constitutive relations of the mechanical and electrical part of the material show the behaviour with strongly non-linear nature. The first one follows the typical behaviour of the hyperelastic materials and for this reason it is studied and modelled through the introduction of an energetic functional for the elastic deformation based on the theoretical model of Mooney-Rivlin. The electrical part, to be more precise the relation that states the electromechanical coupling, is based on the Maxwell law. It links the mechanical stress to a component that depends quadratically from the electric field.

The base of the finite element formulation is the principle of virtual work, specialized for our purpose to the electrostatic and mechanical nature of the materials. A recall of his formulation is proposed.

4.1 The principle of virtual work for electrostatic and mechanical nature of the materials

4.1.1 Basic formulation

The principle of virtual work (PVW) provides an important framework that is used to generate exact and approximate solutions for problems in mechanics and in many others fields of the physics, and is the basis for the finite element method. A PVW for problems of simultaneous

electrostatic and mechanical loading, with material interactions between the resulting strain and polarization, is needed for analyzing the response of electroactive polymers, among other materials. The formulation proposed for the PVW [1][2][3] is based on the displacement and the electric potential as the independent variables, and is suitable as the foundation of a finite element method in which such parameters are taken to be the nodal variables.

Consider a system consisting of dielectric materials, perfect conductors and free space. In the current configuration, the system occupies the volume *V*. The perimeter of the system and the interfaces within it are designated *S* in the current configuration. The internal interfaces separate the dielectric materials, the conductors and free space from each other. In addition, sectors of dielectric with homogeneous or heterogeneous properties may be separated by surfaces included within *S*, as sectors of free space.

Let the free charge per unit volume within *V* be ${}_0^t q$ where the subscript 0 indicates the position of material points in the current configuration and *t* is time. Furthermore, let ${}_0^t \omega$ be the free charge per unit area on the surfaces *S* and define ${}_0^t \phi$ to be the electrical potential everywhere within the system such that it is continuous everywhere in space. Further variables to be considered in the PVW are the velocity ${}_0^t v_i$ of material points, the surface traction ${}_0^t T_i$ defined as the force per unit area acting on *S* and ${}_0^t b_i$, which is the body force per unit volume acting at points in *V* .

Consider the physical laws governing the electromechanical fields in the material [4]. In the quasi-static limit, Maxwell's laws state that the electric field must be curl-free and Gauss's law states that the divergence of the electric displacement must be equal to the volume density of free charge. Therefore, for the electric field, *E* , and the electric displacement, *D* , holds:

$$\varepsilon_{ijk} \frac{\partial E_i}{\partial x_k} = 0 \quad \Rightarrow \quad E_i = \frac{\partial \phi}{\partial x_i} \qquad (18)$$

$$\frac{\partial D_i}{\partial x_i} = q \quad in \quad V \qquad (19)$$

$$n_i \| D_i \| = \omega \quad on \quad S \qquad (20)$$

where ε_{ijk} are the components of the electric permittivity expressed with the permutation symbol.

Here, n_i are the Cartesian components of the unit normal to the surface S pointing from the negative side of the surface out towards the positive side. The notation $\|\ \ \|$ represents the difference or jump in the included quantity across the surface S such that

$$\|D_i\| = D_i^+ - D_i^- \qquad (21)$$

The electric displacement can be decomposed into two parts such that

$$D_i = \varepsilon_0 E_i + P_i \qquad (22)$$

where ε_0 is the dielectric permittivity of free space and P_i are the Cartesian components of the material polarization.

Conservation of mass implies that for a given material volume

$$\frac{d}{dt}\int_V \rho dV = 0 \quad \Rightarrow \quad \frac{\partial \rho}{\partial t} + \rho \frac{\partial v_i}{\partial x_i} = 0 \qquad (23)$$

where ${}_0^t\rho$ is the mass density of the material. The principles of conservation of linear and angular momentum are stated as

$$\int_V (b_i + b_i^E) dV + \int_S (T_i + T_i^E) dS = \frac{d}{dt}\int_V \rho v_i dV \qquad (24)$$

and

$$\int_V \varepsilon_{ijk} x_j (b_k + b_k^E) dV + \int_S \varepsilon_{ijk} x_j (T_k + T_k^E) dS = \frac{d}{dt}\int_V \rho \varepsilon_{ijk} x_j v_k dV \qquad (25)$$

Here the components of the electrical body force b_i^E and surface traction T_i^E have been introduced. These forces arise directly from electric fields acting in the material and are in addition to the mechanical body force and surface traction. Furthermore, it is assumed that the electrical body force can be derived from the Maxwell stress tensor σ_{ij}^M of Eq.(14) such that

$$b_i^E = \frac{\partial \sigma_{ji}^M}{\partial x_j} \quad in \quad V \qquad (26)$$

where the electrical body force is the effect of charges interacting at a distance or equivalently, the force per unit volume arising from electric fields acting on charges. The traction relationship for Maxwell stress is then

$$T_i^E = n_j \left\| \sigma_{ji}^M \right\| \quad on \quad S \qquad (27)$$

Then, in order to satisfy the principle of conservation of linear momentum for a small surface element, the Cauchy stress in the material, σ_{ij} , must balance the total surface traction such that along with Eq. (27)

$$T_i + T_i^E = -n_j \left\| \sigma_{ji} \right\| \quad \Rightarrow \quad T_i = -n_j \left\| \sigma_{ji} + \sigma_{ji}^M \right\| \qquad (28)$$

The sum of the Cauchy and Maxwell stresses will be termed the total true stress, Σ_{ji} .

Next, application of Eqs. (23), (26) and (28) within the principles of conservation of linear and angular momentum and recognition that the resultant integrals must be valid for any arbitrary volume yields

$$\frac{\partial \sigma_{ji}}{\partial x_j} + \frac{\partial \sigma_{ji}^M}{\partial x_j} + b_i = \rho \frac{dv_i}{dt} \quad in \quad V \qquad (29)$$

and

$$\sigma_{ji} + \sigma_{ji}^M = \sigma_{ij} + \sigma_{ij}^M \quad in \quad V \qquad (30)$$

Thus, for the balance of angular momentum to be satisfied, the total true stress must be symmetric, but there is no requirement that the Maxwell and Cauchy stress tensors are individually symmetric.

4.1.2 Principle of virtual work

Now consider the variation of virtual work by external actions to the system. This external virtual work rate, in the form relevant to the so-called electrical enthalpy, is

$$\frac{d^*\widetilde{W}}{dt} = \int_V b_i v_i^* dV + \int_S T_i v_i^* dS - \int_V q \frac{d^*\phi}{dt} dV - \int_S \omega \frac{d^*\phi}{dt} dS \qquad (31)$$

where the asterisk indicates, respectively, a virtual differentiation with respect to time, and a virtual velocity. The first two integral terms represent respectively the mechanical virtual work of the external forces on the volume and surface. The second two integral terms represent respectively the electrical virtual work of the free charge within the volume and on the surface. The material virtual rate of change of potential can be converted to spatial and convected contributions through

$$\frac{d^*\phi}{dt} = \frac{\partial^*\phi}{\partial t} - v_k^* E_k \qquad (32)$$

When this is inserted into Eq.(31), along with Eqs. (20) and (28), we obtain

$$\begin{aligned}\frac{d^*\widetilde{W}}{dt} = \int_V b_i v_i^* dV - \int_S n_j \left\| \sigma_{ji} + \sigma_{ji}^M \right\| v_i^* dS - \int_V q \left(\frac{\partial^*\phi}{\partial t} - v_k^* E_k \right) dV \\ - \int_S n_i \| D_i \| \left(\frac{\partial^*\phi}{\partial t} - v_k^* E_k \right) dS\end{aligned} \qquad (33)$$

Since the virtual velocity and the material virtual rate of change of potential are continuous across *S*, and are zero outside the domain *V*, the divergence theorem can now be used to convert the surface integrals to volume integrals giving

$$\frac{d^*\widetilde{W}}{dt} = \int_V \rho \frac{dv_i}{dt} v_i^* dV + \int_V \left(\sigma_{ji} + \sigma_{ji}^M \right) \frac{\partial v_i^*}{\partial x_j} dV + \int_V D_i \frac{\partial}{\partial x_i} \left(\frac{\partial^*\phi}{\partial t} - v_k^* E_k \right) dV \qquad (34)$$

where Eqs. (19) and (29) have been used to obtain a simplification. The introduction of the material virtual rate of change of the electric field then provides the PVW, namely

$$\begin{aligned}\int_V b_i v_i^* dV + \int_S T_i v_i^* dS - \int_V q\frac{d^*\phi}{dt} dV - \int_S \omega \frac{d^*\phi}{dt} dS \\ = \int_V \rho \frac{dv_i}{dt} v_i^* dV + \int_V \left[\left(\sigma_{ji} + \sigma_{ji}^M - D_j E_i\right) \frac{\partial v_i^*}{\partial x_j} - D_i \frac{d^* E_i}{dt} + \rho \frac{dv_i}{dt} v_i^* \right] dV \\ = \int_V \left[\left(\Sigma_{ji} - D_j E_i\right) \frac{\partial v_i^*}{\partial x_j} - D_i \frac{d^* E_i}{dt} + \rho \frac{dv_i}{dt} v_i^* \right] dV\end{aligned} \qquad (35)$$

This form of the PVW has exactly the form needed for an updated Lagrangian formulation of large strain problems that is the paradigm for finite element analysis [5]. As such, the PVW in Eq. (35) can be considered as the starting point for a finite element formulation for problems of electroactive materials experiencing finite strain, utilizing the physical displacements and the electric potential as the independent nodal variables.

4.2 Numerical solver approach

Let us now address the nonlinear nature of the response and propose a finite element procedure [6] for the analysis of piezoelectric continua, as also proposed in [7]. From a computational viewpoint one of the key advantages of this approach is that already existing finite element programs that solve classical solid mechanics problems and field problems, like heat transfer, can directly be used in a reliable way providing that the constitutive law is modified. It is so possible to include material nonlinearities in the procedure as discussed below.

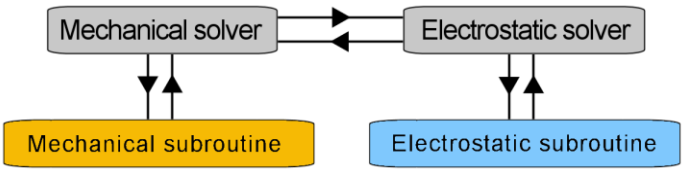

Figure 22. Numerical solver approach.

In order to establish a general solution scheme for nonlinear problems the use of incremental equilibrium equations is necessary; so, we have to use a procedure that is both iterative and also incremental, dealing at every iteration with the mechanical or electrical equilibrium.

The Figure 22 summarizes the numerical solver approach. The heart of the procedure is a finite element code composed of main block with two subroutines, one to solve the governing equations of mechanical models and the other for the electrostatic models. With this approach a coupled electromechanical problem can be simulated with two different models, one for each field. The models interact sharing the calculated values of the electromechanical variables with the main block. The governing equations for the electric field is first solved in the electrostatic subroutine and the values of the electric variables are given as an entry to the mechanical solver that provides a mechanical solution that is, in turn, given back to the electric solver. This procedure iterates until a convergence is reached for both mechanical and electrical variables. The mechanical solver accounts, for the nonlinear behaviour described before, and provide further iterations, as described in the next section.

4.2.1 Mechanical subroutine

The mechanical subroutine is based on the Eq. (16) with an iterative scheme:

$$^{(k)}\Sigma_{ij} = {}^{(k-1)}\sigma_{ij}(W) + {}^{(k-1)}\sigma_{ij}^{M}(E) \qquad (36)$$

The global stress field Σ_{ij} is calculated at iteration k as the sum of the mechanical stress σ_{ij} and the Maxwell stress σ_{ij}^{M}. The mechanical stress depends on the strain energy density W related to

the mechanical state of the system at iteration *k-1*. The Maxwell stress depends on the electric field *E* related to the electrostatic state of the system at iteration *k-1* calculated in the electrostatic subroutine. The Figure 23 shows the input and the output of the mechanical subroutine. The strains from the mechanical solver and the electrostatic field from the electrostatic solver at iteration *k-1* are given as input. The subroutine calculates the stresses and the tangent constitutive matrix to update, in the mechanical solver the stiffness matrix and calculate the stresses at iteration *k*.

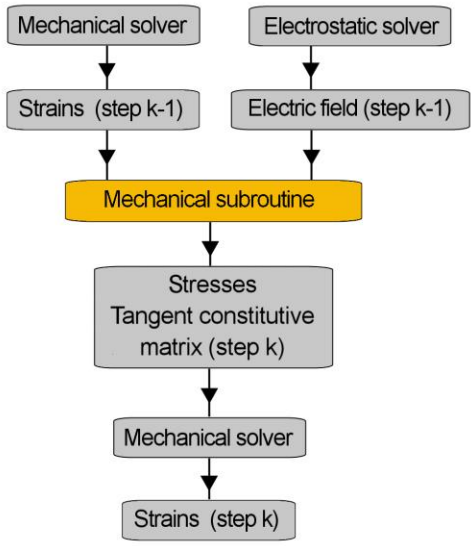

Figure 23. Mechanical subroutine.

A local Lagrangian coordinate reference system is considered. The mechanical constitutive subroutine executes the following operations.

Calculate the right Cauchy-Green deformation tensor:

$$C_{11} = 2\epsilon_{11} + 1 \qquad (37)$$

$$C_{22} = 2\epsilon_{22} + 1 \qquad (38)$$

$$C_{33} = 2\epsilon_{33} + 1 \qquad (39)$$

$$C_{12} = 2\epsilon_{12} \qquad (40)$$

$$C_{13} = 2\epsilon_{13} \quad (41)$$

$$C_{23} = 2\epsilon_{23} \quad (42)$$

Calculate invariants:

$$I_1 = C_{11} + C_{22} + C_{33} \quad (43)$$

$$I_2 = \frac{1}{2}\left({I_1}^2 - \left({C_{11}}^2 + {C_{22}}^2 + {C_{33}}^2 + 2\left({C_{12}}^2 + {C_{13}}^2 + {C_{23}}^2\right)\right)\right) \quad (44)$$

$$I_3 = det\ \boldsymbol{C} \quad (45)$$

Calculate first derivatives of invariants respect to strain components:

$$\frac{\partial I_1}{\partial \epsilon_{11}} = \frac{\partial I_1}{\partial \epsilon_{22}} = \frac{\partial I_1}{\partial \epsilon_{33}} = 2 \quad (46)$$

$$\frac{\partial I_1}{\partial \epsilon_{12}} = \frac{\partial I_1}{\partial \epsilon_{13}} = \frac{\partial I_1}{\partial \epsilon_{23}} = 0 \quad (47)$$

$$\frac{\partial I_2}{\partial \epsilon_{11}} = 2I_1 - 2C_{11} \quad (48)$$

$$\frac{\partial I_2}{\partial \epsilon_{22}} = 2I_1 - 2C_{22} \quad (49)$$

$$\frac{\partial I_2}{\partial \epsilon_{33}} = 2I_1 - 2C_{33} \quad (50)$$

$$\frac{\partial I_2}{\partial \epsilon_{12}} = -2C_{12} \quad (51)$$

$$\frac{\partial I_2}{\partial \epsilon_{13}} = -2C_{13} \quad (52)$$

$$\frac{\partial I_2}{\partial \epsilon_{23}} = -2C_{23} \quad (53)$$

$$\frac{\partial I_3}{\partial \epsilon_{11}} = 2\left(C_{22}C_{33} - {C_{23}}^2\right) \quad (54)$$

$$\frac{\partial I_3}{\partial \epsilon_{22}} = 2\left(C_{11}C_{33} - {C_{13}}^2\right) \quad (55)$$

$$\frac{\partial I_3}{\partial \epsilon_{33}} = 2\left(C_{11}C_{22} - {C_{12}}^2\right) \quad (56)$$

$$\frac{\partial I_3}{\partial \epsilon_{12}} = 2(C_{13}C_{23} - C_{12}C_{33}) \quad (57)$$

$$\frac{\partial I_3}{\partial \epsilon_{13}} = 2(C_{12}C_{23} - C_{22}C_{13}) \quad (58)$$

$$\frac{\partial I_3}{\partial \epsilon_{23}} = 2(C_{12}C_{13} - C_{11}C_{23}) \quad (59)$$

Calculate reduced invariants and first derivatives respect to strain components:

$$J_1 = I_1(I_1)^{-\frac{1}{3}} \quad (60)$$

$$J_2 = I_2(I_3)^{-\frac{2}{3}} \quad (61)$$

$$J_3 = (I_3)^{\frac{1}{2}} \quad (62)$$

$$\frac{\partial J_1}{\partial \epsilon_i} = (I_3)^{-\frac{1}{3}}\left(\frac{\partial I_1}{\partial \epsilon_i} - \frac{1}{3}\frac{I_1}{I_3}\frac{\partial I_3}{\partial \epsilon_i}\right) \quad (63)$$

$$\frac{\partial J_2}{\partial \epsilon_i} = (I_3)^{-\frac{2}{3}}\left(\frac{\partial I_2}{\partial \epsilon_i} - \frac{2}{3}\frac{I_2}{I_3}\frac{\partial I_3}{\partial \epsilon_i}\right) \quad (64)$$

$$\frac{\partial J_3}{\partial \epsilon_i} = \frac{1}{2}(I_3)^{-\frac{1}{2}}\left(\frac{\partial I_3}{\partial \epsilon_i}\right) \qquad (65)$$

with $i = 11, 22, 33, 12, 13, 23$.

The expression of the strain energy density W in Mooney-Rivlin form with nine constants is:

$$\begin{aligned} W = \{&[c_9(J_2 - 3) + c_8(J_1 - 3) + c_5](J_2 - 3) \\ &+ \left[[c_7(J_1 - 3) + c_4](J_1 - 3) + c_2\right]\}(J_2 - 3) \\ &+ \{[c_6(J_1 - 3) + c_3](J_1 - 3) + c_1\}(J_1 - 3) \\ &+ \frac{1}{2}\kappa(J_3 - 1)^2 \end{aligned} \qquad (66)$$

Compute first derivatives of the strain energy density W with respect to reduced invariants:

$$\begin{aligned} \frac{\partial W}{\partial J_1} = &\{3c_6(J_1 - 3) + 2[c_7(J_2 - 3) + c_3]\}(J_1 - 3) \\ &+ [c_8(J_2 - 3) + c_4](J_2 - 3) + c_1 \end{aligned} \qquad (67)$$

$$\begin{aligned} \frac{\partial W}{\partial J_2} = &\{3c_9(J_2 - 3) + 2[c_8(J_1 - 3) + c_5]\}(J_2 - 3) \\ &+ [c_7(J_1 - 3) + c_4](J_1 - 3) + c_2 \end{aligned} \qquad (68)$$

$$\frac{\partial W}{\partial J_3} = \kappa(J_3 - 1) \qquad (69)$$

Calculate 2nd Piola-Kirchhoff stresses tensor:

$$\sigma_i = \frac{\partial W}{\partial J_1}\frac{\partial J_1}{\partial \epsilon_i} + \frac{\partial W}{\partial J_2}\frac{\partial J_2}{\partial \epsilon_i} + \frac{\partial W}{\partial J_3}\frac{\partial J_3}{\partial \epsilon_i} \qquad (70)$$

with $i = 11, 22, 33, 12, 13, 23$.

Calculate Maxwell stresses tensor:

$$\sigma_{11}^{M} = -\frac{1}{2}\varepsilon_0\varepsilon_R {E_3}^2 \qquad (71)$$

$$\sigma_{22}^{M} = -\frac{1}{2}\varepsilon_0\varepsilon_R {E_3}^2 \qquad (72)$$

$$\sigma_{33}^{M} = \frac{1}{2}\varepsilon_0\varepsilon_R {E_3}^2 \qquad (73)$$

$$\sigma_{12}^{M} = \sigma_{13}^{M} = \sigma_{23}^{M} = 0 \qquad (74)$$

Sum of Piola-Kirchoff and Maxwell stresses tensors:

$$\Sigma_{\mathrm{i}} = \sigma_i + \sigma_i^M \qquad (75)$$

with $i = 11, 22, 33, 12, 13, 23$.

Compute second derivatives of the invariants with respect to strain components. All the second derivatives of the invariant I_1 with respect to strain components are zero. The second derivatives of the invariant I_2 and I_3 different to zero are:

$$\frac{\partial^2 I_2}{\partial\epsilon_{11}\partial\epsilon_{22}} = \frac{\partial^2 I_2}{\partial\epsilon_{11}\partial\epsilon_{33}} = \frac{\partial^2 I_2}{\partial\epsilon_{22}\partial\epsilon_{33}} = 4 \qquad (76)$$

$$\frac{\partial^2 I_2}{\partial {\epsilon_{12}}^2} = \frac{\partial^2 I_2}{\partial {\epsilon_{13}}^2} = \frac{\partial^2 I_2}{\partial {\epsilon_{23}}^2} = -2 \qquad (77)$$

$$\frac{\partial^2 I_3}{\partial\epsilon_{11}\partial\epsilon_{22}} = 4C_{33} \quad \frac{\partial^2 I_3}{\partial\epsilon_{11}\partial\epsilon_{33}} = 4C_{22} \quad \frac{\partial^2 I_3}{\partial\epsilon_{11}\partial\epsilon_{23}} = -4C_{23} \qquad (78)$$

$$\frac{\partial^2 I_3}{\partial\epsilon_{22}\partial\epsilon_{33}} = 4C_{11} \quad \frac{\partial^2 I_3}{\partial\epsilon_{22}\partial\epsilon_{13}} = -4C_{13} \quad \frac{\partial^2 I_3}{\partial\epsilon_{33}\partial\epsilon_{12}} = -4C_{12} \qquad (79)$$

$$\frac{\partial^2 I_3}{\partial {\epsilon_{12}}^2} = -2C_{33} \quad \frac{\partial^2 I_3}{\partial\epsilon_{12}\partial\epsilon_{13}} = 2C_{23} \quad \frac{\partial^2 I_3}{\partial\epsilon_{12}\partial\epsilon_{23}} = 2C_{13} \qquad (80)$$

$$\frac{\partial^2 I_3}{\partial {\epsilon_{13}}^2} = -2C_{22} \quad \frac{\partial^2 I_3}{\partial \epsilon_{13}\partial \epsilon_{23}} = 2C_{12} \quad \frac{\partial^2 I_3}{\partial {\epsilon_{23}}^2} = -2C_{11} \tag{81}$$

Compute second derivatives of the reduced invariants with respect to strain components:

$$\frac{\partial^2 J_1}{\partial \epsilon_i \partial \epsilon_j} = {I_3}^{-\frac{1}{3}} \left\{ \frac{1}{3I_3} \left[-\left(\frac{\partial I_1}{\partial \epsilon_i}\frac{\partial I_3}{\partial \epsilon_j} + \frac{\partial I_3}{\partial \epsilon_i}\frac{\partial I_1}{\partial \epsilon_j} \right) + I_1 \left(\frac{4}{3I_3}\frac{\partial I_3}{\partial \epsilon_i}\frac{\partial I_3}{\partial \epsilon_j} - \frac{\partial^2 I_3}{\partial \epsilon_i \partial \epsilon_j} \right) \right] \right\} \tag{82}$$

$$\frac{\partial^2 J_2}{\partial \epsilon_i \partial \epsilon_j} = {I_3}^{-\frac{2}{3}} \left\{ \frac{\partial^2 I_2}{\partial \epsilon_i \partial \epsilon_j} + \frac{2}{3I_3} \left[-\left(\frac{\partial I_2}{\partial \epsilon_i}\frac{\partial I_3}{\partial \epsilon_j} + \frac{\partial I_3}{\partial \epsilon_i}\frac{\partial I_2}{\partial \epsilon_j} \right) + I_2 \left(\frac{5}{3I_3}\frac{\partial I_3}{\partial \epsilon_i}\frac{\partial I_3}{\partial \epsilon_j} - \frac{\partial^2 I_3}{\partial \epsilon_i \partial \epsilon_j} \right) \right] \right\} \tag{83}$$

$$\frac{\partial^2 J_3}{\partial \epsilon_i \partial \epsilon_j} = \frac{1}{2} {I_3}^{-\frac{1}{2}} \left(\frac{1}{-2I_3}\frac{\partial I_3}{\partial \epsilon_i}\frac{\partial I_3}{\partial \epsilon_j} - \frac{\partial^2 I_3}{\partial \epsilon_i \partial \epsilon_j} \right) \tag{84}$$

with $i, j = 11, 22, 33, 12, 13, 23$.

Calculate second derivatives of the strain energy density W with respect to reduced invariants J_1 and J_2 :

$$\frac{\partial^2 W}{\partial {J_1}^2} = 6c_6(J_1 - 3) + 2(c_7(J_2 - 3) + c_3) \tag{85}$$

$$\frac{\partial^2 W}{\partial {J_2}^2} = 6c_9(J_2 - 3) + 2(c_8(J_1 - 3) + c_5) \tag{86}$$

$$\frac{\partial^2 W}{\partial J_1 \partial J_2} = 2\big(c_7(J_1 - 3) + c_8(J_2 - 3)\big) + c_4 \tag{87}$$

Calculate tangent constitutive tensor to update the stiffness matrix:

$$D_{ij} = \left(\frac{\partial^2 W}{\partial {J_1}^2}\frac{\partial J_1}{\partial \epsilon_i} + \frac{\partial^2 W}{\partial J_1 \partial J_2}\frac{\partial J_2}{\partial \epsilon_i}\right)\frac{\partial J_1}{\partial \epsilon_j} + \left(\frac{\partial^2 W}{\partial J_1 \partial J_2}\frac{\partial J_1}{\partial \epsilon_i} + \frac{\partial^2 W}{\partial {J_2}^2}\frac{\partial J_2}{\partial \epsilon_i}\right)\frac{\partial J_2}{\partial \epsilon_j} + \frac{\partial^2 W}{\partial {J_3}^2}\frac{\partial J_3}{\partial \epsilon_i}\frac{\partial J_3}{\partial \epsilon_j} \quad (88)$$

with $i, j = 11, 22, 33, 12, 13, 23$.

4.2.2 Electrostatic subroutine

The mechanical subroutine is based on the Eq. (17) with an iterative scheme:

$${}^{(k)}D_i = \varepsilon_i{}^{(k-1)}E_i \quad (89)$$

with $i = 1, 2, 3$.

The electric displacements D_i are calculated at iteration *k* with the permittivity ε_i and the electric field E_i of iteration *k-1*.

For non-linear materials the permittivity can depend upon the electric field and has a time dependent response. Explicit time dependence can arise if the materials are physically moving or changing in time. For these reasons the permittivity matrix has to be updated and a new electric field calculated. In particular, the thickness of the dielectric can change and a new electric field is evaluated with the electrostatic subroutine at step *k*.

The Figure 24 shows the input and the output of the electrostatic subroutine. The new geometry from the mechanical solver and the electrostatic field from the electrostatic solver at iteration *k-1* are given as input. The subroutine calculates the electric displacement and in the electrostatic solver the new electric field is calculated at iteration *k*.

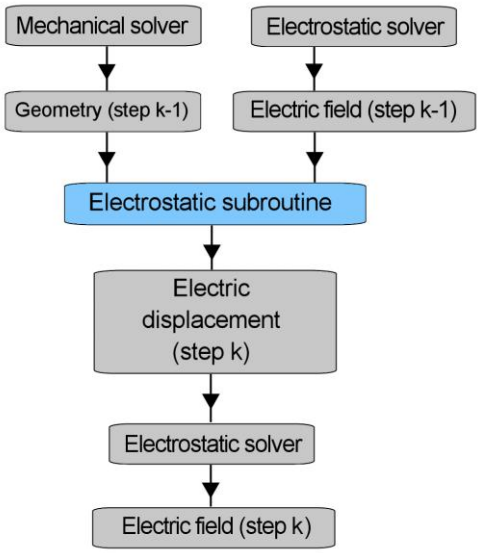

Figure 24. Electrostatic subroutine.

4.3 References

[1] McMeeking R.M., Landis C.M. and Jimenez S.M.A. - *A principle of virtual work for combined electrostatic and mechanical loading of materials* - International Journal of Non-Linear Mechanics 42 (2007) 831 – 838

[2] McMeeking R.M. and Landis C.M. - *Electrostatic forces and stored energy for deformable dielectric materials* - J. Appl. Mech. 72 (2005) 581–590.

[3] Landau L.D. and Lifschitz E.M. - *Electrodynamics of Continuous Media* - Pergamon Press, Oxford, 1960.

[4] Dorfmann A. and Ogden R.W. - *Nonlinear electroelasticity* - Acta Mech. 174 (2005) 167–183.

[5] McMeeking R.M. and Rice J.R. - *Finite-element formulations for problems of large elastic–plastic deformation* - Int. J. Solids Struct. 11 (1975) 601–616.

[6] Bathe K.J. - *Finite Element Procedures* - Prentice Hall, 1996

[7] Gaudenzi P. And Bathe K.J. - *An iterative finite element procedure for the analysis of piezoelectric continua* - Journal of Intelligent Material Systems and Structures, Vol. 6, 1995, 266-273.

5

Multilayered sensor/actuator

The goodness of the numerical procedure is validated in this chapter, where a dielectric elastomer actuator, multilayer type, developed from Risø Danish National Laboratory, is modelled. At this scope a model to reproduce the behaviour of its electrodes (smart metallic compliant electrodes) with a non-linear orthotropic material is developed. A phase of designing approach, through the engineering of the multilayer sensor/actuator follows. A series of numerical parametric analyses focused to the coupling the actuator with a generic host structure, monitoring i.e. the performances of the actuator versus the stiffness of the host structure itself is performed. These analyses are used as background for designing and development of a technological demonstrator for space, optimized to highlight the performances of the actuator.

5.1 The prototype of the multilayered sensor/actuator ESA-C-4

The ESA-C-4 is a dielectric elastomer with smart compliant electrodes (DESCE) actuator. The Figure 25 shows both a picture and a schematic representation of it with geometrical dimensions and electrical connections. This prototype is a multilayered structure (five layers, 37 micron thin each), 100mm long (the elastic part is 90mm) and 70 mm wide.

Four sheets act as actuator and one as sensor. The electrode areas are evaporated on the five films of Elastosil RTV E625 silicone from Wacker [2][3][4][5]. Each electrode is produced by evaporation of silver (Ag) for a thickness of 75nm. Multilayers are glued together using a conductive silicone, Elastosil LR3132. The connectors extend 2.5mm outside the electrode area; the electrical leads are embedded in four connection pads of 5mm, 0.4mm thick each.

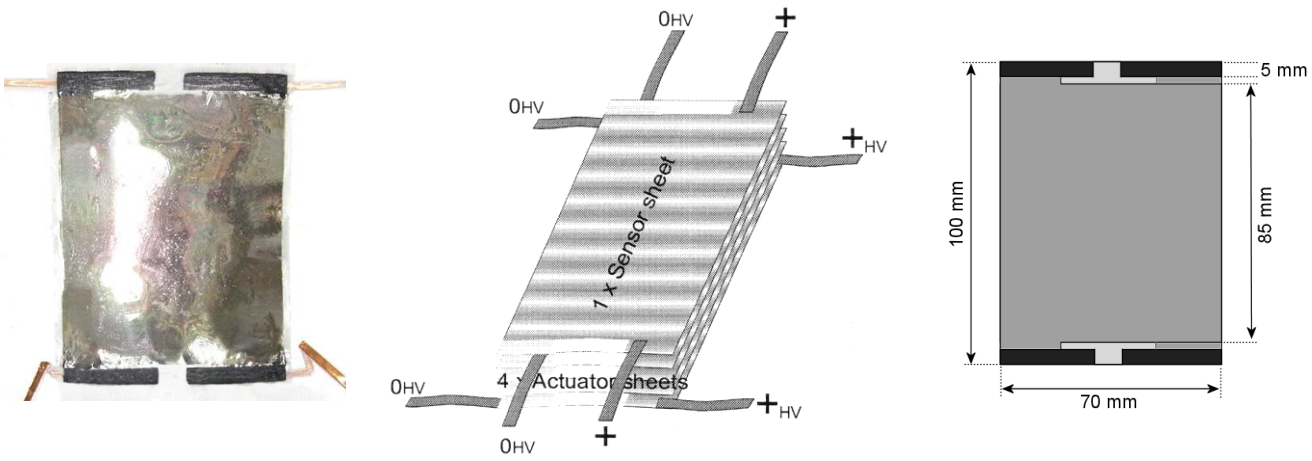

Figure 25. Multilayer ESA-C-4 sensor/actuator.

The basic idea of a "smart" compliant electrode [1][2] is that a thin metal film is deposited on the corrugated side of an elastomeric film. The other side is flat. As it is possible to observe in Figure 26, two such films are assembled to form a layer with corrugated electrodes on both sides. The electrode is compliant in the direction of the wave-pattern but it is as stiff as a flat metallic layer in the perpendicular direction that belongs to the plane of the film. This design allows for elongations in the direction of compliance/actuation only. Corrugation amplitude is 2 μm and corrugation period is 10 μm.

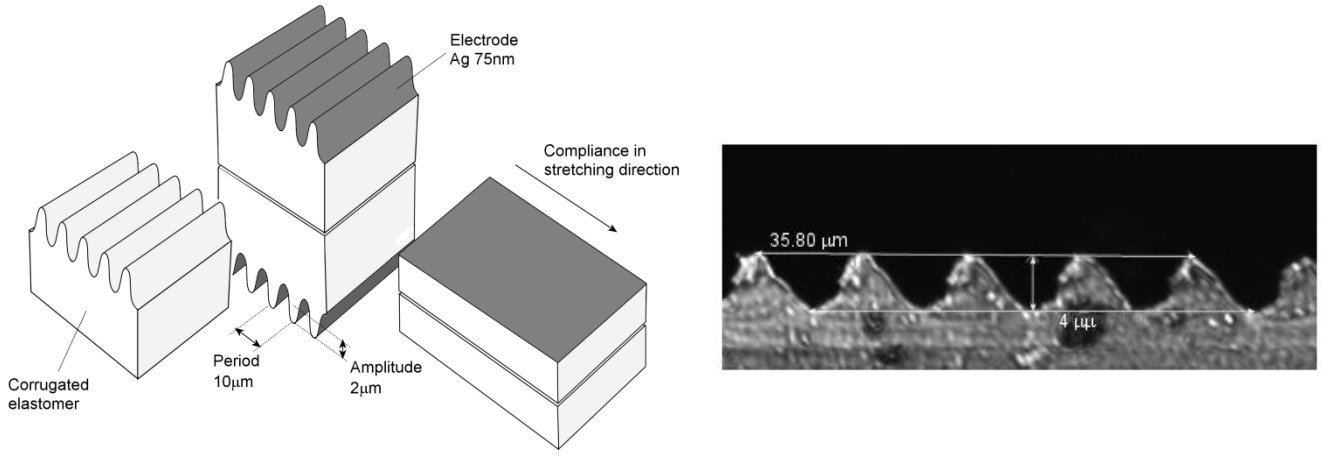

Figure 26. DEA with metallic compliant electrodes.

5.2 The finite element model of the actuator and its experimental set-up

The first step to begin the modelling of the actuator is the characterization of the mechanical behavior of the silicone material used for the fabrication of it, the Elastosil RTV E625. In order to do this a tensile test is performed both in experimental and in numerical way. The material model used for the simulation is hyperelastic in accordance with the Mooney-Rivlin theory. At this aim it is necessary to find the proper material constants to fit the experimental behavior ([1] Sec.11.2.1). The Table 3 resumes the mechanical characteristics used in the numerical models with a constitutive behaviour between stress and stretch expressed in terms of two constants c_1 and c_2.

Elastosil RTV E625
Young's modulus = 0.8 MPa
$\sigma = 2\left(c_1 + \frac{c_2}{\lambda}\right)\left(\lambda - \frac{1}{\lambda^2}\right)$ Mooney-Rivlin theory
c_1 = 100 kPa c_2 = 33 kPa

Table 3. Elastosil RTV E625 material characteristics.

In Figure 27 the non-linear constitutive behaviour is compared with the linear one.

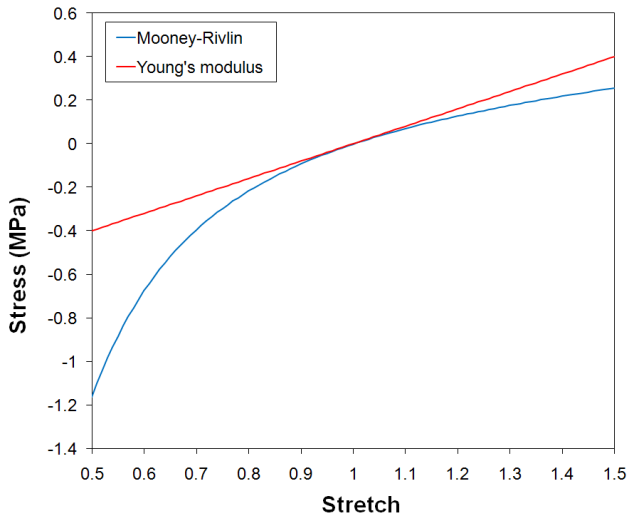

Figure 27. Elastosil RTV E625 constitutive behaviour.

The second step is to reproduce in a numerical way with a finite element approach the experimental set-up. In the Figure 28 the set-up is shown. The aim of the test is to measure the stretching of the actuator subjected to a mechanical load and then to a driving voltage on the electrodes. The mechanical load is a force that provides the actuator of the necessary preload. The actuator is positioned in vertical position clamped at one end and loaded by the weight of a mass attached to it. The Figure 29 illustrates a close-up of the actuator and its clamping system. A rigid bar is attached to the free end in order to distribute the stress homogeneously.

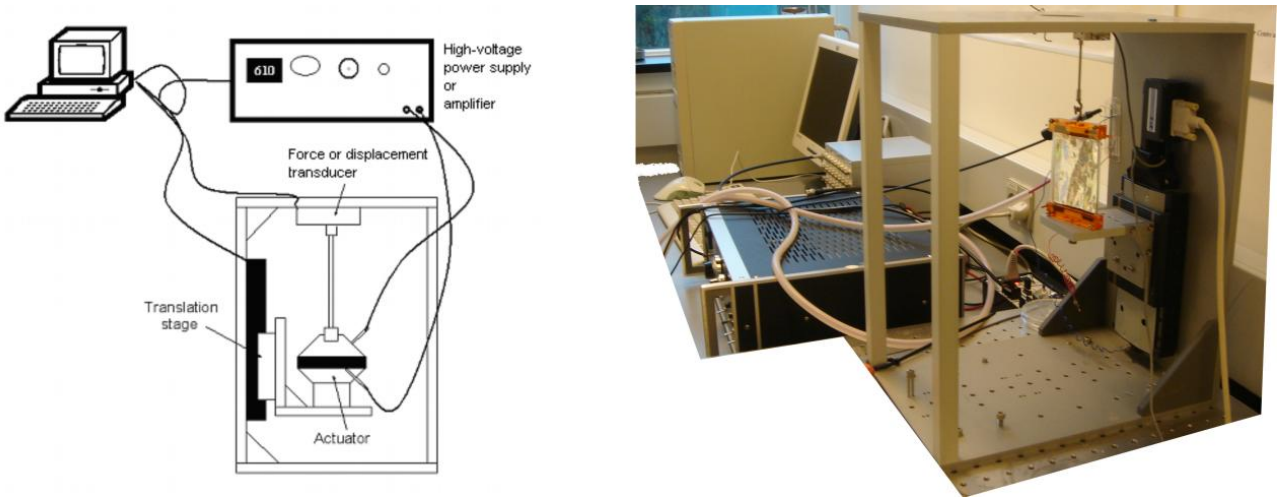

Figure 28. The experimental set-up of the multilayer sensor/actuator.

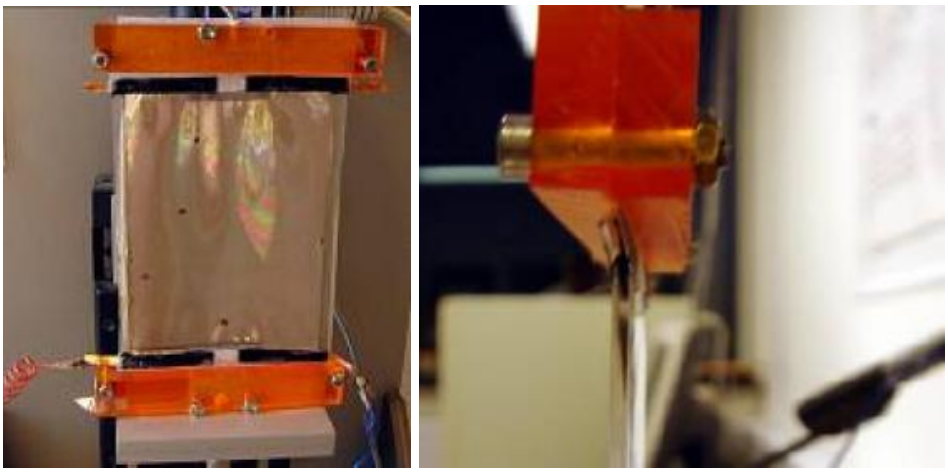

Figure 29. Clamping system.

The main information of the finite element model is summarized in Table 4. The analyses are performed in quasi stationary conditions with the mechanical and electrical loads applied with a linear increase in time. These loads are increased with a slow progression in order to avoid dynamic effects of oscillation. For the mechanical model, the dielectric elastomer is modelled with 3D solid elements 27 nodes, each node with three degree of freedom for the translations. A special material model, that follows the electromechanical behaviour discussed in the previous

part of this thesis, is applied. The electrodes, discussed more in detail in the next section, are modelled with the same type of element but with an orthotropic linear elastic material model. Non-linear 2 nodes spring elements, with a translational single degree of freedom for each node, are superimposed on the electrodes to take into account their non-linear behaviour. The actuator is provided of pads, made with the same material of the dielectric is modelled with 3D solid elements 27 nodes and a Moneey-Rivlin hyperelastic material model. These pads are interposed between the actuator and the clamping system in order to reduce the concentration of stress and failures near the constraints.

The Figure 30 illustrates an exploded view of the finite element model of the ESA-C-4 sensor/actuator.

ESA-C-4
Actuator / sensor layers: 3D solid elements 27 nodes
Elastosil RTV E625
C_1 = 100 kPa
C_2 = 33 kPa
Dielectric constant $\varepsilon = 2.479 \times 10^{-11}$ F/m
Density ρ =1100 kg/m^3
Electrodes:
Linear part: 3D solid elements 27 nodes
Orthotropic Y_{axial}=94.2 MPa, $Y_{thickness}$=94.2 MPa, $Y_{tranverse}$=83 GPa
ν_{12}=0, ν_{23}=0, ν_{13}=0
G_{12}=10 MPa, G_{23}=10 MPa, G_{13}=10 MPa
Non-linear part: Spring element
See Figure 36
Pads: 3D solid elements 27 nodes
Elastosil RTV E625
C_1 = 100 kPa
C_2 = 33 kPa
Density ρ =1100 kg/m^3

Table 4. Finite element model main information.

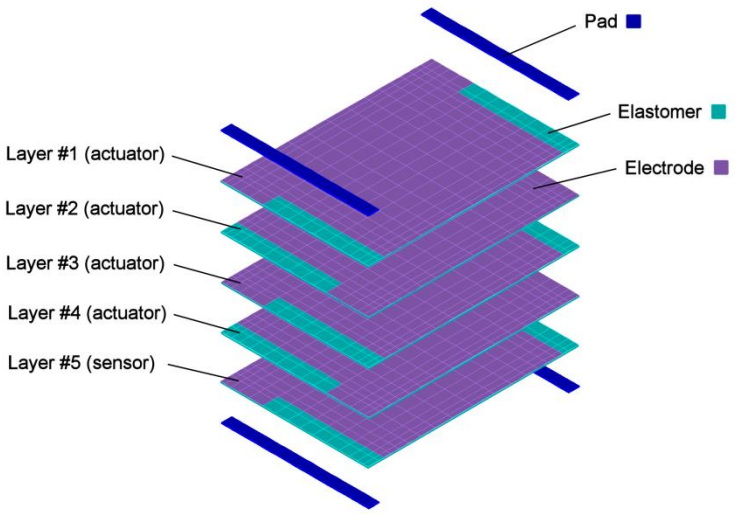

Figure 30. Exploded view of the finite element model of the ESA-C-4 sensor/actuator.

After some tests with different preloads, it has been observed that the best performances of the actuators are obtained for a specific pre-stressed condition. In particular the optimal pre-stress is achievable with a load mass of 50 g/layer, therefore a total of 250 g, to which a force of 2.453 N corresponds. A power supply provides the electrodes of a continuous voltage up to 2500 V. This is the electrostatic limit of the actuator seen as a condenser. Beyond this threshold some discharge induces the breakdown of the system.

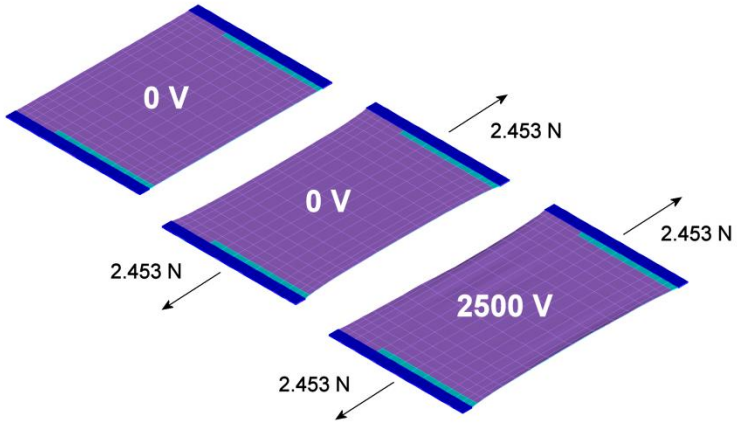

Figure 31. Finite element model of the ESA-C-4 sensor/actuator.

The Figure 31 resumes the two phases of which the simulation is composed.

- Pre-loading phase: no actuation is present. An increasing tensile load from 0 to the optimal force is applied. The ESA-C-4 prototype extends of 10.9 mm, as depicted in the Figure 33. The stretching is quite linear; only the mechanical hyperelastic behaviour is present.
- Actuation phase: starting from the pre-stressed configuration reached at the end of the previous phase and maintaining the loading force of 2.453 N, an increasing voltage from 0 to 2500 V is applied to the electrodes. The actuator extends of 5.9 mm more, as depicted in the Figure 33. The stretching is non-linear; both the mechanical hyperelastic and electro-mechanical behaviour are present.

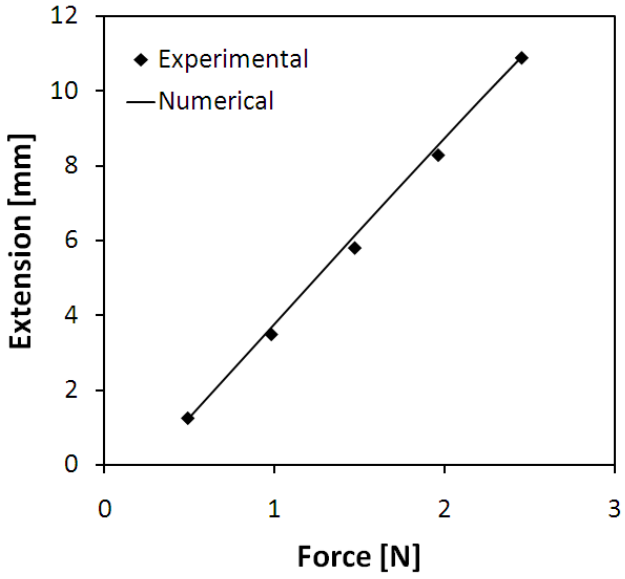

Figure 32. Behavior of the actuator with preload.

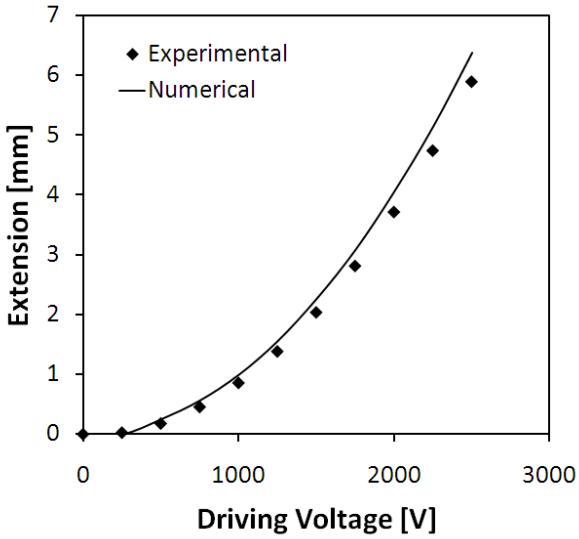

Figure 33. Behavior of the actuator with preload and voltage.

The mesh of the dielectric elastomer is particularly refined along the thickness in a manner to simulate in a good way the stretching along this direction. The Figure 34 shows how the thickness at the centre of one active layer changes during the preloading and the actuation phases. In particular the stretch of the thickness has a strong influence on the electric field and then on the actuation behaviour. The figure shows the difference of the electric field if the stretch of the thickness is considered or not.

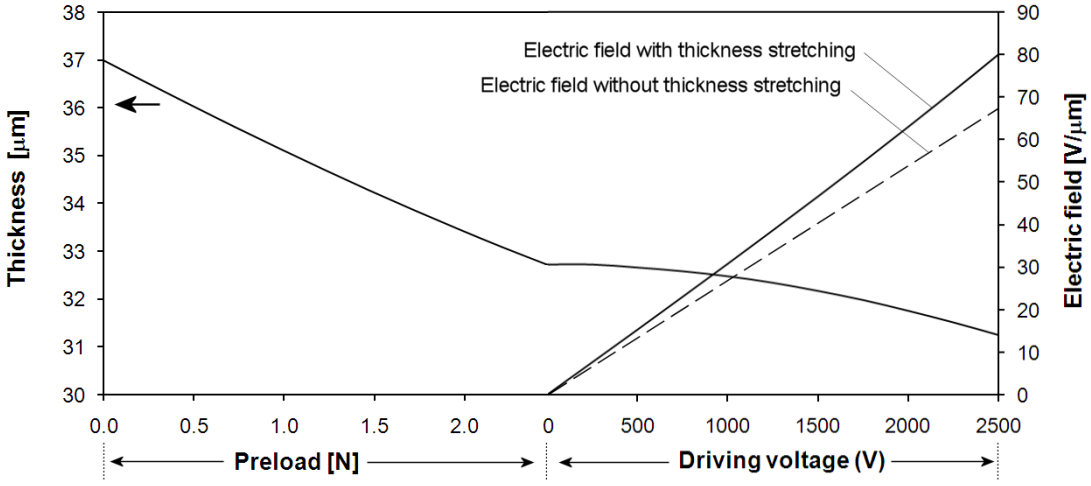

Figure 34. Thickness of a single active layer and electric field behaviour.

A good agreement is reached [6] for the characterization of the model, moreover validated with a convergence analysis. In Figure 35 the total extension of the actuator at the end the activation phase is reported for different refinements of the mesh (number of nodes of the model). Moreover meshes obtained with two different element types (with 8 and with 27 nodes) are compared.

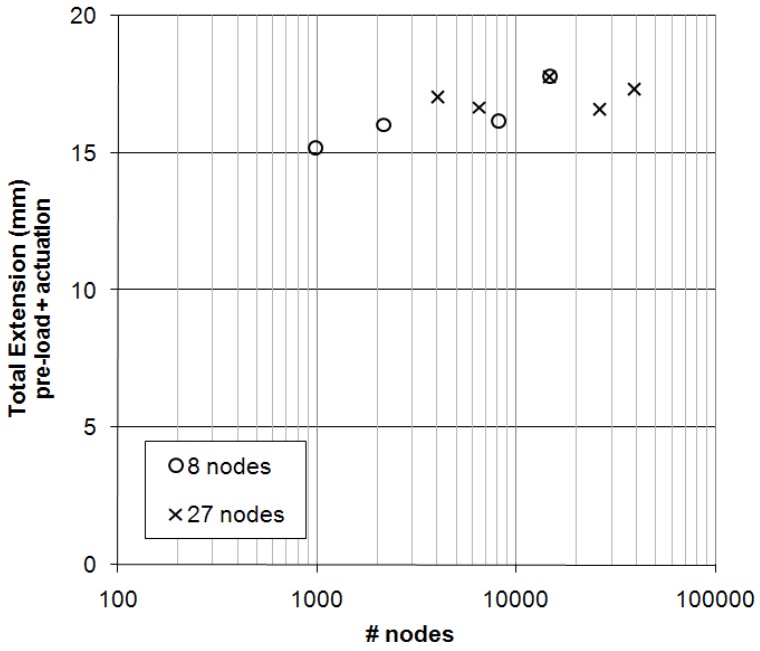

Figure 35. Convergence graph of the FE model.

5.3 Modeling of the metallic compliant electrodes

The most critical part of the model of the DEA is their electrodes. They are corrugated at microscopic level (few nanometers). It is not possible to create a numerical model of it in a macroscopic scale such as the actuator one. For this reason it is necessary to introduce a model that allows to approximate the physical behaviour in terms of stiffness.

This behaviour has a non-linear nature along the actuation direction (axial). The amplitude of the waves decreases and its period increases with the strain. At this effect an increasing of the Young's modulus corresponds until reaching the maximum stretching allowable (flatness) for the

electrode. The non-linearity adopted in the model (Figure 36) derives as a variant of the laws proposed in [1] for a circular arc wave profile. The Young's modulus of the electrode in perpendicular direction to actuation not changes with strain and correspond to a classical value for the silver.

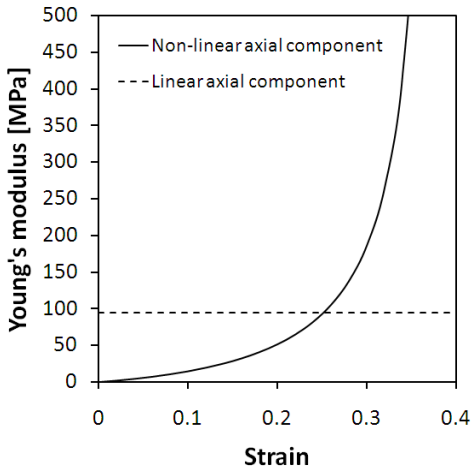

Figure 36. Linear and non-linear components of the Young's modulus of the compliant electrodes.

In order to provide a finite element model of the electrodes, the linear (strain independent) and non-linear (strain dependent) behaviours have been separated. The first one is associated to 3D elements with orthotropic material characteristics Y_{axial}=94.2 MPa, $Y_{tranverse}$=83 GPa and no Poisson's effect (Table 4). The second one is associated to a spring element, superimposed to the electrodes with stiffness $K=YA/l$ where l is the electrode length, A is the transverse area and Y is the non-linear part of the Young's modulus.

5.4 Parametric analyses for the multilayer sensor/actuator

The next step is to include this numerical material model in the frame of a hosting structure, as the model of a breadboard developed to demonstrate the suitability of the DEA actuators in a real case of space structure.

5.4.1 EAP actuator and the hosting structure

In order to underline some important characteristics of the EAP/hosting structure coupling it is possible to analyze a simple scheme with an EAP and a spring representative of the hosting structure stiffness. In the Figure 37 we have that scheme: a) the EAP and the hosting structure are unloaded; b) a stretching is applied to the actuator in order to provide with a preload to increase the performances and then it is joint to the hosting structure: the equilibrium is reached and both the elements are preloaded; c) under activation, the actuator elongates and the host structure recovers part of his unloading. A new equilibrium state is reached.

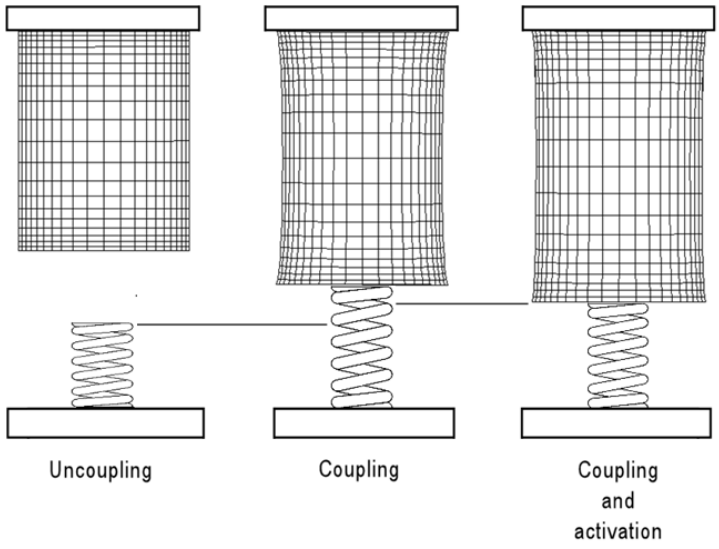

Figure 37. EAP/Hosting structure coupling scheme.

As observed in the past sections, the best performances of the actuator are achieved with an optimal pre-load. It is very important to underline that the hosting structure deformation produces a progressive decrease of the actuation capability of the EAP, because of the consequent decrease of the actuator pre-load (reaction force). The more the actuator elongates, the less is the pre-load applied on it. For a correct sizing of the actuator it is important to take into account this effect to obtain a right compromise between the elongation and the best actuation performance.

In Figure 38 and Figure 39 some charts that underline the above described effect are shown. The tests are performed with an initial pre-load of 2N (optimal) of the EAP.

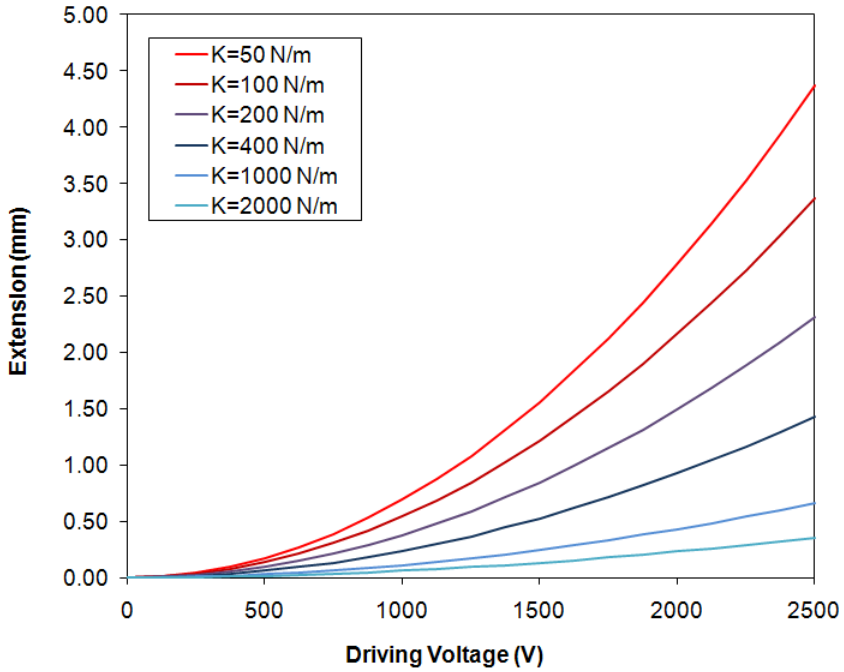

Figure 38. Extension vs. applied potential (for several spring stiffness K).

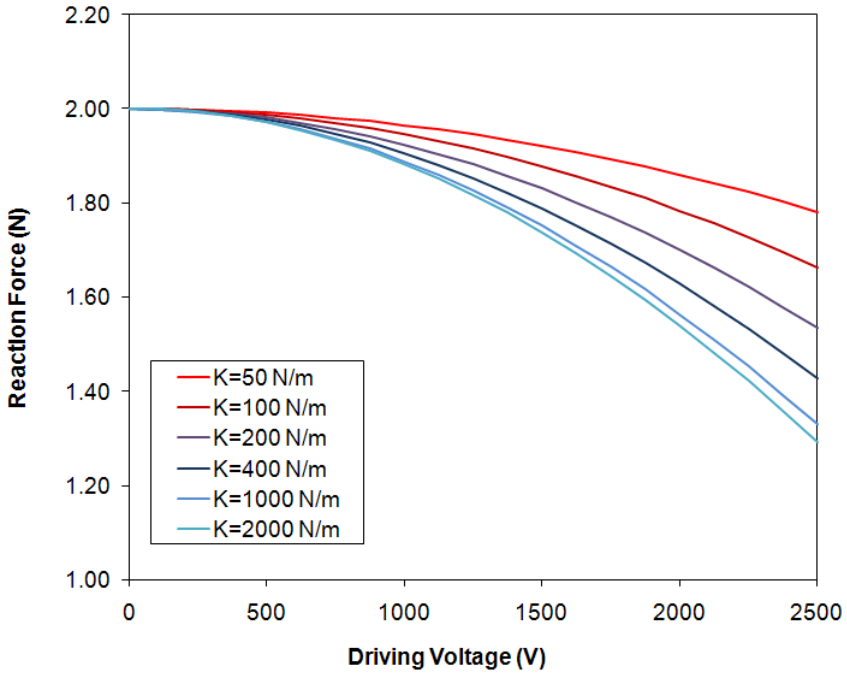

Figure 39. Decreasing of reaction force (for several spring stiffness K).

From the datasheet of the sensor/actuator it is possible to estimate a mathematical relation of the electric capacity (C/nF) as function of extension ($\Delta x/mm$) in the range $0 < \Delta x < 21.7$:

$$C = 0.079\,\Delta x + 3.78$$

Combining of this expression with the graph of Figure 38 gives some information about the influence of the hosting structure on the sensing capability.

5.4.2 Number of active layers

The multilayer sensor/actuator studied until now is composed of a stack of layers, four active and one passive to sense. The sensor layer, with his stiffness, in effect decreases the performance of the active part. The aim of the following analysis is to simulate different configurations, varying the number of active layers, and to compare.

The first evident consideration we can do is that the performances increase with this number. In fact the ratio between the active layers and the sensing one (not active) is more and more high. Less evident it is to evaluate what is the optimal configuration, that means what the optimal number of active layer is. Above a certain value the performances do not increase noticeably. The effort, and the cost, to produce more staked configurations is not compensate with the performances we can obtain, if the weight of the device is also take into account.

The following four configurations are considered:

- 4 + 1 layers (namely 4 active layers and 1 layer for the sensing)
- 9 + 1 layers
- 19 + 1 layers
- 39 + 1 layers

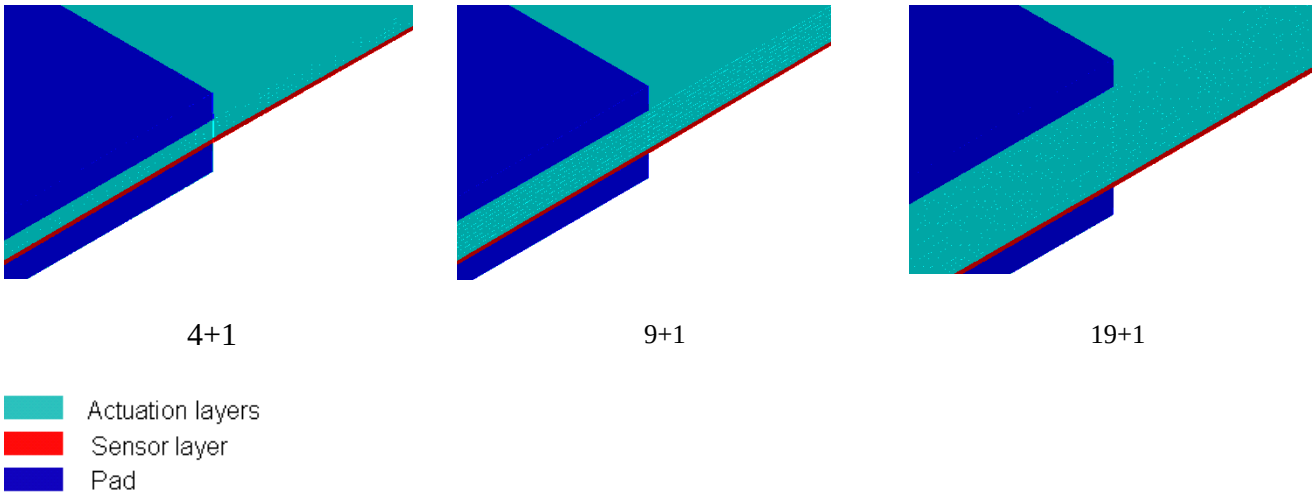

Figure 40. Sketch of the multilayer sensor/actuator with his number of layers.

The main characteristics and the performances of the four configurations are compared in the following table:

	4+1 layers	9+1 layers	19+1 layers	39+1 layers
Total Thickness (mm)	0.185	0.37	0.74	1.48
Pre-load (N)	2	4.5	9.5	19.5
Extension pre-load (mm)	10.9	12.5	13.3	13.7
Extension at 2500 V (mm)	6.3	8.3	8.9	9.3

Table 5. Performance comparison.

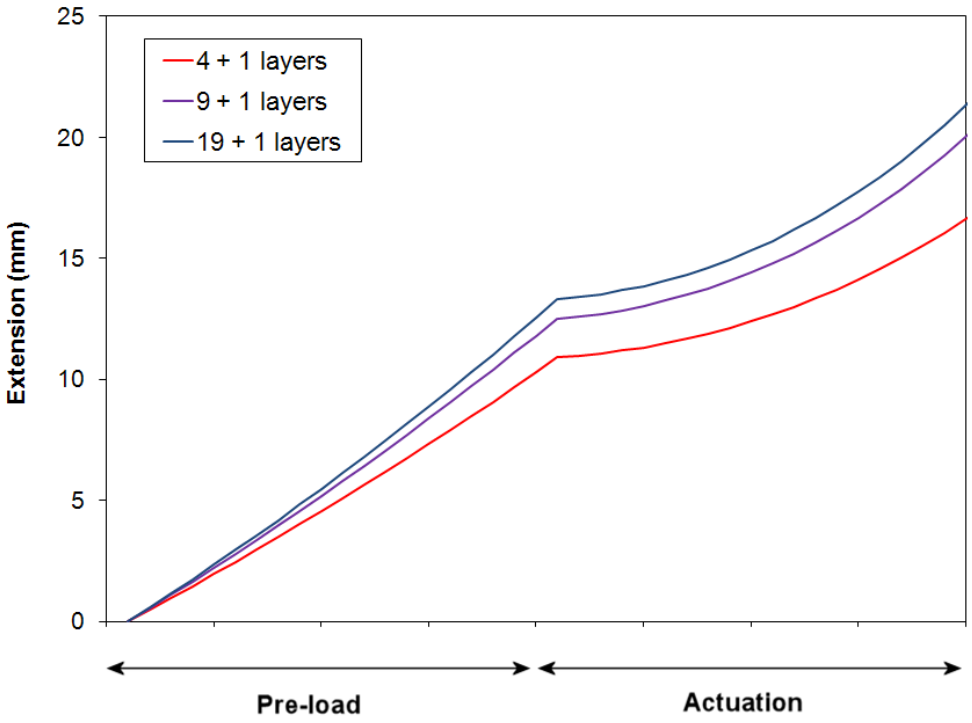

Figure 41. Preload and actuation sequence for the first three configurations.

As evidenced from Figure 42, after a configuration with 20 layers the maximum extension of the device not change noticeably. If we consider the performances as function of the weight of the actuator (Figure 43), the behaviour is different. The pre-load/weight ratio increases with the number of layers but the extension/weight ratio decreases dramatically.

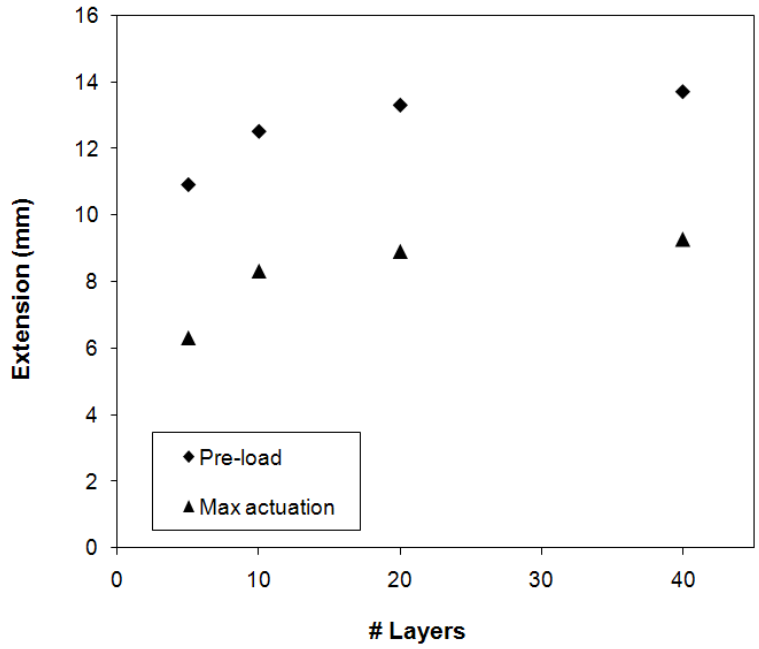

Figure 42. Comparison of the max extension under actuation of four configurations.

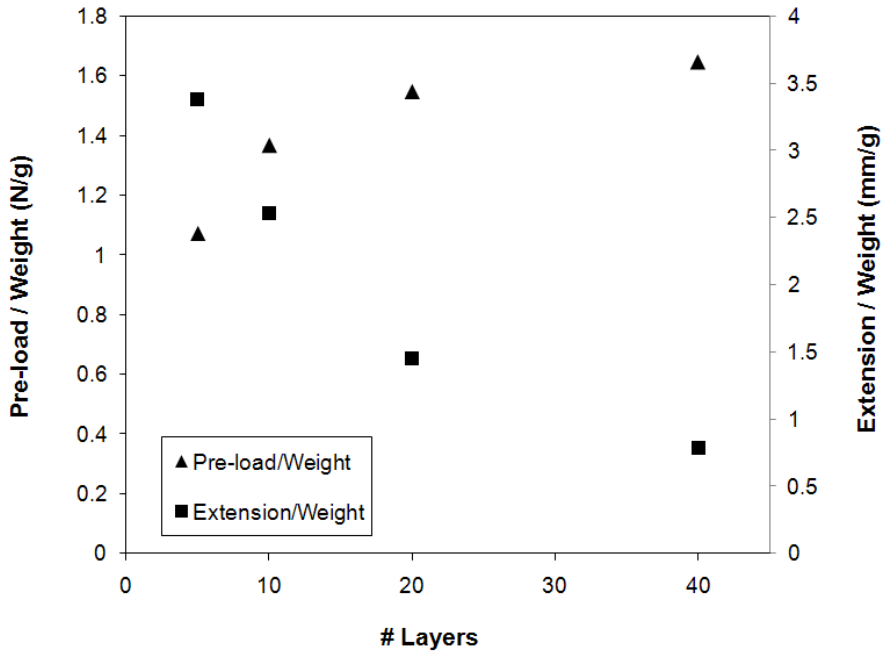

Figure 43. Comparison of the specific performances of four configurations.

5.5 References

[1] Carpi F., De Rossi D., Kornbluh, R. Pelrine R. and Sommer-Larsen P. - *Dielectric Elastomers as Electromechanical Transducers Fundamentals, Materials, Devices, Models and Applications of an Emerging Electroactive Polymer Technology* - Elsevier Science, March 10, 2008

[2] Benslimane M., Gravesen, P. and Sommer-Larsen P. - *Mechanical properties of dielectric elastomer actuators with smart metallic compliant electrodes* - Smart Structures and Materials 2002: Electroactive Polymer Actuators and Devices (EAPAD) Edited by Bar-Cohen, Yoseph. Proc. SPIE Vol. 4695, p. 150-157

[3] Sommer-Larsen P., Kofod G., Shridhar M.H., Benslimane M. and Gravesen P. - *Performance of dielectric elastomer actuators and materials* - Proc. SPIE Vol. 4695, p. 158-166, Smart Structures and Materials 2002: Electroactive Polymer Actuators and Devices (EAPAD), Yoseph Bar-Cohen; Ed.

[4] Kofod G. and Sommer-Larsen P. - *Silicone dielectric elastomer actuators: Finite-elasticity model of actuation* - Journal: Sensors and Actuators A:Physical. Vol./Iss.:122, 2 , 2005

[5] Pelrine R.E., Kornbluh R.D. and Joseph J.P. - *Electrostriction of polymer dielectrics with compliant electrodes as a means of actuation* - Journal: Sensors and Actuators A 64 (1998) 77-85

[6] Baldacci S., Serafini L., Zolesi V.S., Thurecht F., Pfeiffer E.K., Sommer Larsen P., Carpi F., De Rossi D., Lampani L. and Gaudenzi P. - *Development of Electro Active Polymers Configurations to Monitor and Control Deployable Space Structures* - 1st CEAS (European Air and Space Conference) 10-13 September 2007, Berlin (Germany).

6

Buckling sensor/actuator

Different kind of polymeric electroactive sensor/actuator, based on a buckling functioning scheme, produced and developed from Centro Piaggio of the University of Pisa are modelled. The choice to model such kind of actuator is motivated for its strong three-dimensionality, in order to validate the numerical procedure also for non-planar deformations.

6.1 The working principle

The buckling sensor/actuator is a dielectric elastomer actuators specifically designed [1] to operate with out-of-plane unidirectional displacements of a rubbery membrane with sensing capabilities. The aim is to produce an actuator, dielectric elastomer type, capable of showing large displacement in response to applied electric field, more than others. When a flat sample of elastomer coated with compliant electrodes is considered, electrically induced deformations are not able to produce any curvature of the sample, unless specific 'tricks' are adopted.

Basically, two main strategies can be recognized as effective for this purpose: the first one is to use electrodes with different stiffness, the second is to operate on the boundary condition in order to induce a buckling effect.

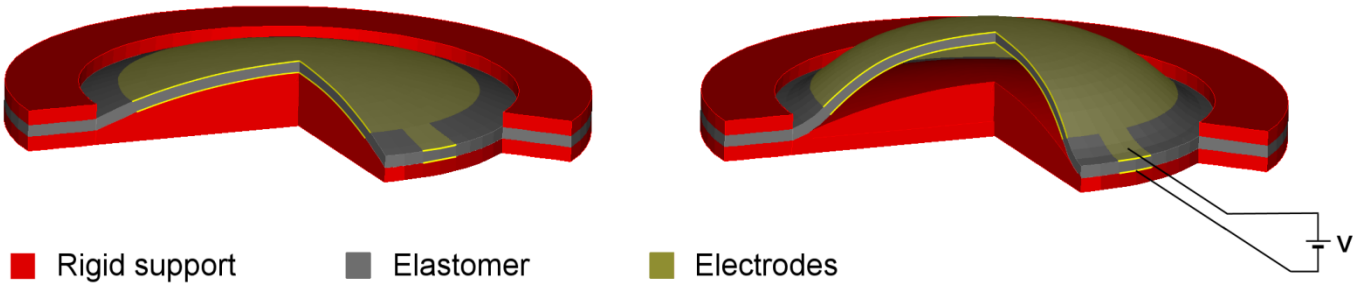

Figure 44. Working principle of a buckling actuator.

The Figure 44 illustrates this second device that is the argument of the thesis. The prototype of actuator is composed of an elastomeric membrane, circular shaped, coated with two electrodes with the same compliance. This disk is constrained by a rigid ring with the aim of avoid the membranal expansion of its bound. When an electric field is induced in the dielectric elastomer through a high voltage difference between the electrodes, an electromechanical stress state is produced in the membrane. This stress field determines a in-plane expansion of the membrane but the constraint of the ring forces a typical situation of elastic instability, the buckling. In this manner a in-plane expansion is transformed in a out-of-plane deformation.

Nevertheless such as deformation produces a not controlled wavy shape. In order to drive the deformation out-of-plane to take a regular shape it is necessary to force the membrane with an hemispheric rigid support. The Figure 45 shows the buckling shapes without (a) and with (b) the presence of the rigid support. In the first case a non-axisimmetric deformation is produced.

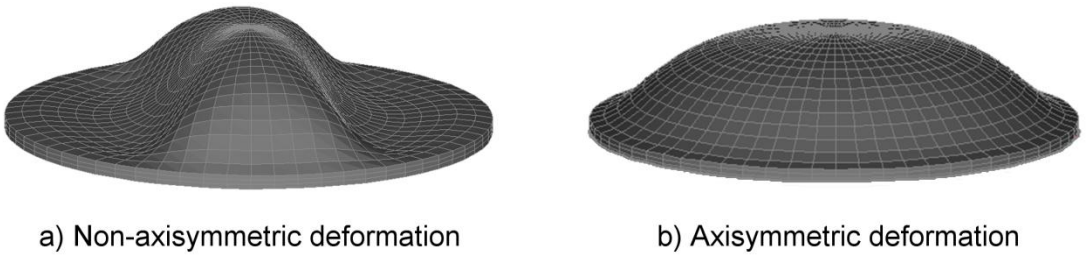

Figure 45. Buckling shapes without (a) and with (b) rigid support.

The support is pushed on the membrane and produces a stress field already during its (electrically) inactive state. Then, a high voltage difference applied between the electrodes and the membrane moves in the direction identified by the pre-deformation, as a combined result of both the pre-deformation itself and the electrically sustained surface expansion.

In terms of sensing capability, two configurations can be considered: the first one relies on a piezoresistive sensing, while the second on a piezocapacitive effect.

Piezoresistive sensing

A sketch of the constitutive components of a buckling actuator with an integrated piezoresistive sensor is presented in Figure 46. The actuation part of the device consists of a thin circular membrane of dielectric elastomer coated with two compliant concentric circular electrodes. The membrane is arranged onto a rigid hemispheric support. A concentric ring-like frame provides boundary constraints for the actuator. In order to provide the device with a sensing function, a piezoresistive displacement sensor is coupled to the upper side of the actuator; it consists of a resistive compliant strip fabricated on a second thin layer of dielectric elastomer. The sensing strip can be made of the same material used for the actuation electrodes.

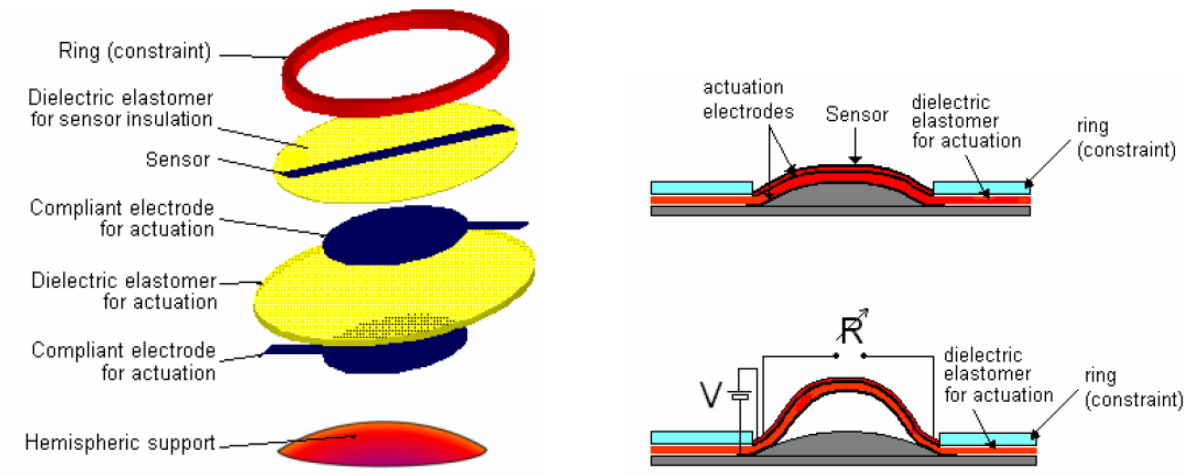

Figure 46. Assembly and working principle of a buckling actuator with integrated piezoresistive sensor.

When a high voltage V is applied between the electrodes, the opposite charges on their surfaces generate an attractive force, which compresses at constant volume the intermediate dielectric membrane. Accordingly, its thickness tends to be reduced while its area tends to be increased. However, the membrane cannot radially expand, owing to the boundary ring. Nevertheless, the initial out-of-plane arrangement enabled by the underlying hemisphere makes the membrane to lift up. Conversely, without any initial pre-deformation the activation would basically induce just an uncontrolled wrinkling of the elastomer surface. Following the actuation of the membrane, the overlaying sensing strip deforms and varies its resistance R accordingly. By monitoring the value of the resistance, the displacement of the device can be measured and followed.

Piezocapacitive sensing

The basic actuation part of the device consists again of a thin circular membrane of dielectric elastomer coated with compliant electrodes and arranged onto a rigid hemispheric support. However, for this second configuration (Figure 47) a thin layer of dielectric elastomer is coupled to the lower side of the actuator. This insulating layer hosts a third compliant electrode, working as one of the two electrodes of the sensing capacitor. The second sensing electrode, that is rigid and fixed, is fabricated directly on the surface of the hemispheric support. For this purpose a thin metallized Mylar film is used, so as to easily have both the electrode and its insulation.

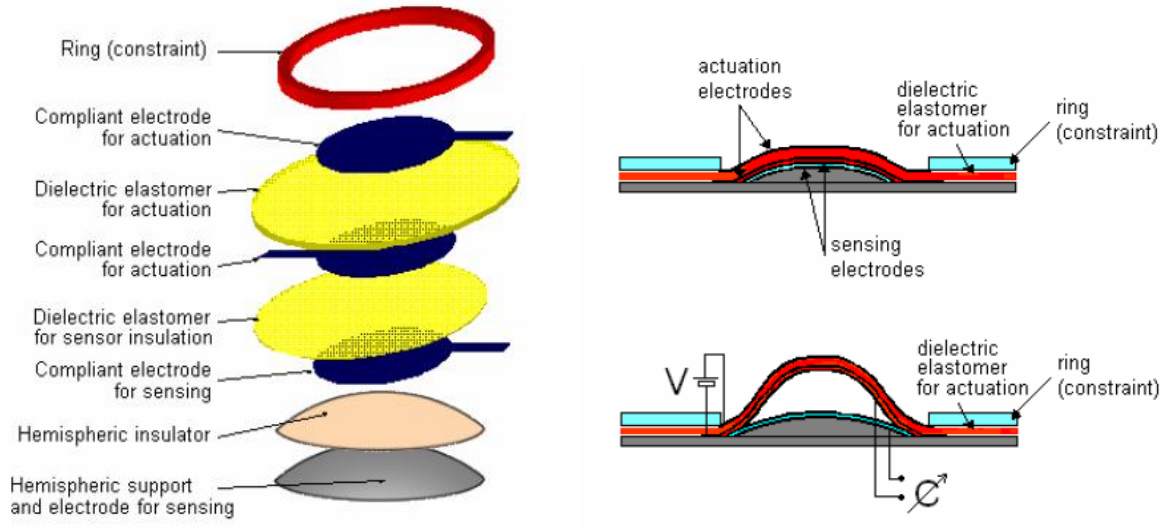

Figure 47. Assembly and working principle of a buckling actuator with integrated piezocapacitive sensor.

By applying a high voltage difference between the two electrodes of the actuator, the induced membrane displacement causes an increase of the separation between the electrodes of the sensing capacitor. In particular, the compliant sensing electrode lifts up with respect to the fixed sensing electrode; this generates a decrease of the measurable capacitance.

6.2 The prototype of the buckling sensor/actuator

Some prototypes have been manufactured from Centro Piaggio with different size. A finite element model is referred to one [1] of these devices and the performances are compared. The prototype under analysis is composed of a membrane fabricated by using a silicone rubber (TC-5005 A/B-C, BJB Enterprises Inc., USA) as a dielectric elastomer. The characteristic of this rubber is to be very soft, with an elastic modulus of about 60 kPa, in order to enables high deformations. The active part of the membrane is a disk of 30mm diameter and 0.85mm thick. The hemispheric support is made of an insulating resin and had a height h_0 of 3mm. A thin conductive silicone layer is used to create each electrode. The actuator is driven with a maximum voltage of 8.5 kV that induces in the dielectric an electric field of about 10 V/μm. For higher values the device risks the breakdown of the dielectric.

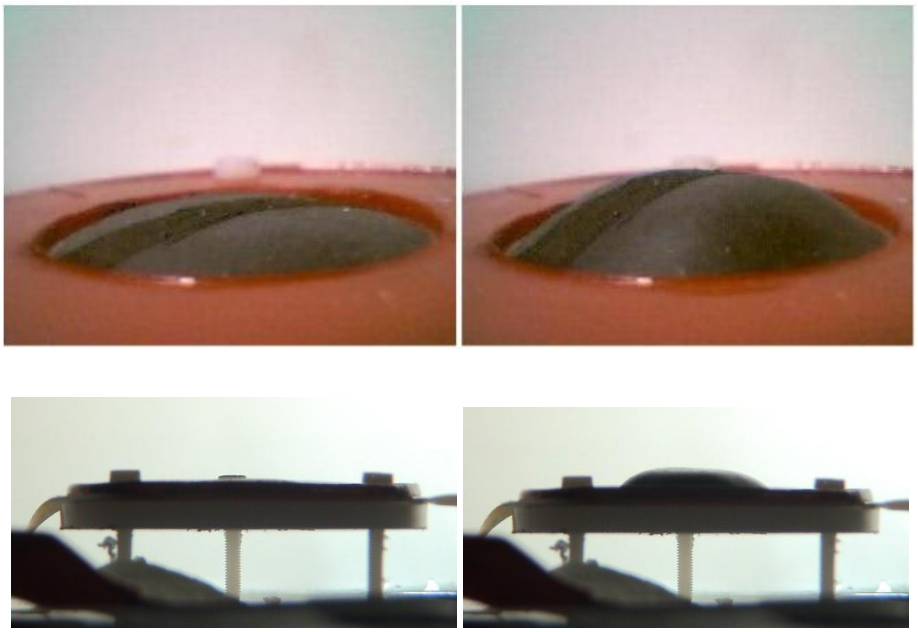

Figure 48. Prototipe of EAP Buckling sensor/actuator

The static displacement in response to increasing step-wise electric fields is measured by using an optical technique. In particular, data are used to quantify the difference between the electrically-induced value h and the rest value h_0 of the membrane height with respect to the base of the hemispheric support; moreover, the difference h - h_0 is normalised by h_0, in order to obtain the following relative displacement along the vertical direction:

$$Relative\ displacement = \frac{h - h_0}{h_0}$$

6.3 The finite element model

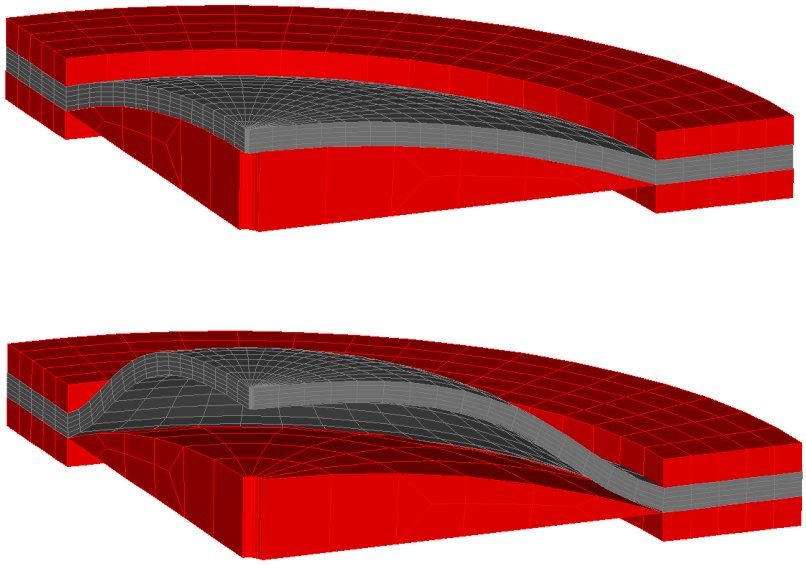

Figure 49. FE model of the buckling actuator.

In order to reproduce the behaviour of the buckling actuator through a numerical model it necessary to simulate before a pre-load phase and then the actuation one. During the assembling, the elastomeric layer is placed on a rigid substrate and forced to assume his shape. This operation induces into the elastomer a stress state we have to take in account before the simulation of the actuation. The finite element model is composed of two different geometries: the substrate and the actuator. For both 3D solid elements 8 nodes have been used. In the first phase the substrate is pushed in contact of the elastomer, originally plane, until to induce a spherical cap shape (Figure 50). A series of contact elements with 4 nodes are distributed on the surface of the bodies to avoid their compenetration. The bound of the elastomer disk is clamped.

In the second phase, starting from the configuration with the stress state included, a driving voltage linearly growing to a final value of 8500 V is applied. An electric field into the active layer of the elastomer is generated by the electrostatic subroutine of the code. This second phase is illustrated in Figure 51.

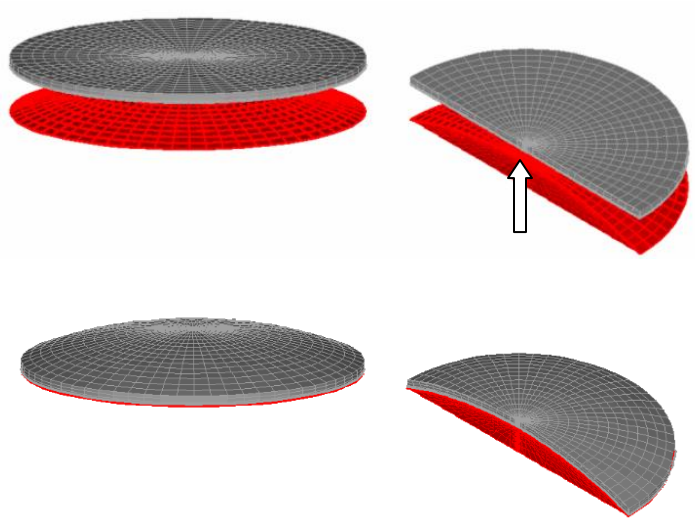

Figure 50. Pre-loading step of the FE model of the buckling actuator.

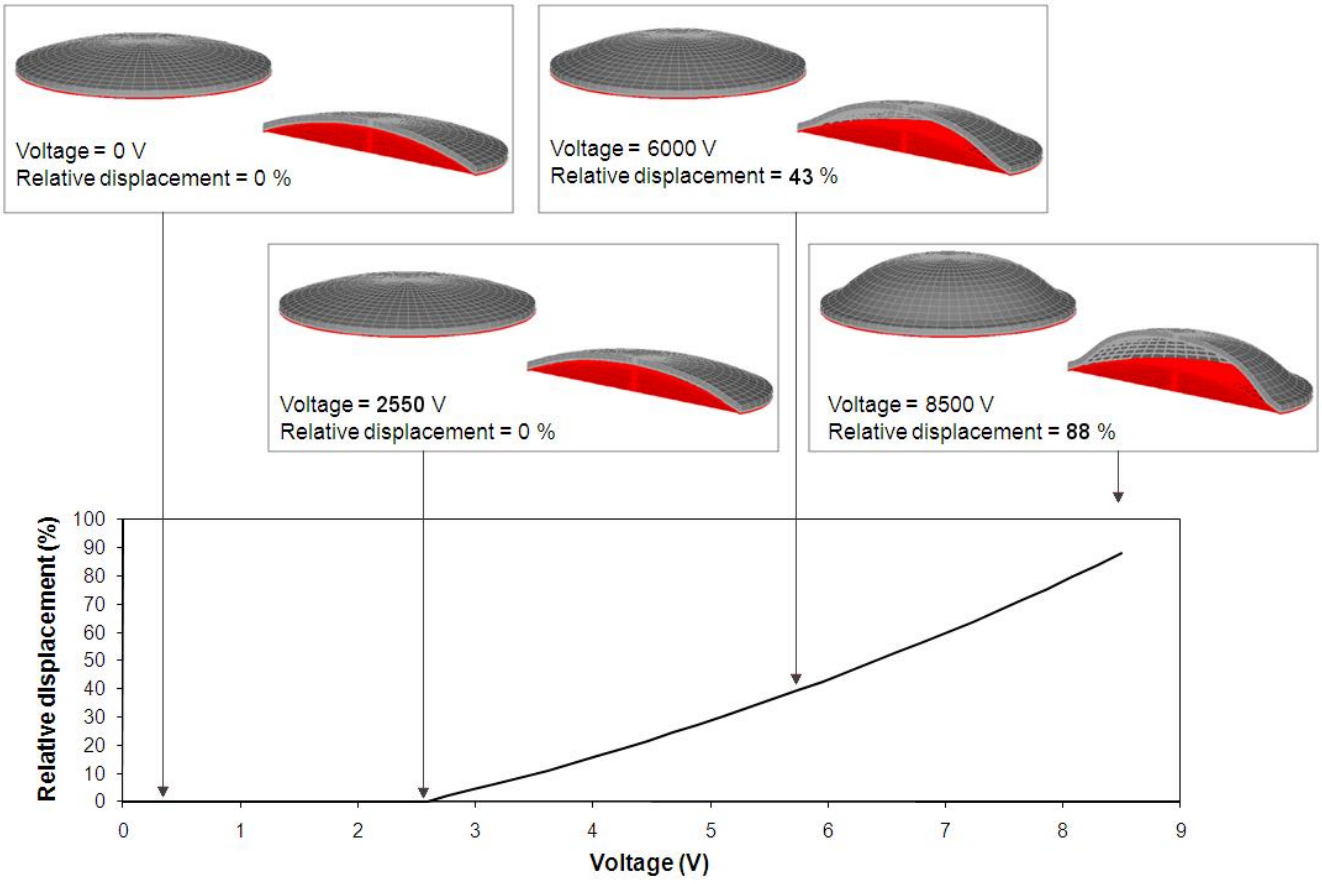

Figure 51. Simulation of the actuation phase.

It is possible to observe in the numerical results a not regular behaviour. Into the range 0-2550V any displacement is produced. The elastomer has to recover the initial pre-stress: the extension balances the initial stretching. At 2550V all the pre-stress is recovered and the membrane is not stressed. After this value the effects of the driving voltage begin to produce the displacement.

The Table 6 resumes the mechanical characteristics used in the numerical models with a constitutive behaviour between stress and stretch expressed in terms of two constants c_1 and c_2.

In Figure 52 the non-linear constitutive behaviour is compared with the linear one.

Silicone TC-5005
Young's modulus = 60 kPa
$\sigma = 2\left(c_1 + \frac{c_2}{\lambda}\right)\left(\lambda - \frac{1}{\lambda^2}\right)$ Mooney-Rivlin theory
c_1 = 10 kPa c_2 = -0.6 kPa Density ρ = 1090 kg/m^3 Dielectric constant ε = 5.3x10^{-11} F/m

Table 6. Silicone TC-5005 material characteristics.

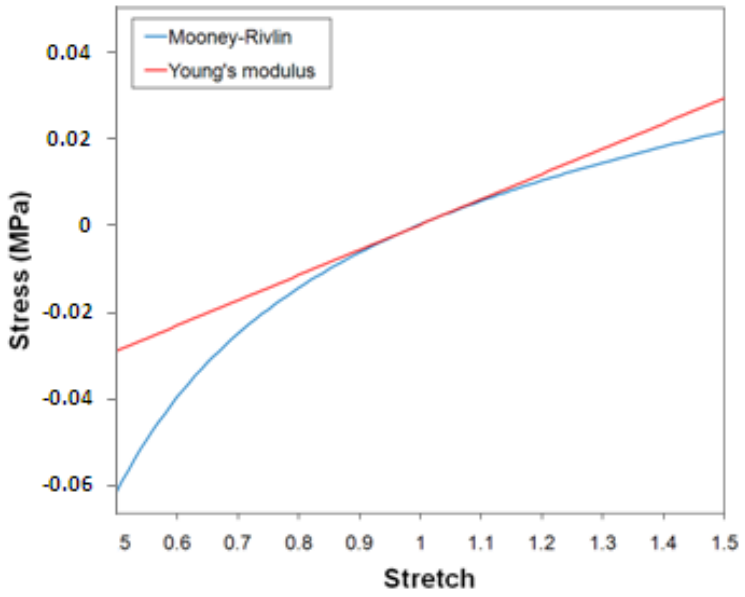

Figure 52. Silicone TC-5005 constitutive behaviour.

The comparison graph between the numerical and experimental displacement of the top of the bubble vs the driving electric field is reported in Figure 53. The numerical model approximates sufficiently the experimental behaviour very hard to reproduce. The strongly non-linear nature of the problem superimposes the difficulty we encounter in an analysis of elastic instability. Such as combination not allows to obtain better results at the moment.

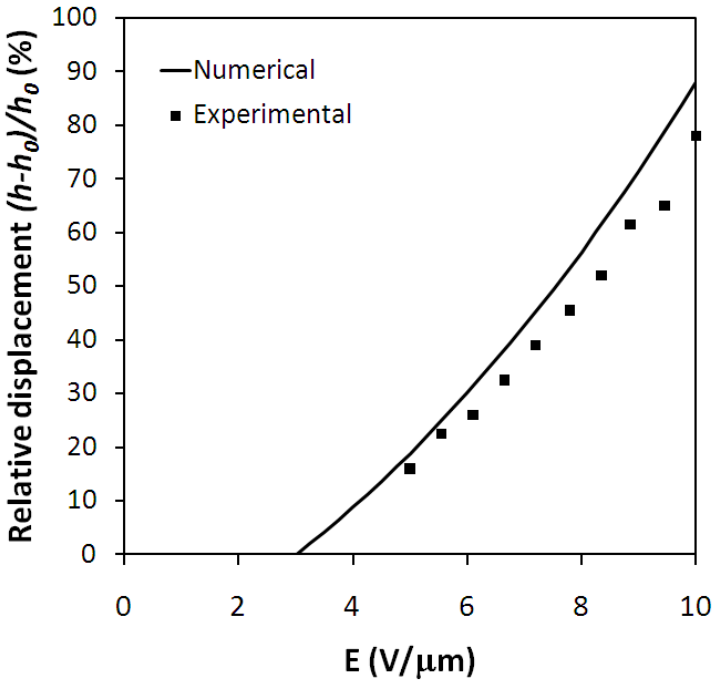

Figure 53. Bucking actuator – numerical/experimental comparison.

6.4 Effect of the gravity on the actuation behaviour

An interesting comparison can be done between two different cases of gravity effect. Until now the actuator has worked against the gravity. In a new configuration the actuator is placed in up-side-down position and it works with the support of the gravity.

Observing of the graph reported in Figure 54 can evidence the following considerations: working in the direction of the gravity increases the performances. The actuation is progressive and the threshold of actuation droops (wider range of actuation). Working against the gravity decreases the performances and increases the buckling effect: the actuation is less progressive and the threshold of actuation highs (shorter range of actuation). The behaviour without the gravity, important for a space application, is obviously in between.

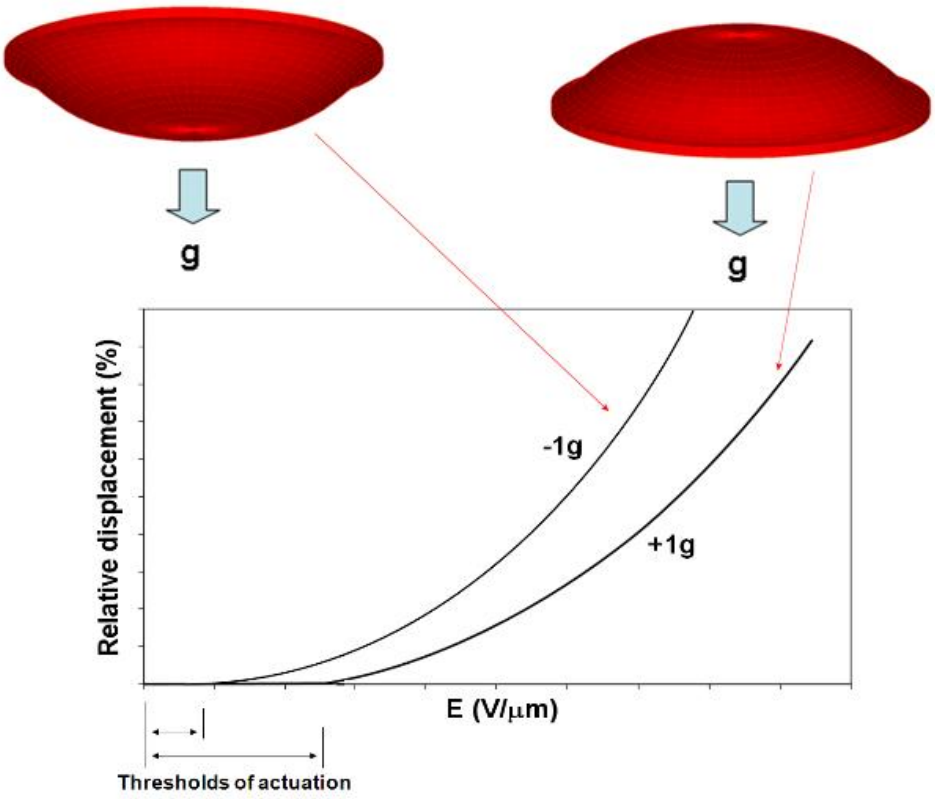

Figure 54. Effect of the gravity on the actuation behavior.

6.5 References

[1] Carpi F., Fantoni G., Frediani G. And De Rossi D. – *Buckling actuators with integrated displacement sensor* – In Dielectric Elastomers as Electromechanical Transducers Fundamentals, Materials, Devices, Models and Applications of an Emerging Electroactive Polymer Technology - Elsevier Science, March 10, 2008

7

A space application for the multilayered sensor/actuator: CFRP deployable/inflatable boom

In this chapter the development of a technological demonstrator, such as an active boom, is reported. During this phase a new engineering solution to control the vibration of such kind of structure, based on the morphing of his cross-section and then acting on the inertia moment terms is proposed. This kind of control allows to vary at local level the stiffness of this pipe structure through four sensor/actuators positioned internally. With the aim of develop an adequate control law, a multibody numerical model with flexible elements is built. In this manner the finite element model of the boom is associated with the multibody model equipped with sensors and actuators and controlled with a loop implemented in Matlab-Simulink environment. The designing development of this technological demonstrator is then completed with the study of a control algorithm.

7.1 Potential Spacecraft Applications for the EAP

7.1.1 Gossamer structures

In recent years, NASA has introduced the “gossamer” expression to label those forms exceptionally low in mass and suitable for packaging into very small volumes (when compared to conventional space items): in general, this term applies to inflatable and membrane structures for

space use. The technology of gossamer structures has been increasingly taken into consideration in the frame of space applications (Figure 55) to allow for an optimization process of the mass-to-size ratio of large structures such as solar arrays, but also antennas as well as scientific equipment. The "foldability" of a structure becomes more and more efficient as the actuator's size decrease, since the mass gain of a structure which strength is optimized for weightlessness might be reduced by the adoption of sometimes necessary bulky actuator to perform the deployment once in space. In this frame the adoption of EAP as actuators for deployable/foldable structures is certainly the path to provide a further step ahead in the optimization of the launch mass of such structures.

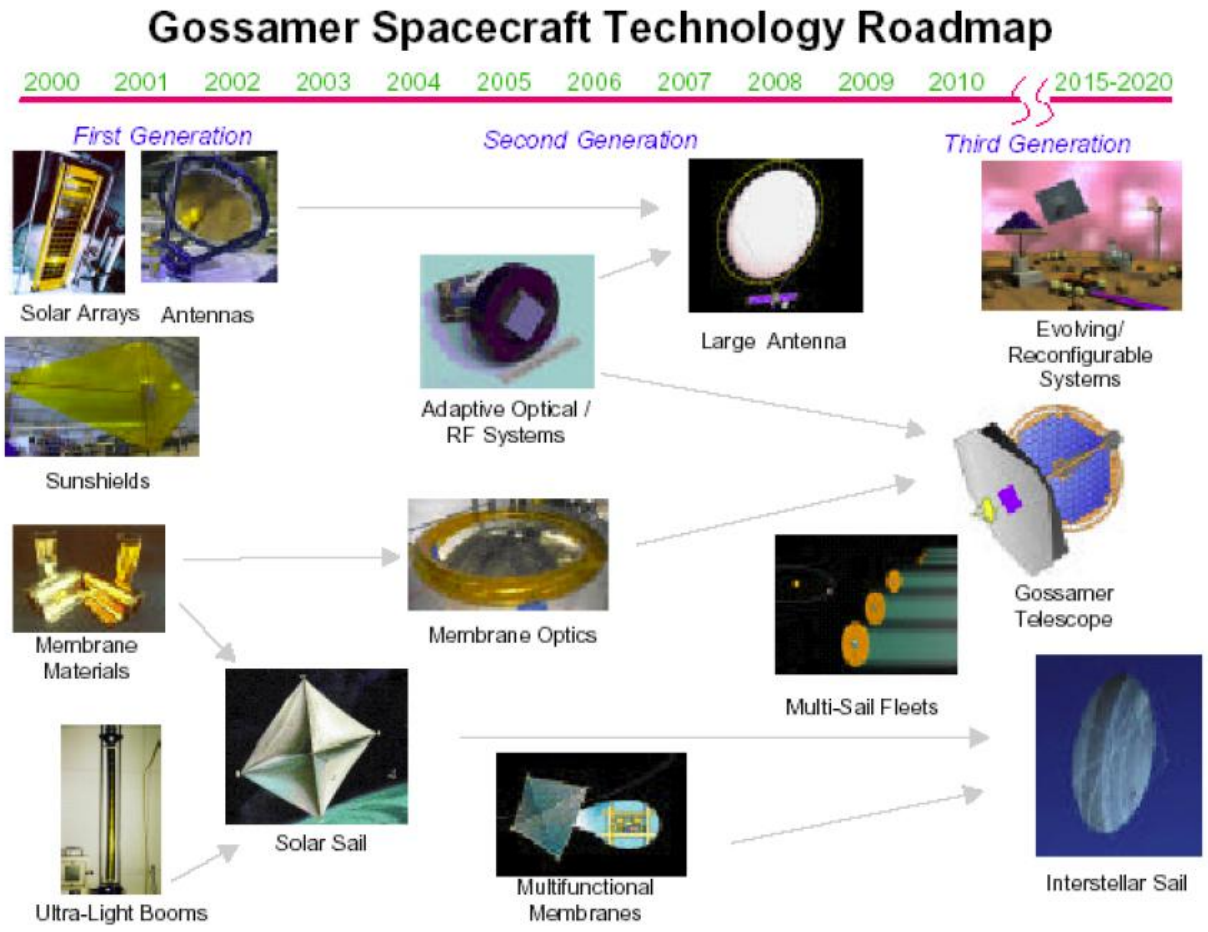

Figure 55. Technology roadmap of gossamer spacecrafts.

We find Flexible Wall Expandable Structures (FWES) a better, more descriptive term, as it is this initial compliance of the walls that allows both a compact packaging and a geometric efficient use of the materials that – in combination with a design for the space environment proper – also leads to the items' low mass. The installation sequence on station may include a material's rigidization procedure (mechanical, physical, or chemical), spinning the spacecraft (for a rotationally-stabilized object), pressurization (for continuously-inflated objects), etc. The range of technological approaches to FWES implementation seems as vast as that of the applications for such structures.

One can organize the field, for instance by sorting structures in accordance to use and major requirements as shown in Figure 56:

Mechanically extendable

- Deployable: those structures which extension is generally due to a linear actuation of segment in different sizes (telescopic motion). Telescopic booms for solar arrays is a typical application of deployable structure
- Unfurlable: likewise an umbrella, “unfurlable” are those structures which are characterized by large surfaces that are kept extended by bracings which are actuated by a linear motion along a rigid boom. Solar sails are the typical application of furlable structures
- Foldable: those structures which packed configuration is characterized by a stack of identical segments connected by a flexible joint, or a hinge. Antennas can be realized also as foldable structures, as well as solar arrays.

Inflatable

- “Lightly-loaded” structures: generally sized from stability requirements, and for high packaging efficiency, very low specific mass, large size; the tension within an element's wall is of the order of 0.1 kN/m; one further distinguishes between:

    - "backbones" support structures, with a small integration between structure and system function occurs, and
    - "precision structures" where the structural element and its shape have a direct system function impact
- "Heavy-duty" structures: sized to carry larger loads (generally, pressurization forces), with a typical requirements: large enclosed volume, moderate packaging efficiency, specific mass; often, compatibility with crew presence; the tension within an element's wall is of the order of 100 kN/m.
- "High-temperature" structures: sized to sustain significant temperature levels (above 1000K), e.g. as induced by entry into a planetary atmosphere.

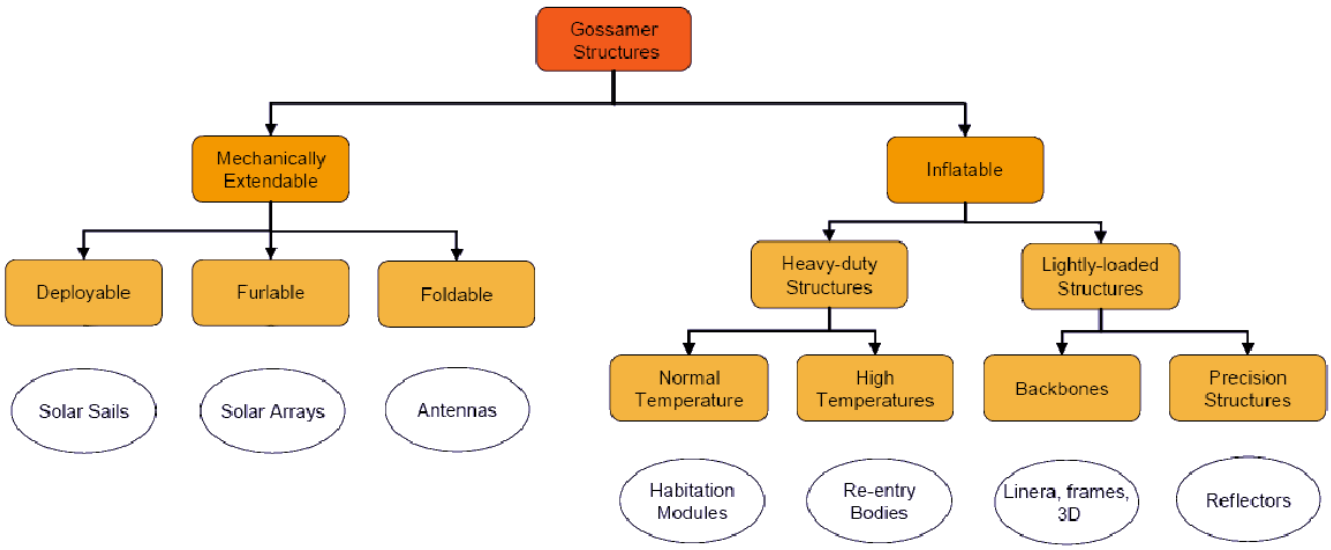

Figure 56. Classification of gossamer structures.

7.1.2 Multifunctional and adaptive space systems

In the same manner as the classification done for the gossamer structures an overview of the existing and future space technologies for active structures is provided. The requirements and

constraints which these potential applications impose on the materials and on the active part of the structure itself are derived.

Technologies

- Shape control on telescope mirrors and antenna surfaces
- Adaptive optics and antenna feeds for correcting wavefront errors
- High-precision metrology systems for determining surface errors
- Control of flexible structure dynamics
- Multifunctional membranes
- Self-healing materials

Benefits

- Breakthrough reduction in mission cost
- Reconfigurable systems for handling new scientific opportunities as they arise
- Systems that reactively respond to environmental stimuli
- Robust operational capability
- Substantial reductions in system mass and launch volume

From matching of gossamer structures and technologies for adaptive structure for space, several potentially interesting missions application [1][2][3][4] have been identified for the implementation of electroactive polymers: Heliopause Express (solar sail with deployable CFRP booms), Vigiwind (solar sail with inflatable booms and inflatable sustaining torus), GESS GEO SAR (maypole radar with inflatable booms), ARISE (inflatable booms, inflatable torus and inflatable secondary reflector) and ODISSEE (solar arrays with inflatable booms). In principle all missions can be "reduced" to the following main types of "structures" in which EAPs can work as actuators and/or sensors: deployable booms, inflatable booms, inflatable torus, inflatable reflectors, interfaces between membranes and torus or booms, in-between membrane segments.

7.1.3 Innovative technology: the CFRP inflatable boom with active vibration control

In order to produce a prototype for a breadboarding test activity, the efforts in designing and manufacturing have been directed on a single configuration, representative of a basic structural element analogous to a beam: the boom.

The aim is to produce a beam element for space with large dimensions, capable to be folded during earth-to-orbit transportation phase and auto-deployed in orbit. An innovative technology has been developed at this scope. The boom is composed of a skin in prepreg composite material layered around an inflatable mould made in polymeric film. Originally stowed in a folded configuration, it is then deployed by inflation in orbit and rigidized through the exposition to the solar ultrawave radiation. Lightweight nature of this structural element is synonymous of flexibility and then the boom is provided of EAP active components that allow a vibration control.

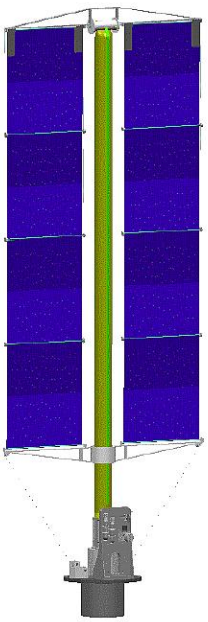

ODISSEE Solar Sail (NASA/DLR)

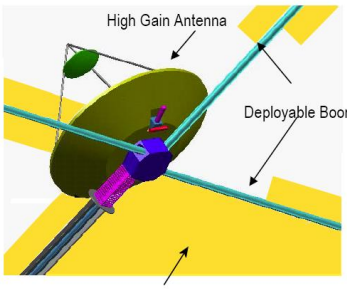

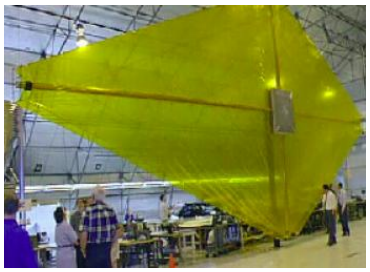

SAS split blanket solar array (Astrium)

ARISE Inflatable Reflector

Figure 57. Space applications for deployable boom.

7.2 New concept of boom vibration damping system

In order to use EAP sensor/actuators to reduce the vibrations [5]-[11] of a boom structure, a new system of damping has been developed. The working principle is to modify the cross section of a boom or a torus so that the structure can change its stiffness by changing its cross-section shape. E.g. with reference to the Figure 58 a 10% diameter decrease in Y results in an almost 25% decrease of bending stiffness in Z direction (7% increase of stiffness in Y direction). This purpose can be achieved by mean of a EAP actuator, multilayered type, mounted internally along a diameter. By an intelligent control loop one might get a relatively quick settling effect of a low frequency boom vibration. Due to the fact that EAP sheets have only an elongation performance, they must be mounted in pretension. In the case of an originally circular boom (lower manufacturing cost) the nominal configuration (without actuator power on) is an elliptical shape. Once the actuator is powered, it elongates and the boom shape becomes circular.

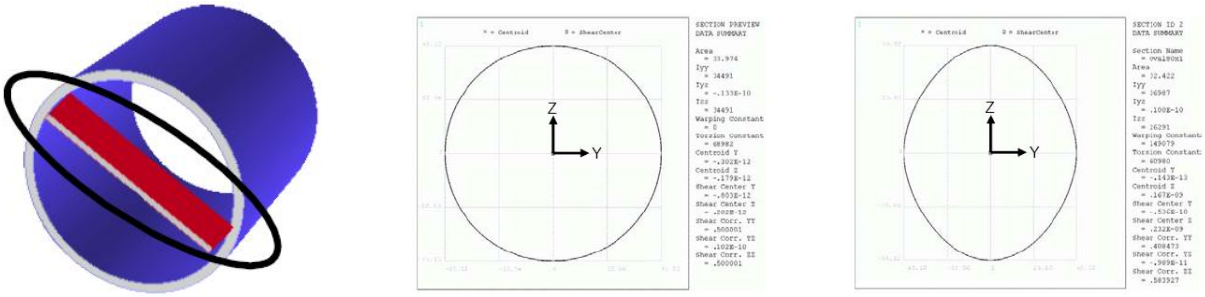

Figure 58. Working principle of boom vibration damping system

Here, the embedding structure supplies the pre-load: the inner walls of the boom have low flexural stiffness and the actuator is stretched out between them (Figure 59); hence the boom profile is compressed in the direction of the actuator and balances the actuators contractile force.

Activating the actuator will extend it and allow the cross-sectional profile of the boom to return to its natural configuration. Upon discharging, the actuator will force the structure back in the initial compressed configuration. The actuator works over its full stroke, and the induced local change of the booms longitudinal bending stiffness can be utilized to damp large-scale

vibrations. By varying the cross-sectional shape of the boom at certain points, the actuators provide a variation of the bending stiffness of the section. This effect creates the actuation effect in the structural behavior of the boom.

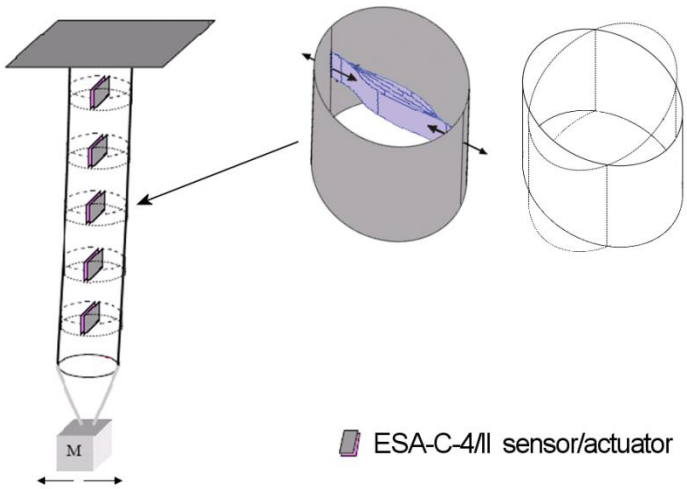

Figure 59. Working principle of the boom with EAPs for vibration control.

7.3 Preliminary study on a numerical model of the boom

The EAP actuators are characterized by large stroke and low force. The work density, the product of stress and strain, is however among the highest of all electromagnetically driven actuator technologies. In order to efficiently utilize it, e.g. to damp large-scale vibrations, it is necessary to allow the actuator to work over its full stroke range. For this reason a preliminary numerical model of boom has been developed and sized with geometrical and material characteristics optimized to obtain the maximum performances of the multilayered type actuators. Moreover it represents a starting point for the production of a breadboard.

The boom model is a tube, circular shaped, made in composite material ±45° / 0° CFRP 3.5m long, with a diameter of 130mm. Four actuators are distributed along the axis. The position of them is case study.

The configuration is cantilever in vertical position in order to reduce the effects of the gravity. The boom is closed with two end plugs in aluminium, necessary to maintain the circular shape. One is clamped to the ground, the other one has a mass that represents a payload.

The first finite element model is composed of composite shell elements. The first test is finalized to give an order of magnitude for the ovalization of the cross-section when the boom bends thorough a transversal force applied at the free end. This test is performed for a configuration without actuators. The magnitude of the ovalization of the cross-section is an indicator to determine the further insertion of the sensor/actuators. The sensing and acting capabilities are better as this parameter is large. The result of this test determines the optimal positioning of the actuators.

The Figure 60 and Figure 61 show the behaviour of the section along the axis of the boom. The ovalization effect is reduced for the presence of the constraints at the ends. The maximum effect is obtained in the middle of the length. For a tip displacement of 45mm, a maximum stretch of 2.65% of the diameter corresponds.

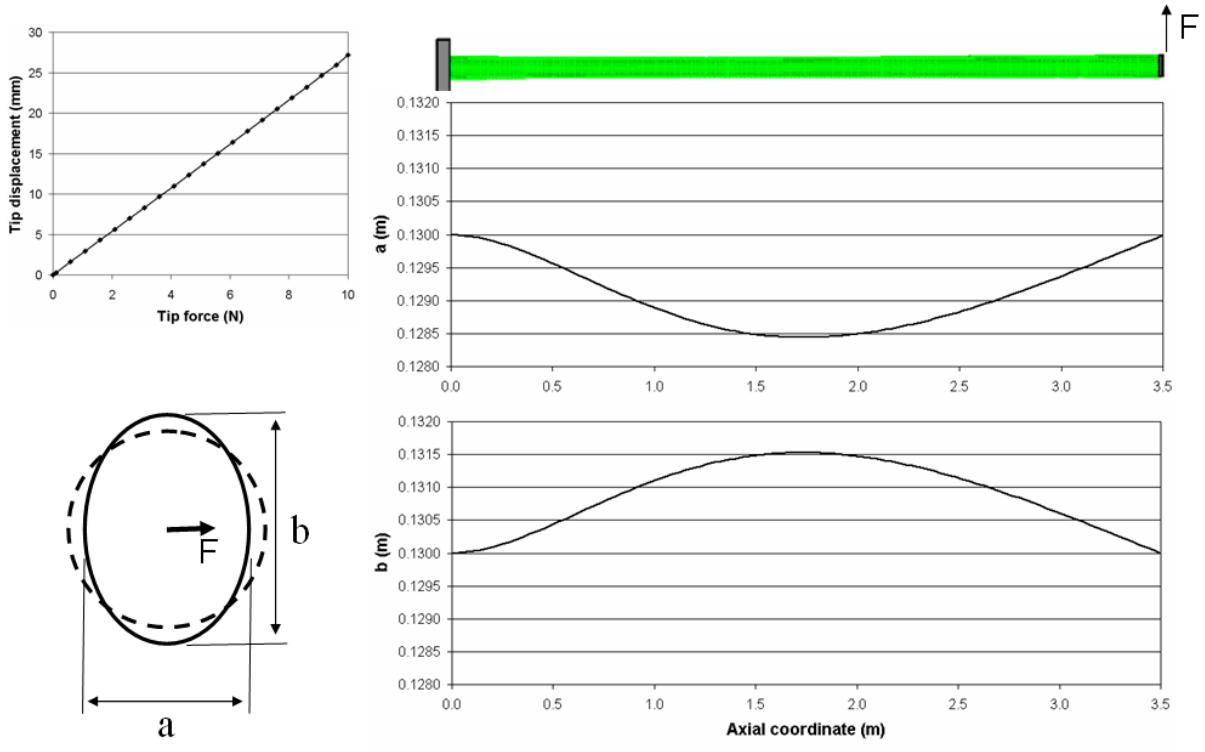

Figure 60. Ovalization effect of the cross-section along the boom under bending.

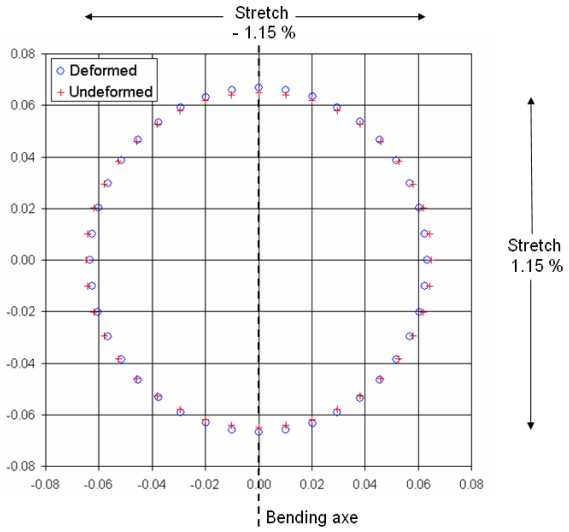

Figure 61. Maximum ovalization effect of the cross-section.

The second test performed on the finite element model of the boom is finalized to evaluate, both at global and local level, the effects of the insertion of the four actuators into the structure. In this case the boom is not subjected to external load. At global level the presence of the actuators introduces an ovalization of the section. At local level, at the connection points with the skin of the boom, a depression on the surface is evident. The sizes of these depressions are strongly dependent on the pre-loading of the actuators. Where these depressions are present the section has a reduced bending stiffness. It means the insertion of the actuators can produce a "hinge effect".

The Figure 62 resumes the results of this test.

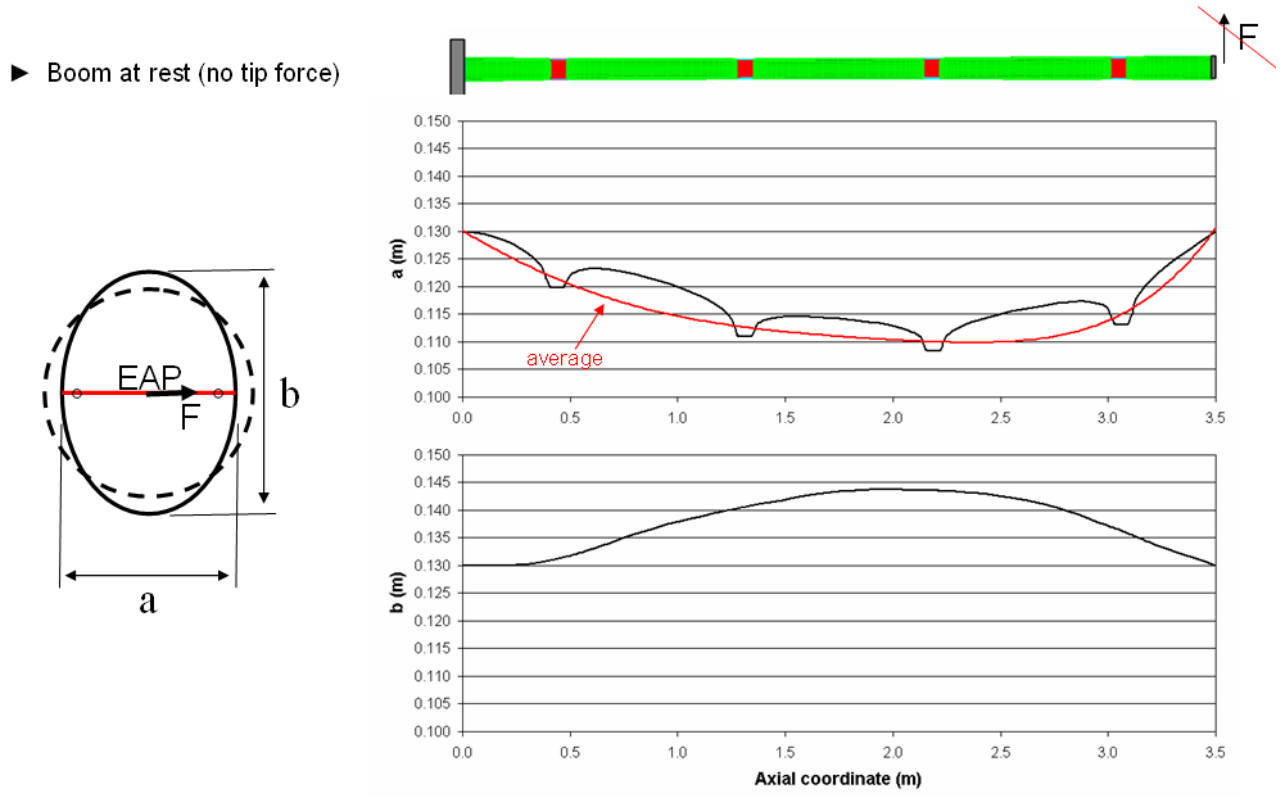

Figure 62. Ovalization effect of the section of the boom due to the presence of the actuators.

The third analysis is focused on the evaluation of the sensing capability of the EAP coupled with the boom structure. The input is a periodic transversal force applied to the free end to produce an oscillation. The load is sinusoidal and its amplitude grows linearly at beginning phase, and constant after. Two cases of load, and bending, are studied depending if the tip force lays into the same plane as the actuators or orthogonally.

The output is reported in terms of electrical capacity, through the direct measurement of the extension of each actuator, following the formula characteristic of the ESA-C-4 sensor/actuators:

$$C = 0{,}079\ \Delta x + 3{,}78$$

where the capacity C is expressed in nF and the extension Δx in mm. It is important to observe as each of four actuators feel the bending of the boom and how much its position is relevant at this scope.

From the Figure 63 is evident that the system senses two time each period, it means with a frequency double of the excitation load.

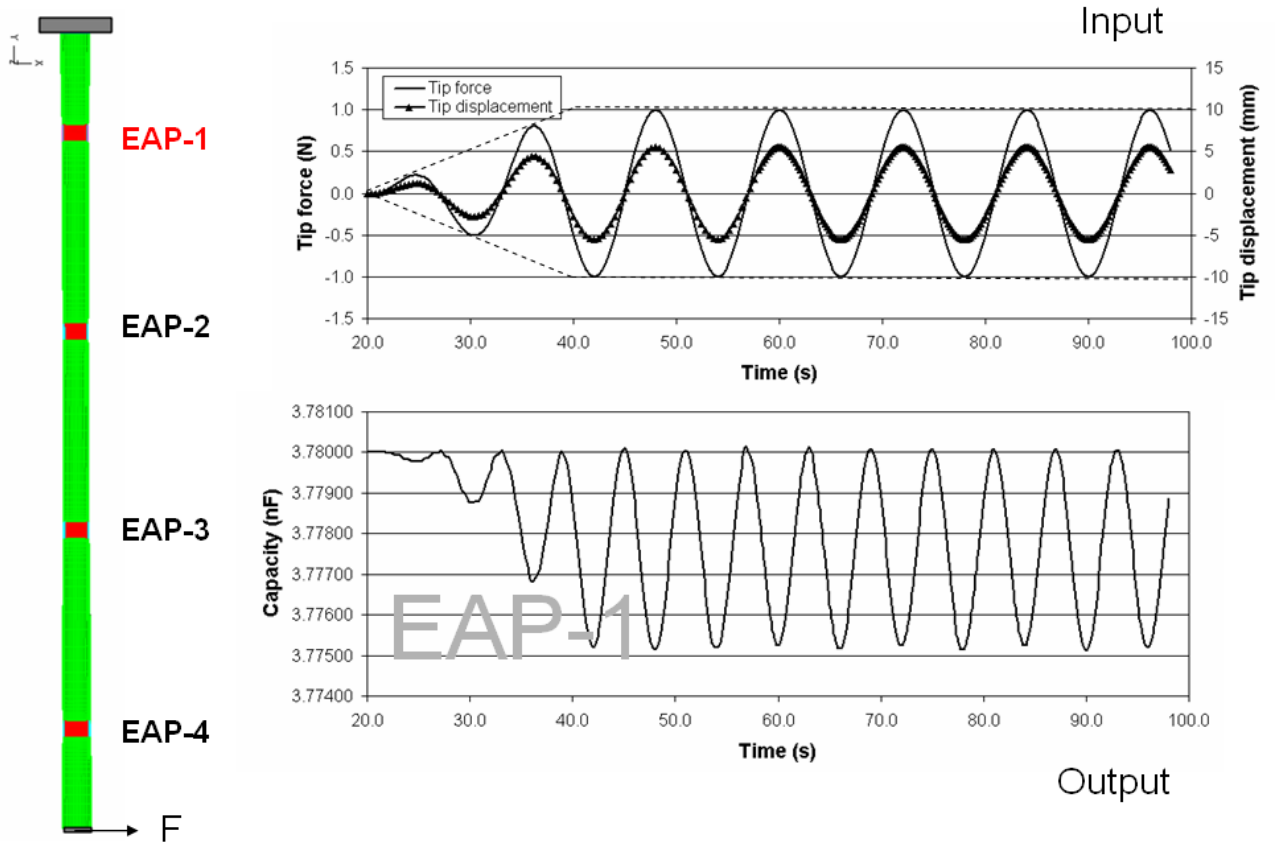

Figure 63. Sensing capability of EAP sensors/actuators for in plane excitation.

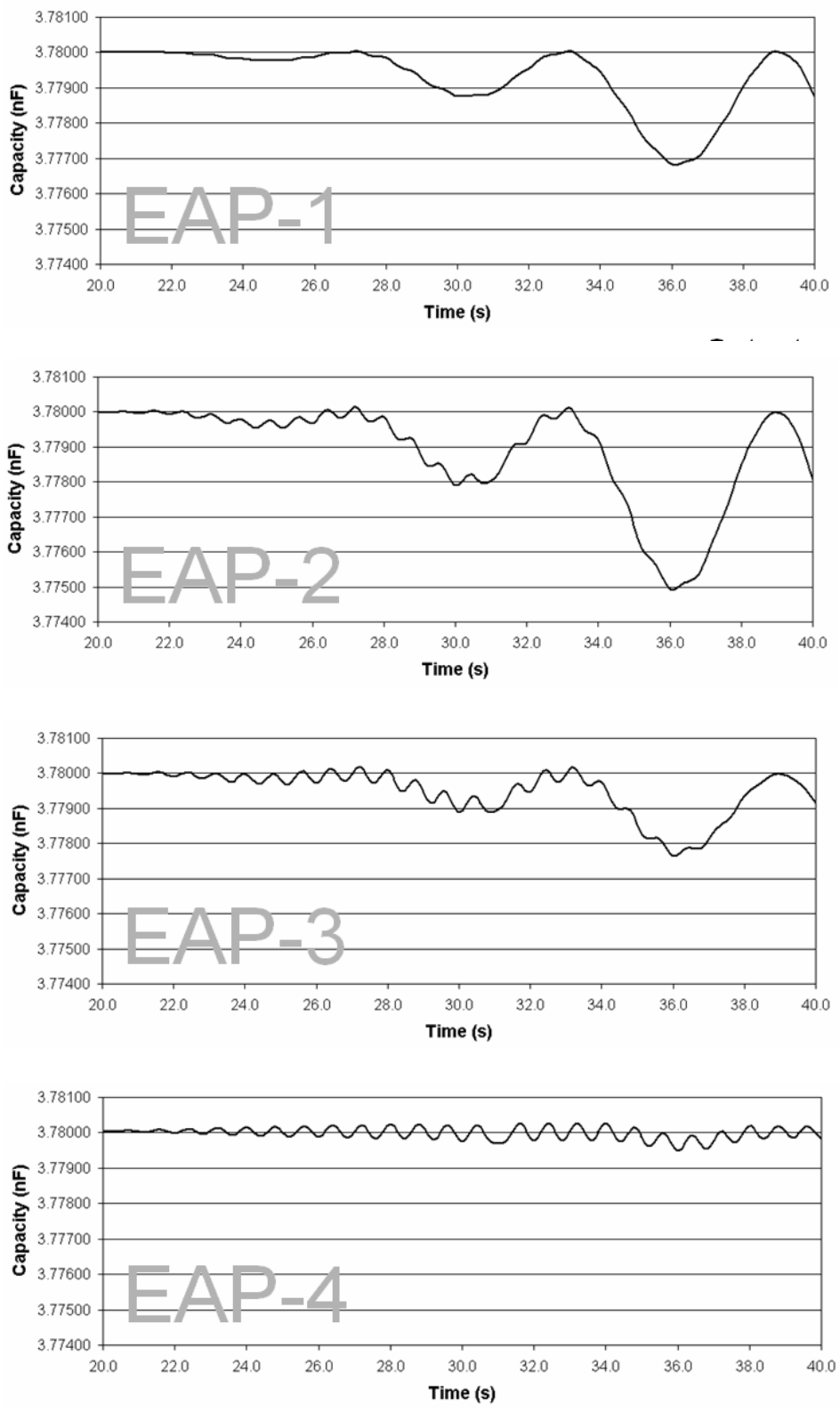

Figure 64. Load case in plane excitation – electrical capacity measurement.

The second load case concerns the bending in the plane normal to the EAP plane.

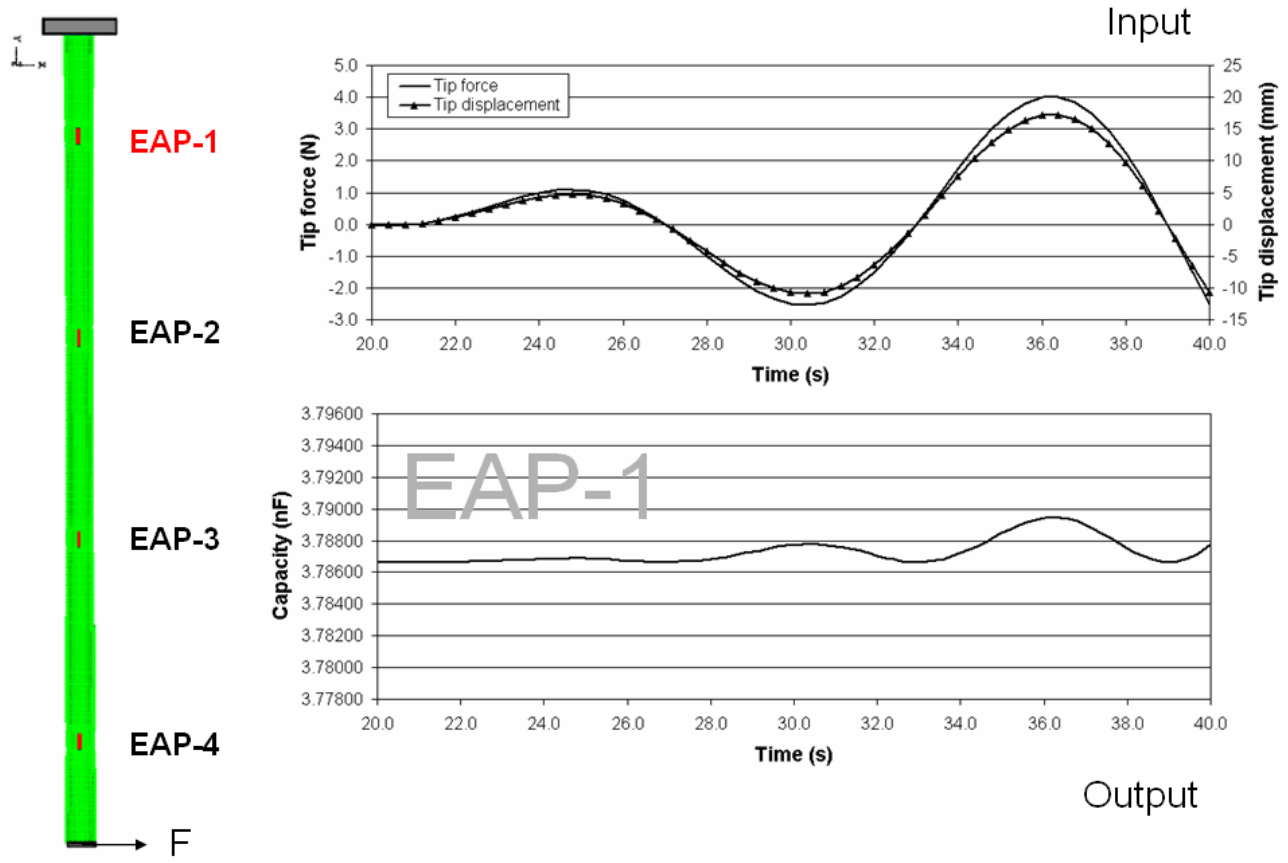

Figure 65. Sensing capability of EAP sensors/actuators for orthogonal excitation.

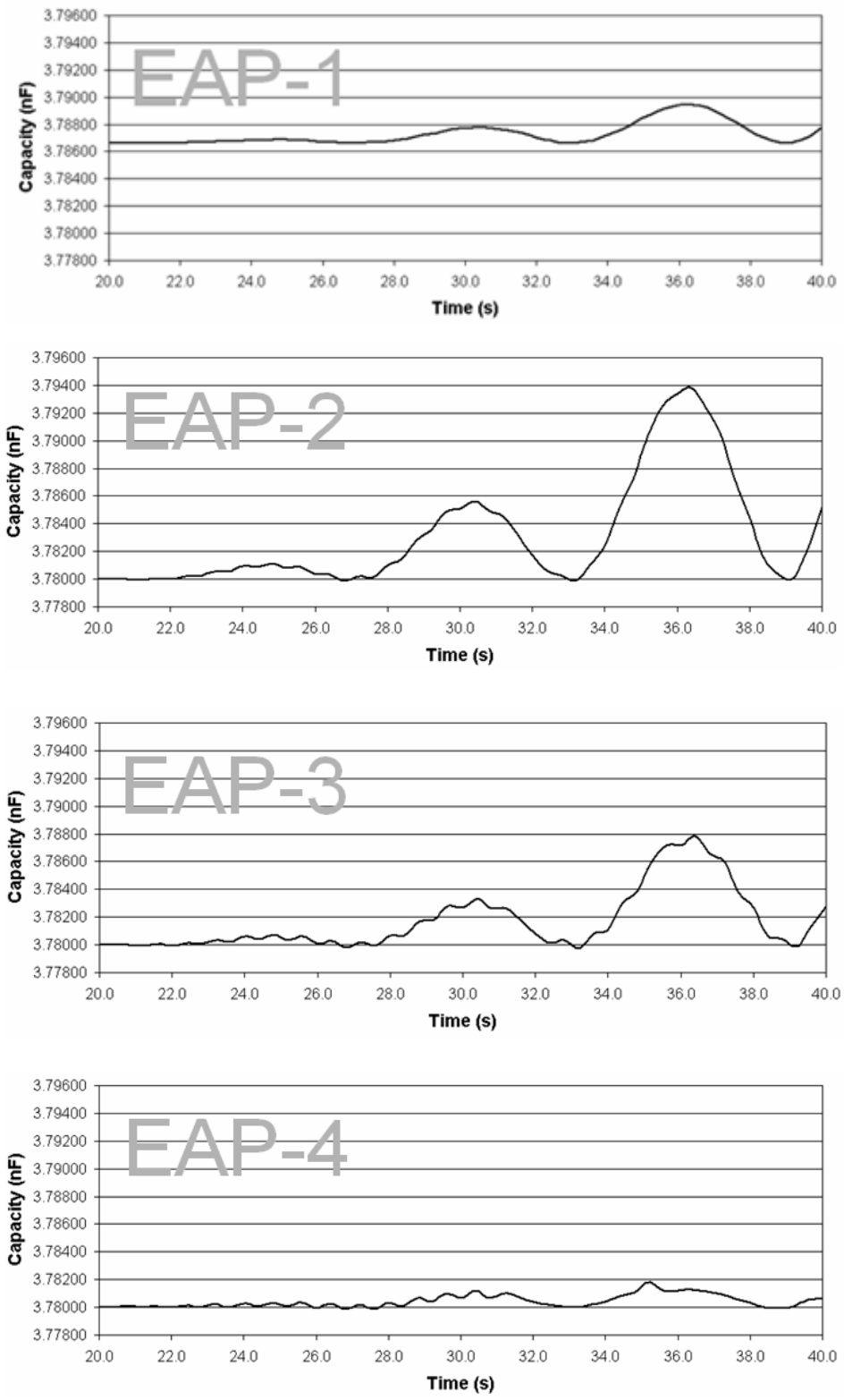

Figure 66. Load case orthogonal excitation – electrical capacity measurement.

The results of this analysis can be resumed as follow. For both load cases the EAP #2 feels better than the others. For a cantilever beam, the maximum curvature for the first bending mode is observed near the root. The EAP #1 in this sense is positioned better than the others but its capability of sensing is partially compromised by the constraint of the wall. The section of the wall is constrained to be circular and affects the section in correspondence of EAP #1, that in this manner can be less ovalized.

7.4 The breadboard

Figure 67. Breadboard of the deployable/inflatable boom with EAPs.

The breadboard [5] is dedicated for testing the capabilities of EAP actuators for damping boom oscillations. Its purpose is not the development of inflatable structures though this aspect was regarded as well. The boom was built therefore as an inflatable structure which was cured before the integration of the EAP actuators. So valuable experience was gained without an excessive risk of damage for the EAP actuators.

The boom has a nominal length of 3.5m and a diameter of 134 mm. It is made in carbon fiber reinforced polymer (CFRP): two layers of carbon fiber prepregs are applied onto an inflated nylon hose. The inner layer is made from a 45° plain weave carbon fiber prepreg with a mass of 95g/m² while the outer layer is made from a unidirectional CF prepreg with a mass of 150g/m². Thickness of the laminate is 0.6 mm (+/- 45°ply: 0.17 mm, UD-ply 0.43 mm). Two flanges in aluminium, 3.5kg of weight, are used as end caps. One of them provides the clamping to the

ground, the other represents a tip mass as a generic payload. Four actuators are positioned at 0.5, 1.0, 1.5 and 2.0m from the clamped base.

The breadboard is built in a deflated state; the prepregs lay onto the inflated inner nylon hose. The mandatory overlap of the +/- 45° layer could not be handled the other way. Further problems arose when the inner layer of nylon foil developed several small holes so that air escaped into the laminate and partly caused separation of the layers. It was found that the leeks must have been caused during production or handling of the nylon hose, because they appeared on regular distances along the boom (distance equals circumfluence of the original boom). This problem could be solved by applying a stiff bandage of nylon peel ply on the entire length of the boom. By doing so, the prepregs are compressed between the inner bladder and the outer, load taking bandage, which is able to exhaust leek air. This proved to be a better solution than the outer layer from nylon foil also because the pressure can be raised to higher values and there is less risk of laminate failures. After curing the peel ply was removed.

After laminating the boom, the pressure was released but the boom was not folded or rolled. Repeated repressurising produced a result equal to the state directly after manufacturing. Curing was first tried in a hanging position with a foil-tent and an electrical heater. Unfortunately this method did not ensure the required temperatures, so the boom was hardened in a lying position in a modular curing chamber with insulated walls built for this purpose. Temperature was controlled and kept to 87.5°C +/- 2.5°C, curing took 32 hours.

Because the gravity in this case is causing bending moments, the boom experienced some buckling and bending at the position where it was supported. These imperfections in the geometry cause a higher sectional stiffness compared to an ideal cylindrical boom.

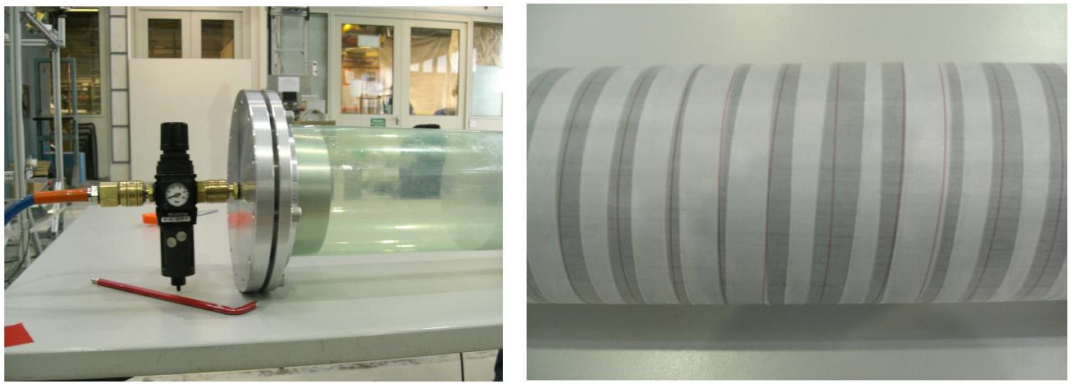

Figure 68. Flange and inner nylon hose under pressure (left). Peel ply bandage (right).

Figure 69. Boom after curing and removal of peel ply.

Some slots are produced on the boom in order to insert the actuators. EAP actuators being totally flexible are by nature ideal components in foldable structures. Therefore a solution of interfacing actuators had to be found which is flexible too. They are provided of a textile connection to be glued to the skin o the boom. For the correct integration of the actuator, the boom section has to be squeezed so that the optimum pretension of is achieved. In Figure 70 the phases of the insertion of one EAP in the boom are depicted.

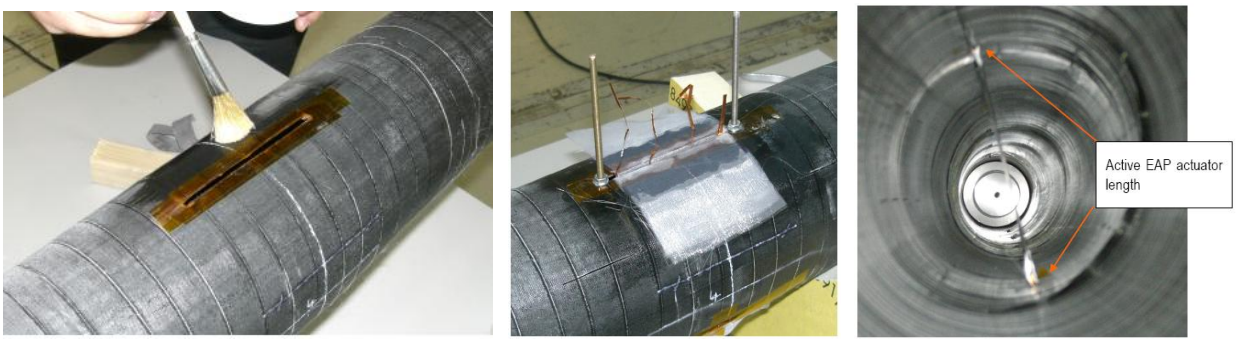

Figure 70. EAPs sensor/actuator insertion.

Figure 71. Breadboard experimental set-up.

A measurement of the stiffness of the cross-sections estimated to be a little too rigid respect to the design specifications. The complexity of the innovative technique of manufacturing not permitted to obtain the exact design parameters. In order to reduce the stiffness of the cross-sections in correspondence of the actuators, some trenches (better explained in the next section) have been cut on the composite.

7.5 Tuning of the finite element model

The finite element model

The model of the boom, with the four ESA-C-4 actuators integrated reproduces the experimental breadboard. The boom structure is modelled by composite shell elements and the actuator in the same manner as explained in the previous chapters. The laminate is composed of two layers: 0° (UD), ±45° (fabric). Thickness of the laminate is 0.6 mm (+/- 45°ply: 0.17 mm, UD-ply 0.43 mm). The characteristics of materials are reported in Table 7.

	±45° layer			***UD layer***	
E_{11}	6.360E+10	N/m^2	E_{11}	1.392E+11	N/m^2
E_{22}	6.360E+10	N/m^2	E_{22}	9.528E+09	N/m^2
ν_{12}	0.072		ν_{12}	0.311	
G_{12}	1.230E+10	N/m^2	G_{12}	2.484E+09	N/m^2
ρ	1760	kg/m^3	ρ	1536	kg/m^3

Table 7. Material characteristics from reference data

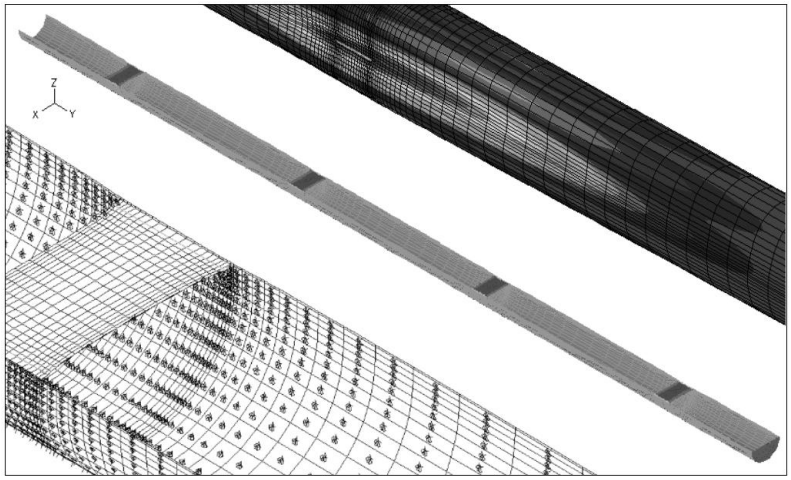

Figure 72. FE model of the boom with EAPs for vibration control.

In order to produce the shrinkage of the section of the boom, the actuator is pre-stretched before attaching it to the skin of the boom. At the equilibrium, also the section of the boom is pre-loaded. The numerical sequence adopted is to stretch the actuator to the diameter as first step, then to attach its ends (provided of fabric end-connectors) to the skin of the boom, and to release gradually the body to reach the configuration of equilibrium.

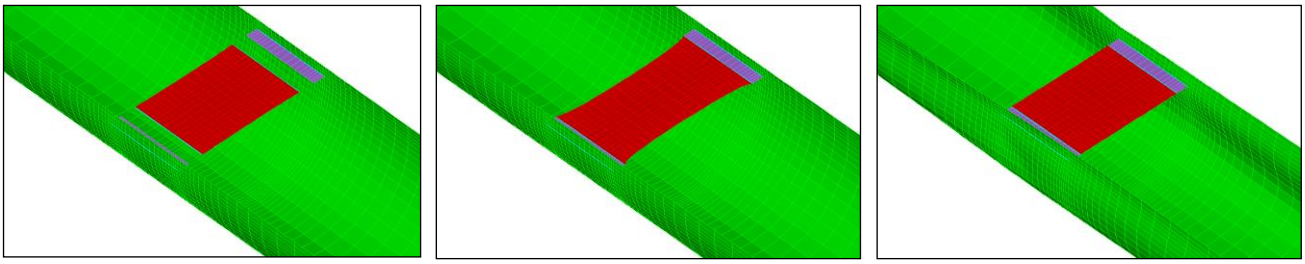

Figure 73. Simulation of insertion sequence of the actuators into the boom structure.

The breadboard produced is provided of 133 trenches to increase the flexibility around the areas where the actuators are localized. The finite element model has been improved with these trenches. A modal analysis is performed in order to investigate a possible change in behavior.

The shift of the first two bending frequencies is not relevant. The presence of the trenches does not affect the bending behavior of the boom.

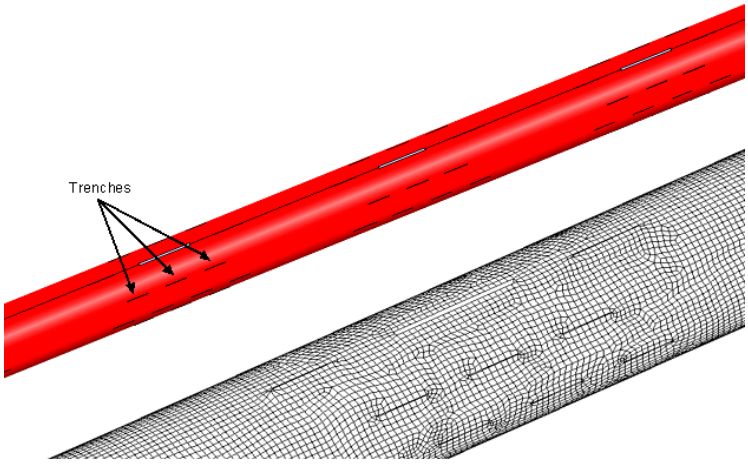

Figure 74. Finite element model of the boom improved with 133 trenches.

The dynamic characterization of the breadboard

The data acquired through the experimental test campaign are used to characterize the modal behaviour of the boom structure and to estimate the natural vibration frequencies.

In order to calibrate the finite element model, a fitting of the two first bending frequencies is performed. The first experimental frequency is 2.75 Hz, the second is 78 Hz . In the Figure 76 it is possible to observe the resonance peaks of these frequencies. There are others peaks in between; they represent the vibration modes of the "skin" of the boom and not the bending.

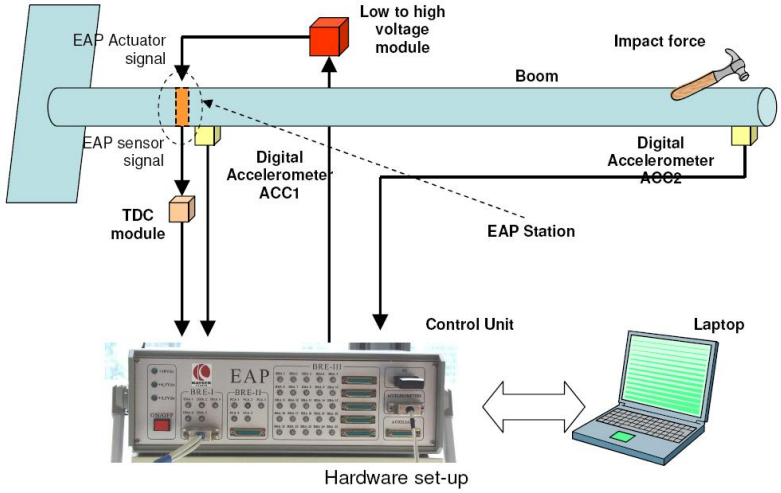

Figure 75. Dynamic characterization set-up.

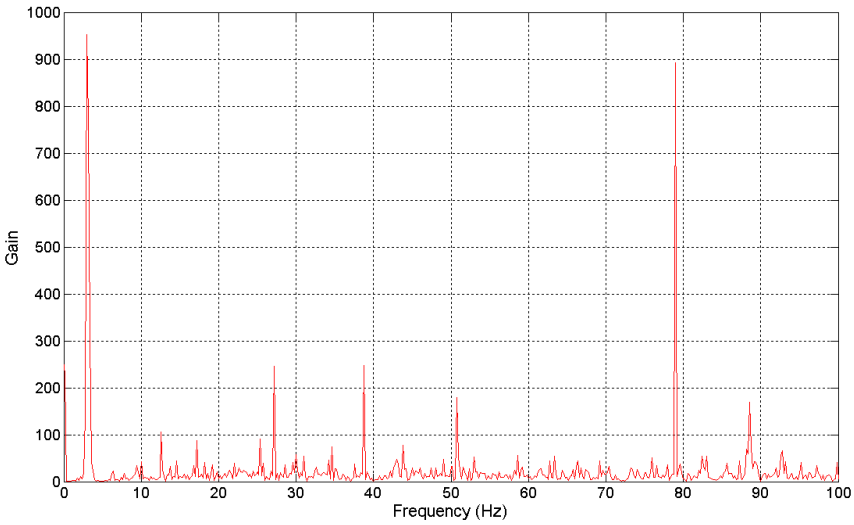

Figure 76. Experimental frequency response spectrum.

The boom is provided of a big mass at the free end (aluminium flange, 3.498 kg). This mass is an order of magnitude heavier than the mass of the boom + actuators. The presence of this mass, that represent the payload, is also necessary to decrease the dynamics of the first modes in a range available for the EAP actuators that have a not fast response (<5Hz).

As it is possible to observe from Figure 77, the tip mass is more static in the second mode. The first mode is more energetic and has to be controlled.

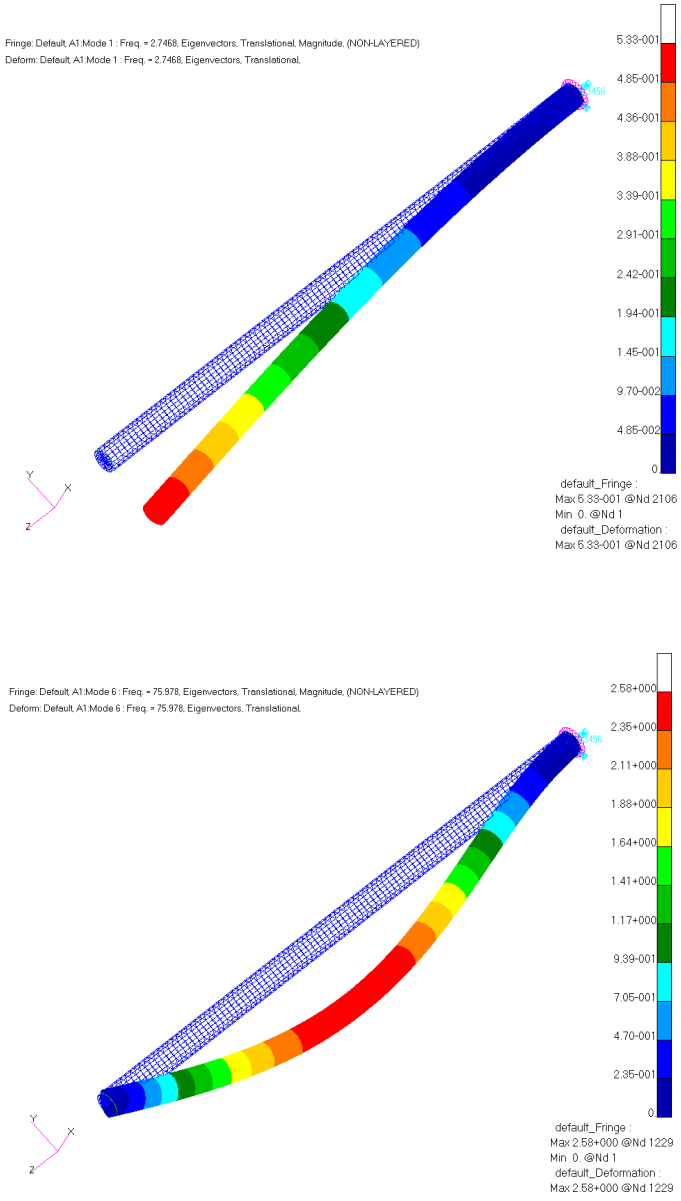

Figure 77. 1st and 2nd modes of the finite element model.

An estimation of the natural damping coefficient for the first mode is obtained from the information of the accelerometer at the free end of the boom.

Time constant [s]	= 7.6790849
Standard Deviation [%]	= 1.8520605
Amplitude	= 0.1392887
Standard Deviation [%]	= 5.6350072
Frequency [Hz]	= 2.7666667
Standard Deviation [%]	= 1.605D-14

Table 8. Data of time history.

After 10 seconds, the wave amplitude is decreased to 30%

$$\tau = 7.679 \quad s$$

$$c = \frac{1}{\tau} = 0.13 \quad Hz$$

$$\zeta = \frac{c}{c_{cr}} = \frac{0.13}{2\pi \quad 2.77} = 0.007$$

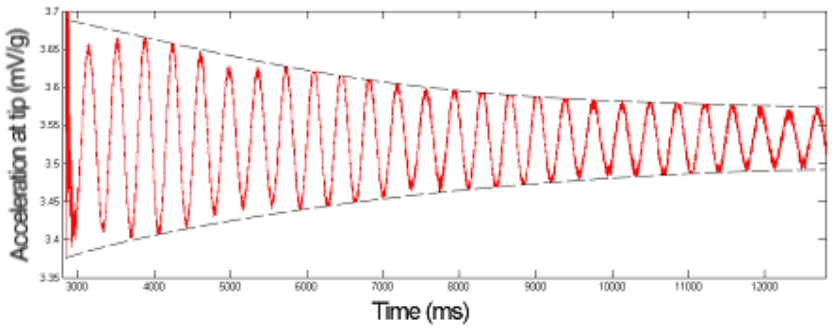

Figure 78. Tip acceleration time history.

All these information allow to identify completely the structure of the breadboard. The frequencies and the damping are resumed in the following graph obtained through a FRF analysis.

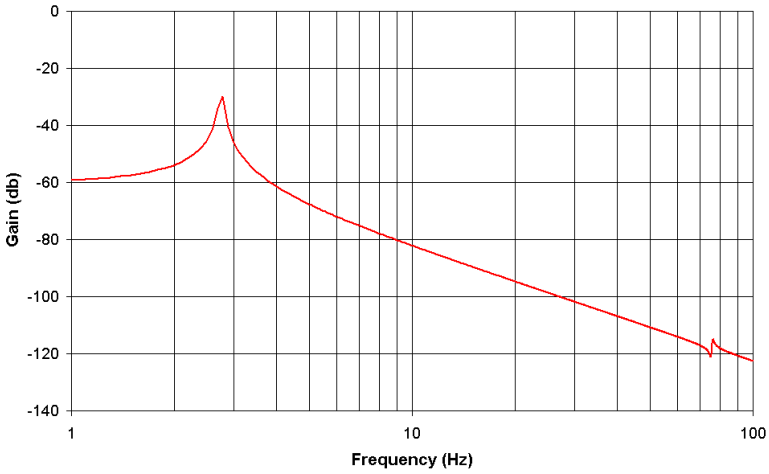

Figure 79. Numerical frequency response spectrum – gain

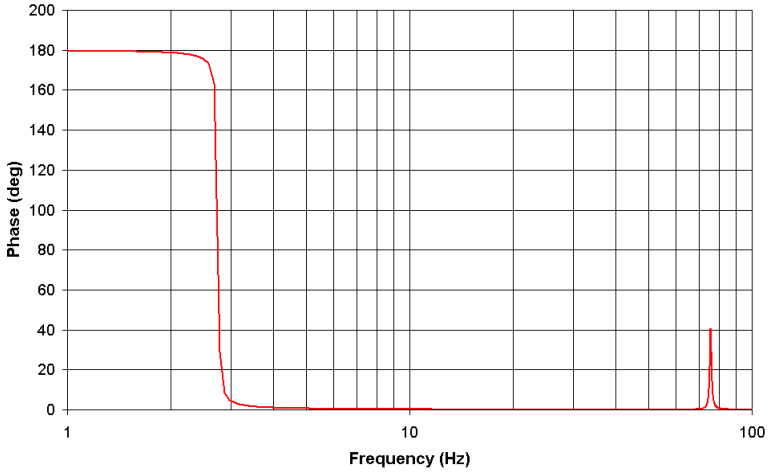

Figure 80. Numerical frequency response spectrum - phase

7.6 Multibody model

In order to develop a control algorithm to reduce the amplitude of the oscillation of the boom induced because of an external perturbation, a multibody model is created.

The boom structure is represented as a flexible body. The finite element model is imported in a multibody code (DCAP) thorough the *pre_flex* routine. Each EAP is modeled with a couple of actuators. The multibody code is then interfaced with Matlab Simulink code to provide a numerical close loop control.

During the experimental tests, some problems are encountered coupling high tension in actuation and capacity measurement in sensing. To avoid these problems, the EAP_1,3,4 work just as actuators, instead of EAP_2 that works just as sensor. As we explain in a previous section the best sensing capability for the first bending mode is achieved by the second EAP.

In DCAP model the actuators play a double role: they work to apply a preload (EAP_1,2,3,4) and to apply the control (EAP_1,3,4).

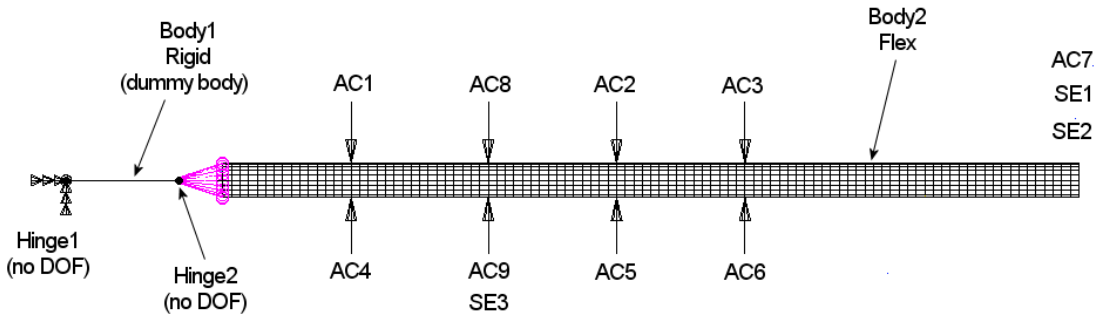

Figure 81. Multibody flexible model.

At the free end of the boom an acceleration and a position sensor are placed. These sensors are used to observe the effective oscillations of the structure and to appreciate the effectiveness of the control, but it is not used inside the control loop. The only information used in the control algorithm comes from the sensor of EAP_2.

Moreover at the free end an actuator is placed to produce an external perturbation.

We can resume the input/output to the structure as follow with reference to the Figure 81:

- *EAP_1*: preload + control actuation by AC1 and AC4
- *EAP_2*: preload actuation by AC8 and AC9 + sensing by SE3
- *EAP_3*: preload + control actuation by AC2 and AC5
- *EAP_4*: preload + control actuation by AC3 and AC6
- *Accelerometer at tip*: sensing by SE2
- *Position sensor at tip*: sensing by SE1
- *External perturbation at tip*: actuation by AC7

The experimental set-up to which the model refers is described in Figure 82. The free end of the boom is excited with a sinusoidal force generated by a shaker and monitored through an accelerometer and an oscilloscope. The second EAP, used as a sensor, transmits the information of the variation of the cross-section to the control unit, a single input multiple output (SIMO). The control unit drives the other three EAP that work as actuators.

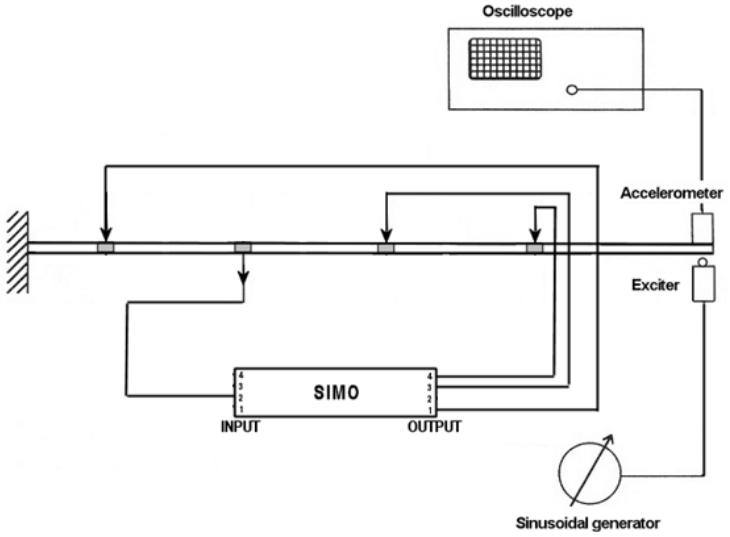

Figure 82. Control experimental set-up.

7.7 Simulink model

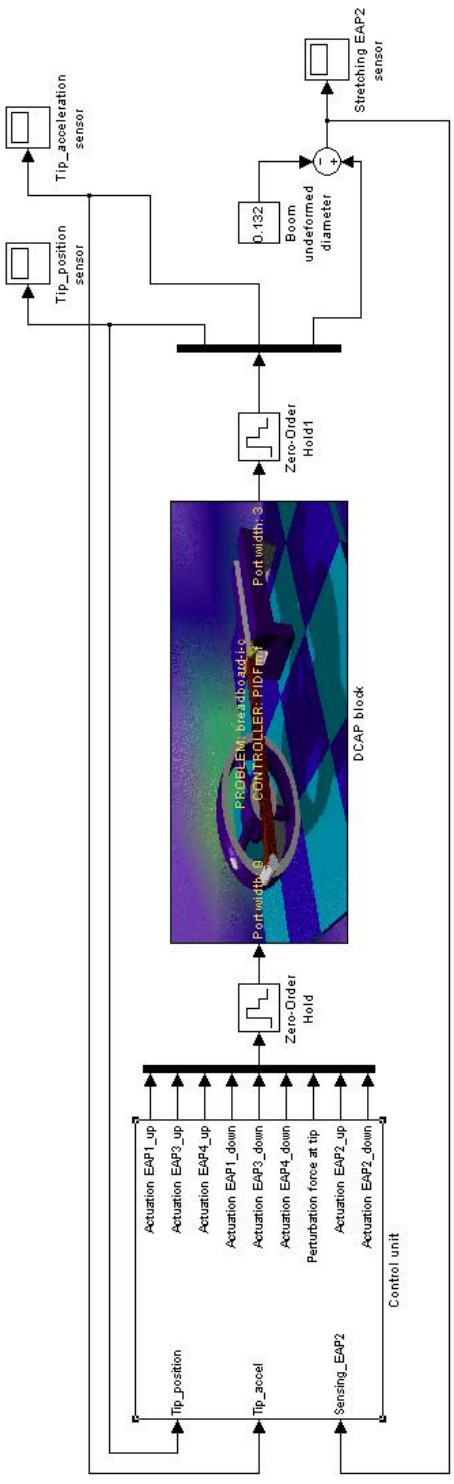

The overall control algorithm is implemented into the Simulink environment. The DCAP block resumes all the structural information of the flexible multibody model. It is interfaced with the control unit with 9 input (actuators) and 3 output (sensors).

The control unit (Figure 83) provides the management of all the actuator and sensors. Inside the control unit, the control box with the algorithm (next section) is present.

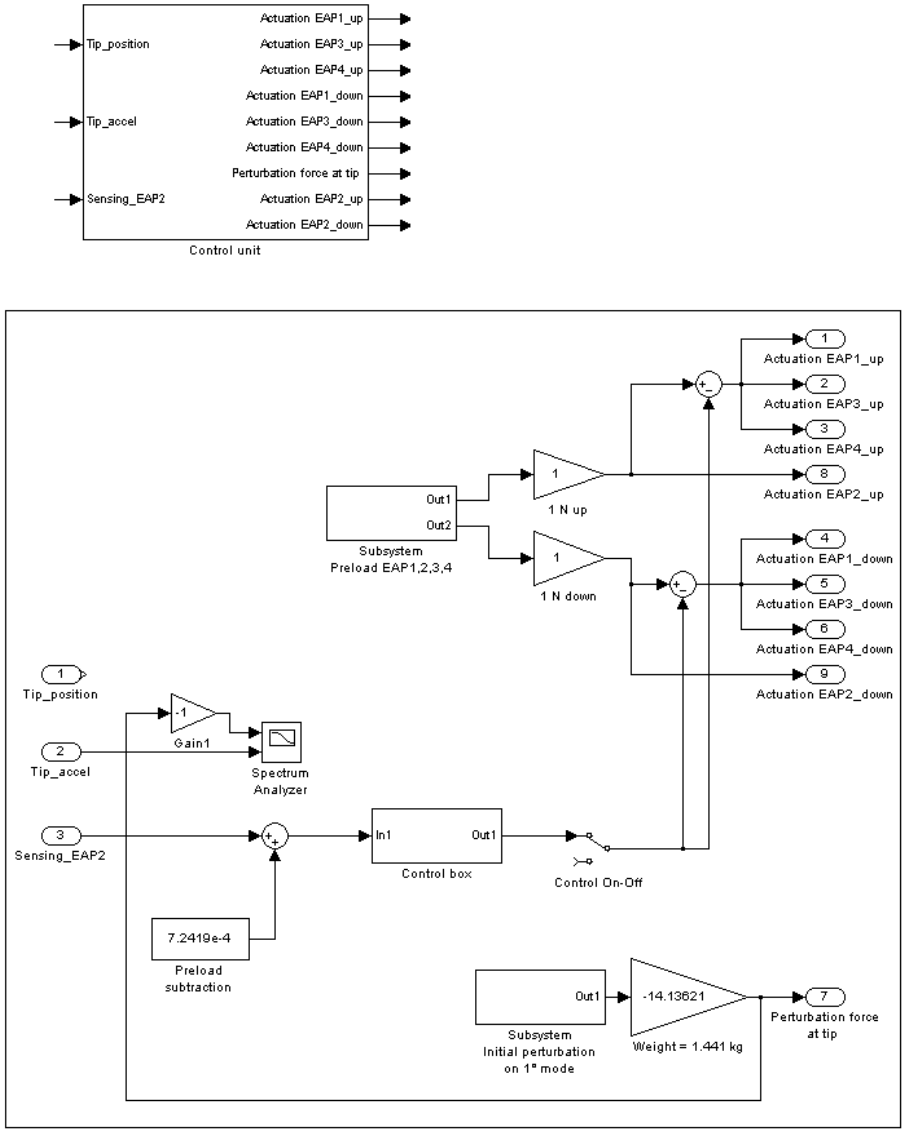

Figure 83. Control unit.

7.8 The logic of control

A logic of control is developed and applied in order to reduce the amplitude of the vibrations of the system. We apply a pull-release excitation to the free end to induce a bending oscillation mainly on first mode. This is the input. The output is acquired from an accelerometer and a position sensor on the free end.

Experimental results were obtained with different types of controls. Some not good results have been achieved with a Proportional Integrative Derivative (PID) control at first. After numerical simulations, a derivative control with a thresholded non linear block has been implemented. A block diagram of the implemented control is shown in Figure 84.

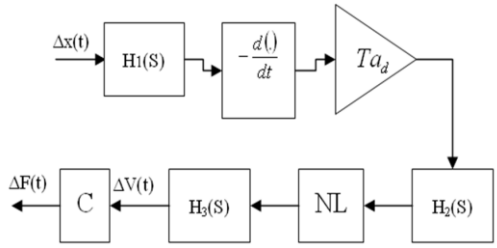

d(t)/dt → is the derivative operator

T_a → is an amplification factor

Δx(t) → is the elongation variation of the EAP sensor

ΔV(t) → is the voltage variation of the EAP actuator

ΔF(t) → is the variation of the output equivalent force

H1,H2,H3 → are linear filters

NL→ is a non-linear block whose characteristic is shown below

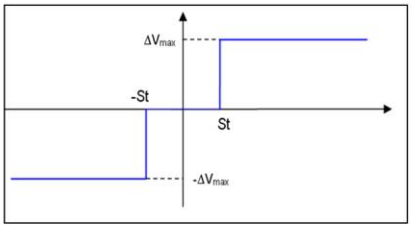

C → is the block that describes the elastic force variation as a function of the applied voltage

Figure 84. Block diagram of the vibration damping control.

This kind of control appears to be more effective in damping the vibrations because the action of the elastomers is held at the maximum strength as long as the vibration itself is present and then set to null when the vibration falls below a threshold (Figure 85). The threshold also helps preventing unwanted oscillations due to the noise inherent to the high voltage modules and the noise generated by the derivative block.

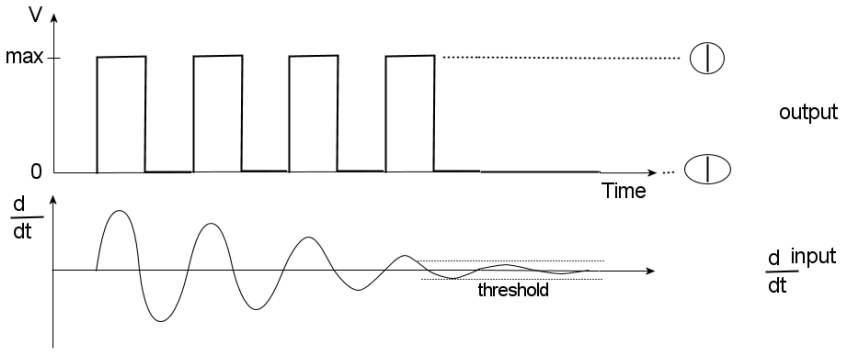

Figure 85. Maximum strength actuation signal.

Small amount of vibration damping was achieved for the experimental breadboard due to the high stiffness of the boom compared with the actuation performances of the DEA configurations in terms of maximum force and stroke. The manufacturing process of the boom is rather complex and it was difficult to control the thickness of the carbon fiber which in the end resulted to be too stiff. Simulations carried out after the experimental tests have shown that a less stiff boom would have been dampened more effectively.

In the Figure 86 and Figure 87 the time response of the position and the acceleration are reported for the firsts 10 seconds with and without the application of the control. Moreover a spectrum analysis provides to plot the transfer function between the input and output (acceleration) of the system in magnitude and phase. In Figure 88 and Figure 89 the same transfer functions are reported for the firsts 5 seconds.

The comparison of the peaks with and without control for this more flexible configuration gives a reduction in magnitude of about 15db after 5 seconds from the beginning of the vibrations and 50db after 10 seconds.

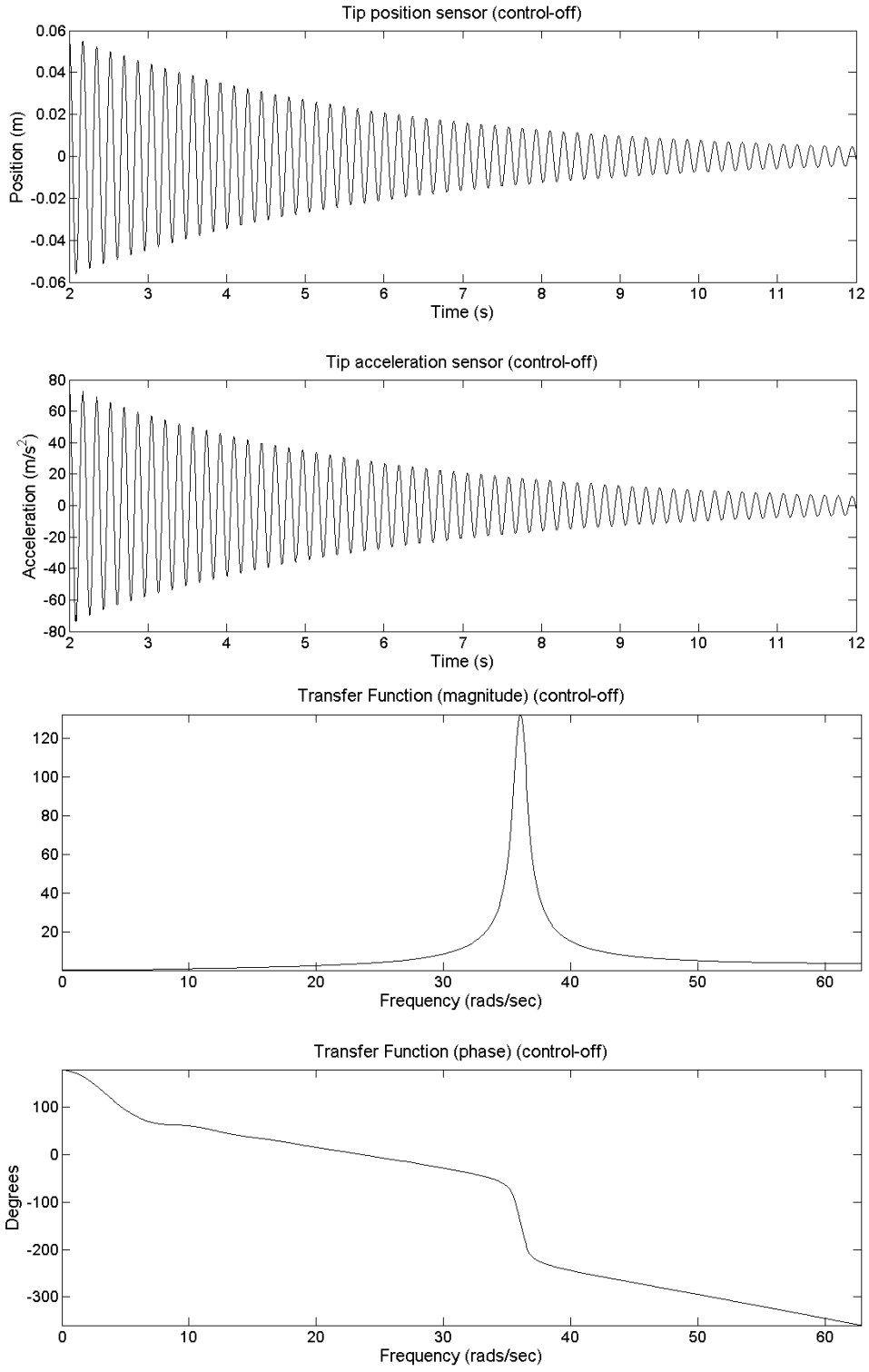

Figure 86. Time history and transfer function of the free end of the boom (control off) after 10 seconds

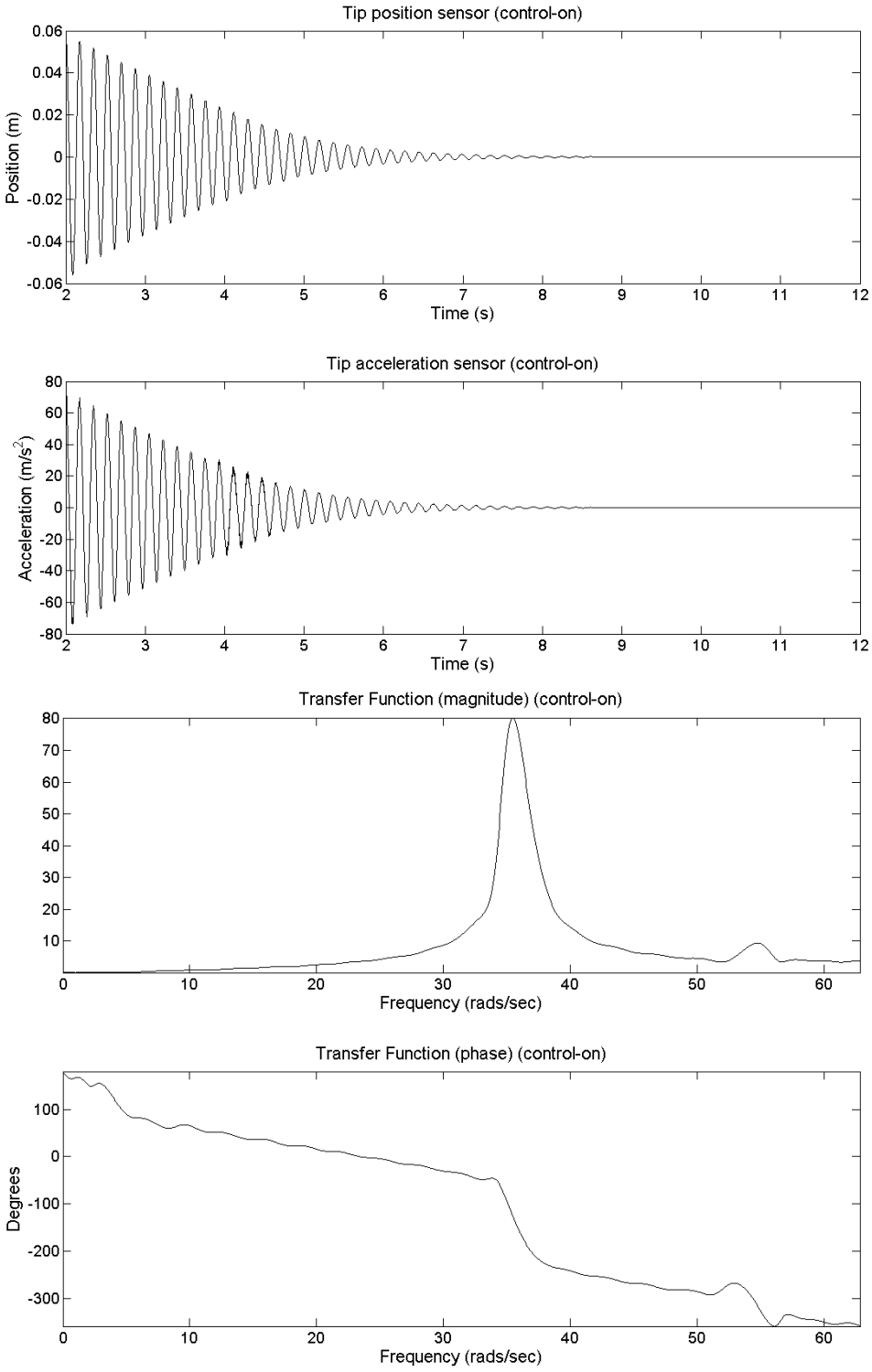

Figure 87. Time history and transfer function of the free end of the boom (control on) after 10 seconds

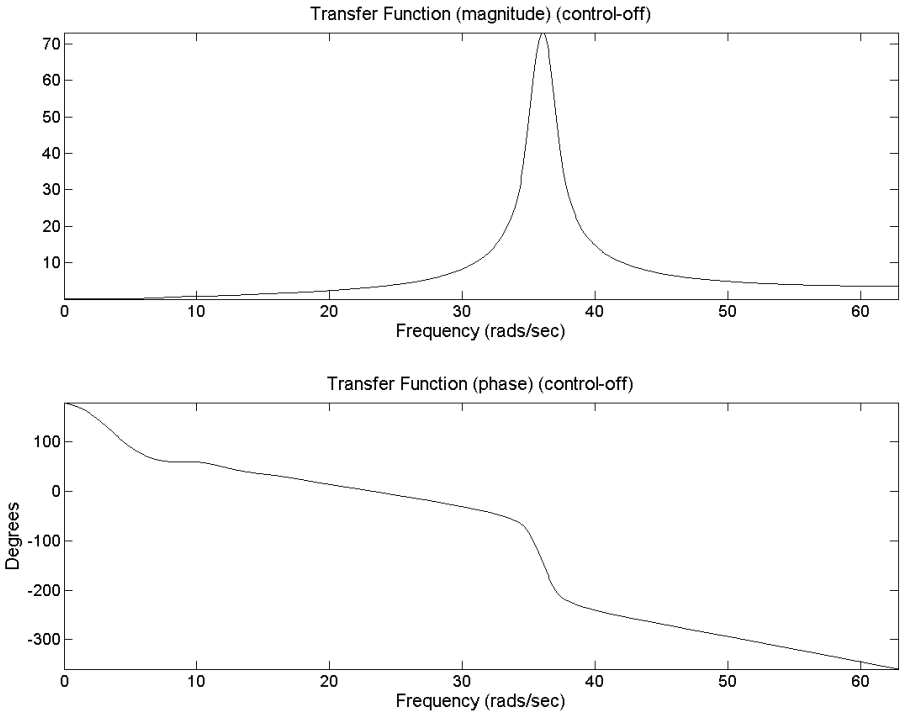

Figure 88. Transfer function of the free end of the boom (control off) after 5 seconds

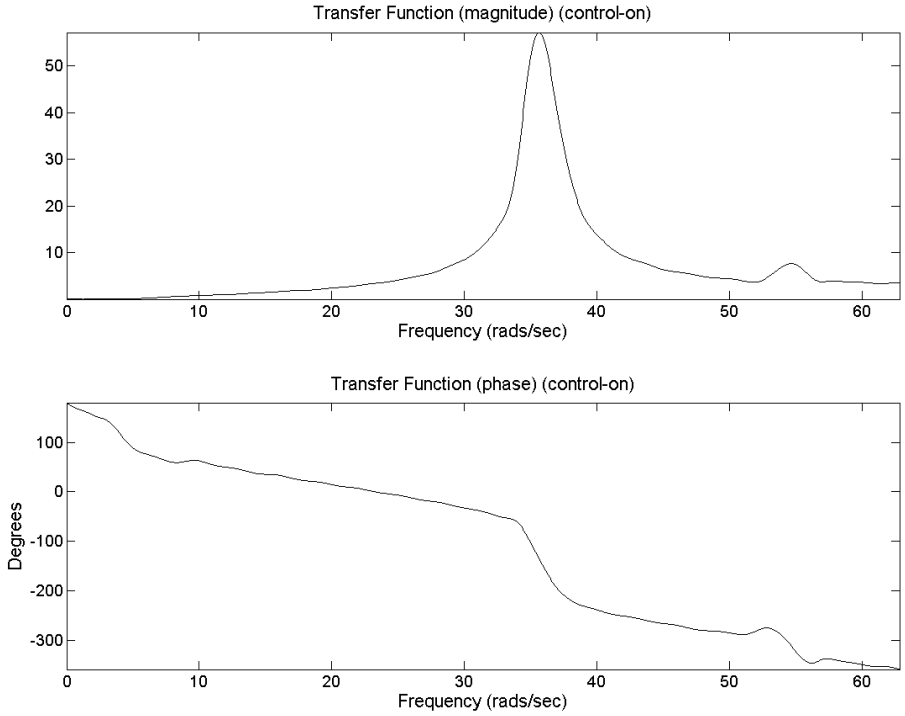

Figure 89. Transfer function of the free end of the boom (control on) after 5 seconds.

7.9 References

[1] Leipold, M. et al. - *Solar Sail Technology Development and Demonstration* - 4th IAA International Conference on Low-Planetary Missions, May 2-5, 2000, Johns Hopkins University, Maryland, USA

[2] Herbeck L., Eiden M., Leipold M., Sickinger Chr. and Unckenbold W. - *Development and Test of Deployable Ultra-light Weight CFRP Booms for a Solar Sail* - Proceedings European Conference on Spacecraft Structures, Materials and Mechanical Testing, ESTEC, November/ December 2000

[3] Fang H., Lou M., Huang J., Hsia L.-M. and Kerdanyan G. - *An Inflatable/ Self-Rigidizable Structure for the Reflectarray Antenna* - 10th European Electromagnetic Structures Conference, Munich (Germany), October 1-3 (2001).

[4] Frisbee R.H. and Brophy J.R. - *Inflatable Solar Sails for Low-Cost Robotic Mars Missions* - AIAA-97-2762, 33rd AIAA/ ASME/ SAE/ ASEE Joint Propulsion Conference & Exhibit, Seattle (WA), July 6-9 (1997).

[5] Baldacci S., Serafini L., Zolesi V.S., Thurecht F., Pfeiffer E.K., Sommer Larsen P., Carpi F., De Rossi D., Lampani L. and Gaudenzi P. *Development of Electro Active Polymers Configurations to Monitor and Control Deployable Space Structures* - 1st CEAS (European Air and Space Conference) 10-13 September 2007, Berlin (Germany)

[6] Carpi F., De Rossi D., Kornbluh, R. Pelrine R. and Sommer-Larsen P. - *Dielectric Elastomers as Electromechanical Transducers Fundamentals, Materials, Devices, Models and Applications of an Emerging Electroactive Polymer Technology* - Elsevier Science, March 10, 2008

[7] Freymann R.F. and Stümper E. - *Active Damping of a Large Structure Using Piezoelectric Sensors and Actuators* - Proceedings of the 32nd AIAA Structures, Structural Dynamics and Materials Conference, Baltimore, 8.-10. April 1991

[8] Herbeck L., Eiden M., Leipold M., Sickinger C. and Unckenbold W. - *Development and Test of Deployable Ultra-Lightweight CFRP-Booms for Solar Sail* - Proceedings of the

European Conference on Spacecraft Structures, Materials and Testing, 29.11.-1.12.2000, Noordwijk

[9] Locatelli G. - *Piezo-actuated adaptive structures for vibration damping and shape control – modeling and testing* - PhD-Thesis, Techn. Univ. Munich, Chair of Lightweight Structures, 2001

[10] Preumont A. - *Vibration control of active structures* - Kluwer Academic Publisher, Dordrecht, 1997

[11] Fanson J.L. and Caughey T.K. - *Positive position feedback control for large space structures* - AIAA Journal, Vol. 28, No. 4, April 1990, p. 717-724

[12] Courau E., Guay P. and Bousquet P.W. - *CASTOR Experiment Reults* - Proceedings of the 42nd AIAA Structures, Structural Dynamics, and Materials Conference, 16.-19.4.2001, Seattle, WA

Conclusions

The research work realize in the framework of this thesis has been for me extremely challenging and of great satisfaction. It allowed to give an innovative contribution to the modelling of a class of new generation smart materials, as the electroactive polymers with dielectric elastomer, and to find technological solutions for their application into the space environment.

The heart of the work is described in the forth chapter where the work for the implementation of a new numerical procedure, thorough the finite element method, to model the electromechanical behaviour of these materials is sustained. Both the constitutive relations of the mechanical and electrical part of the material show the behaviour with strongly non-linear nature. The first one follows the typical behaviour of the hyperelastic materials and for this reason it is studied and modelled through the introduction of an energetic functional for the elastic deformation based on the theoretical model of Mooney-Rivlin. The electrical part, to be more precise the relation that states the electromechanical coupling, is based on the Maxwell law. It links the mechanical stress to a component that depends quadratically from the electric field.

The goodness of the numerical procedure is validated in the fifth chapter, where a dielectric elastomer actuator, multilayer type, developed from Risø Danish National Laboratory, is modelled. In particular at this scope a model, totally new, to reproduce the behaviour of its electrodes (smart metallic compliant electrodes) with a non-linear orthotropic scheme is developed.

Another kind of actuator, based on a buckling functioning scheme, produced and developed from Centro Piaggio of the University of Pisa is studied and modelled in the sixth chapter.

A technological demonstrator of a structural space application for the electroactive polymers is described in chapter seven. It is a rigidizable inflatable boom made in carbon fiber reinforced polymer with sensors and actuators inserted. A new engineering solution to control the vibration of such kind of structure, based on the morphing of his cross-section is proposed. This kind of control allows to vary at local level the stiffness of this pipe structure through four sensor/actuators positioned internally along the diameter.

All this work allows further in-depth examinations, as i.e. the modelling of the viscoelastic behaviour of such materials for a better simulation of the dynamic process or the investigation of new configurations of sensor/actuators or new active structures.

The electroactive polymers opens the way to very interesting and surprising applications in the human life and it is opinion of the author that this argument will find more and more place in the future.

Acknowledgments

This work has been developed in the context of the research project of ESA/ESTEC “Electro-active polymers” contract no. 18548/04/NL/PA directed by Kayser Italia with which the Dipartimento di Ingegneria Aerospaziale e Astronautica, Sapienza – Università di Roma, collaborated in partnership with Risø Danish National Laboratory, Università di Pisa Centro Piaggio, HPS High Performance Space Structure Systems GmbH, DLR Germany's National Research Centre.

A special thank to Prof. Paolo Gaudenzi for his continuous support in the development of the present work, to the reviewers Prof. Renato Barboni, Prof. Luigi Balis Crema, Prof. Giuliano Coppotelli for their precious contributions and to Prof. Paolo Gasbarri for coordination.